

The Integrated Rotary Inverted Pendulum An Open and Configurable System With Digital Motor Controller Technology

Table of Contents

1. INTRODUCTION	3
OVERVIEW OF THIS MANUAL	5
2. INTEGRATED ROTARY INVERTED PENDULUM SYSTEM OVERVIEW	7
3. INTEGRATED ROTARY INVERTED PENDULUM CHARACTERISTICS	10
4. INTEGRATED ROTARY INVERTED PENDULUM: ROTOR SYSTEM MODEL.....	11
5. SUSPENDED PENDULUM DYNAMIC RESPONSE.....	17
6. SUSPENDED PENDULUM SINGLE PID CONTROLLER: ROOT LOCUS DESIGN	19
7. SUSPENDED PENDULUM DUAL PID CONTROLLER: ROOT LOCUS DESIGN.....	28
8. SUSPENDED PENDULUM SINGLE PID CONTROLLER: FREQUENCY RESPONSE DESIGN	35
9. SUSPENDED PENDULUM DUAL PID CONTROLLER: FREQUENCY RESPONSE DESIGN	47
10. INVERTED PENDULUM SINGLE PID CONTROLLER: ROOT LOCUS DESIGN.....	55
11. INVERTED PENDULUM DUAL PID CONTROLLER: ROOT LOCUS DESIGN	67
12. INVERTED PENDULUM SINGLE PID CONTROLLER: FREQUENCY RESPONSE DESIGN	73
13. INVERTED PENDULUM DUAL PID CONTROLLER: FREQUENCY RESPONSE DESIGN	87
14. INVERTED PENDULUM DUAL PID CONTROLLER: CONTROL OF AND UNSTABLE PLANT	95
15. STATE SPACE MODERN CONTROL: THE LINEAR QUADRATIC REGULATOR	104
16. STATE SPACE MODERN CONTROL: THE LINEAR QUADRATIC REGULATOR FOR STABLE SUSPENDED PENDULUM OPERATING MODE.....	115
17. REFERENCES	122
18. APPENDIX A: PENDULUM ANGLE ERROR AUTOCOMPENSATION SYSTEM	124
19. APPENDIX B: INTEGRATED ROTARY INVERTED PENDULUM: REAL TIME VIEWER AND MATLAB INTERFACE.....	126
1. APPENDIX C: INTEGRATED ROTARY INVERTED PENDULUM: SERIAL CONTROL INTERFACE	127
RESPONSE MESSAGES FROM IRIP SYSTEM	127
2. APPENDIX D: INTEGRATED ROTARY INVERTED PENDULUM: INDIVIDUALIZATION FOR INSTRUCTION	129

1. Introduction

Control systems engineering increases in importance ever more rapidly with the appearance of self-driving vehicles, novel aerial vehicles, medical robotics, and countless consumer products. These applications require not only engineers with hands-on experience in control systems, but also very importantly, in the management and control of electric motor actuators and precise position sensors.

Digital control has evolved to advance nearly every electronic system. In contrast, *direct digital electric motor interfaces* has most recently appeared. Integrated system on chip power electronics now provides accurate electric motor actuation control with combined sensing of motor shaft angle. This presents critical new capabilities and requirements for control systems. Training and instruction in direct digital motor interfaces is essential for engineers today with the appearance of these systems in every form of mechatronics and robotics.

Control systems engineering design skill relies on understanding of both theory and practice. This is important to both experienced, professional engineers addressing a new control problem or students learning control systems engineering for the first time. Engineering education for fields, including electronics and computer engineering have taken advantage of hands-on instruction for all students for many decades. However, understanding of control systems practice, requiring hands-on-experience, has not been available for control systems students due to the cost of platforms.

The Integrated Rotary Inverted Pendulum has been designed to provide every engineer learning control systems with a flexible, low cost, *personal* design platform. A diverse and fascinating set of design challenges are available. These include the unique characteristics of state-of-the art motor control systems. This introduces the concepts of motor control and power electronics with classic and important control problems.

The Integrated Rotary Inverted Pendulum has been developed to provide engineers with experience in both Control Systems as well as state-of-the-art Motor Control interfaces. This includes opportunities for both development of stable control, with a suspended pendulum mode, and the classic unstable control problem with the inverted pendulum. This also includes a state-of-the-art high speed, precise, and configurable electric motor interface integrated with a processor hosting user composed controller systems.

An important feature of the Integrated Rotary Inverted Pendulum system is the opportunity to demonstrate the limitations of classic control and introduce *modern control*. Thus, this system includes stable and unstable plants as well as conventional PID control, parallel PID control structures, and LQR control based on design optimization.

Recent advances in state-of-the-art motor control systems by STMicroelectronics now enables the development of powerful control system kits that are sufficiently low in cost to be owned by every student. Further, it is possible for an individual to purchase and use this system for a cost less than a textbook. It can further be used in multiple courses from introductory level through senior and graduate level.

Hands-on experience with the Integrated Rotary Inverted Pendulum can be gained with many paths:

- 1) **Introduction to Control and Motor Control:** An introduction to control systems can be gained by students and users who access the Integrated Rotary Inverted Pendulum from any computer over a serial interface to adjust a real-time controller, configure control architectures, acquire data and both experience control as well as design advanced control methods.
- 2) **Matlab, Terminal Command Line Access, or C-Code Real Time Development:** Real time controllers are included along with demonstration systems. This also includes methods for configuration by Matlab or Terminal session command line interfaces.
- 3) **Open Source C-Code Real Time Development:** The real time C-Code control systems may be examined, modified, or replaced by users, offering a very wide range of instruction and research opportunities in advanced control systems.
- 4) **Matlab Real Time Viewer:** Live data is displayed via a Matlab “scope” interface of all physical system and control system parameters and signals.
- 5) **Example Instruction Sequences:** The Integrated Rotary Inverted Pendulum control systems can also be used in the Control Systems course curriculum with a sequence of projects focusing on PID control of stable systems, PID control of unstable systems, and State Space LQR control of unstable systems. This includes reference simulation and design methods based on Mathworks Matlab.
- 6) **Example Advanced Instruction Sequences:** The Integrated Rotary Inverted Pendulum control systems can also be used in advanced Control Systems course, mechatronics courses, and embedded systems courses where users have direct access to the real-time C-code implementation of the control system and the ability to view the control system template, modify and replace any or all components. This is supported by the STM32 system and open source Integrated Development Environment (IDE) tools compatible with Windows and Apple OS X operating system platforms.
- 7) **Individualization for Each Student:** An important characteristic of the Integrated Rotary Inverted Pendulum is its adaptability to enable *individualization for each student and for each assignment. This ensures that individual students or selected student groups may operate independently with assurance of independent results when assessing assignment results. This is described further in Appendix C.*
- 8) **Shared and Open Environment:** *First, our objective is to continuously adapt and advance the Integrated Rotary Inverted Pendulum to address the needs of students and instructors. All requests for new features, new analyses, and new instructional approaches will be pursued. Also, all components are open and available for any innovations at any level by all users.*

This description, intended for Instructors who wish to learn about the Integrated Rotary Inverted Pendulum, describes system configuration, system dynamics, control system design examples, and experimental measurements.

Overview of This Manual

- 1) *Introduction*
 - a. This describes the motivation for the Integrated Rotary Inverted Pendulum, the introduction of direct digital actuators and the difference between this platform and prior systems.
- 2) *Integrated Rotary Inverted Pendulum System Overview*
 - a. This describes the system physical architecture
- 3) *Integrated Rotary Inverted Pendulum System Characteristics*
 - a. This describes the system critical dimensions and motor control parameters
- 4) *Integrated Rotary Inverted Pendulum: Rotor System Model*
 - a. This describes the second order model developed for the response of the Motor Controller
- 5) *Suspended Pendulum Dynamic Response*
 - a. This describes the dynamic response characteristic of the Pendulum when operating in a suspended, and stable mode.
 - b. This permits an introduction to control system development with an inherently stable plant.
- 6) *Suspended Pendulum Single PID Controller*
 - a. This describes the design and implementation of a Single Input Single Output (SISO) PID controller stabilizing Pendulum Angle
- 7) *Suspended Pendulum Dual PID Controller*
 - a. This describes the design and implementation of dual, parallel, controllers stabilizing Pendulum Angle and Rotor Angle.
 - b. This approach of dual PID controllers enables a method for implementing stable control. However, a strategy for optimal control is not available with this method.
- 8) *Inverted Pendulum Single PID Controller*
 - a. This describes the design and implementation of a Single Input Single Output (SISO) PID controller stabilizing Pendulum Angle for the Inverted Pendulum operating mode.
 - b. The Inverted Pendulum operating presents an inherently unstable control challenge ideal for gaining experience in modern control.
- 9) *Suspended Pendulum Dual PID Controller*
 - a. This describes the design and implementation of dual, parallel, controllers stabilizing Pendulum Angle and Rotor Angle for the Inverted Pendulum operating mode.
 - b. This approach of dual PID controllers enables a method for implementing stable control. However, a strategy for optimal control is not available with this method.
- 10) *State Space Modern Control: The Linear Quadratic Regulator for Inverted Pendulum Operation*
 - a. This describes the design and implementation of a Multiple Input Multiple Output (MIMO) State Space Linear Quadratic Regulator (LQR) control system for the Inverted Pendulum operating mode.
 - b. This provides an introduction and experience in Modern Controls and optimal control methods.
- 11) *State Space Modern Control: The Linear Quadratic Regulator for Suspended Pendulum Operation*
 - a. This describes the design and implementation of a Linear Quadratic Regulator (LQR) control system for the Suspended Pendulum operating mode.
 - b. This provides additional experience in optimal control methods and the limitations of classic control for MIMO systems.
- 12) *Appendices:*

- a. Appendix A: Pendulum Angle Autocompensation System
- b. Appendix B: Integrated Rotary Inverted Pendulum Real Time Viewer and Matlab Interface
- c. Appendix C: Integrated Rotary Inverted Pendulum Individualization for Instruction
- d. Appendix D: Integrated Rotary Inverted Pendulum: Dual PID Controller Matlab Design and Simulation For Suspended Pendulum Mode
- e. Appendix E: Integrated Rotary Inverted Pendulum: Dual PID Controller Matlab Design and Simulation For Inverted Pendulum Mode
- f. Appendix F: Integrated Rotary Inverted Pendulum: LQR State Space Modern Control of Inverted Pendulum Mode Operation
- g. Appendix G: Integrated Rotary Inverted Pendulum: LQR State Space Modern Control of Stable Suspended Pendulum Mode Operation

2. Integrated Rotary Inverted Pendulum System Overview

The Integrated Rotary Inverted Pendulum System includes an Inverted Rotary Pendulum [Furuta_1992] structure with a rotor system based on a Stepper Motor, Motor Control System based on the STMicroelectronics L6474 Motor Controller [ST_L6474_2019] and IHM01A1 [ST_IHM01A1_2019] support board, and finally a Nucleo F401RE board supporting the STM32 processor[ST_Nucleo_2019]. Figure 1 shows the system architecture with the following definitions for dimensions and angle values in Table 1 and *Table 2*. Figure 2 through Figure 4 show images of the system.

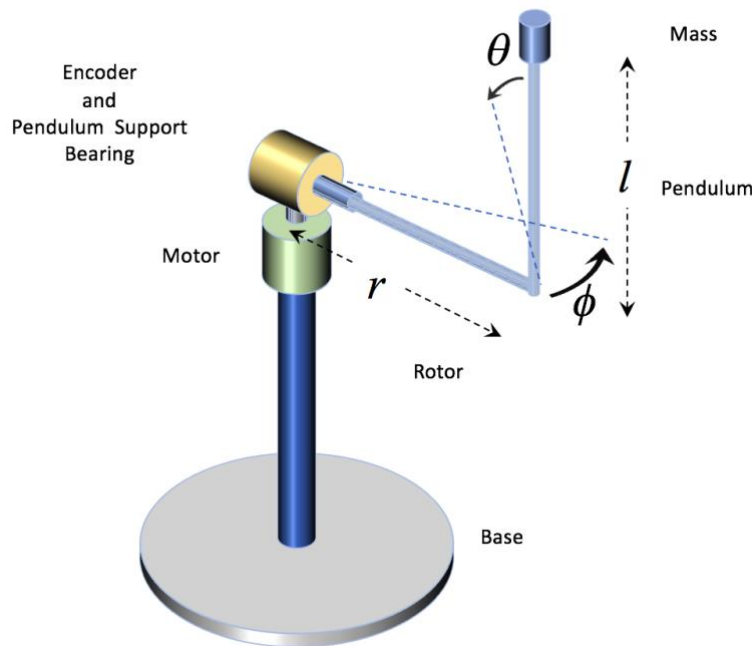


Figure 1. The Integrated Rotary Inverted Pendulum System shown with pendulum inverted. This shows its components including Motor providing rotation actuation of the rotor, Encoder providing sensing of rotor axial rotation angle, and the pendulum upright component with its supported mass. The definitions of dimensions and rotation angles defining pendulum position are also shown.

System Structure Characteristic	Definition
l	Pendulum Vertical length from Rotor Arm to supported Mass
r	Rotor Arm length
ϕ	Angle of Rotor relative to start reference angle
θ	Angle of pendulum relative to gravity vertical

Table 1. The Integrated Rotary Inverted Pendulum System Structure Characteristics

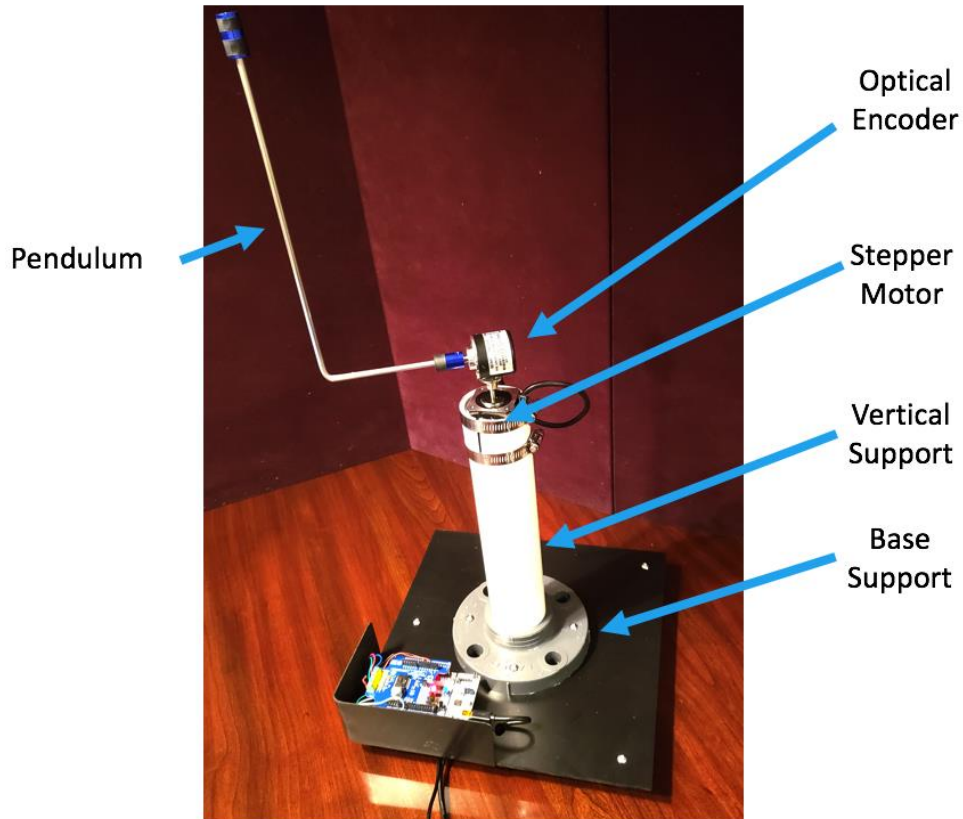


Figure 2. Rotary Inverted Pendulum System view during operation with active control and pendulum stabilized in vertical orientation

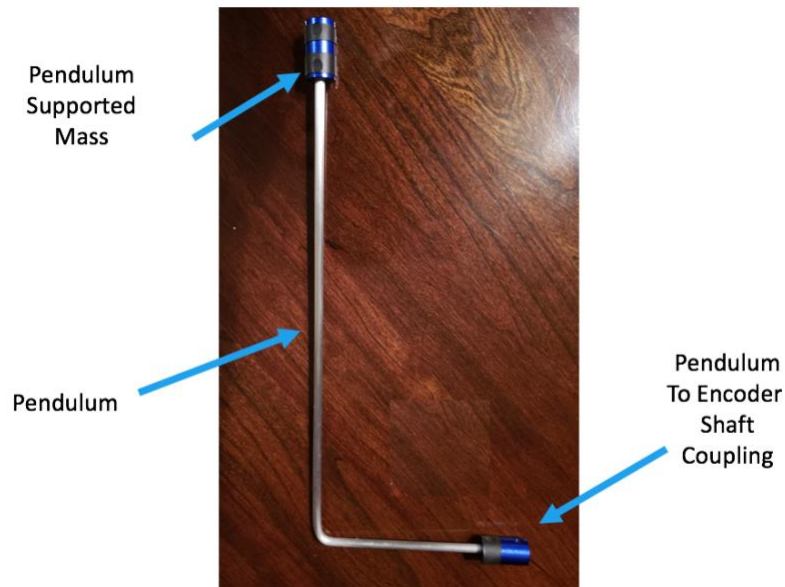


Figure 3. Pendulum System showing upper shaft Mass. The Pendulum structure is based on a 4.5mm diameter aluminum bar. This is fastened by a shaft coupling to the Optical Encoder shaft.

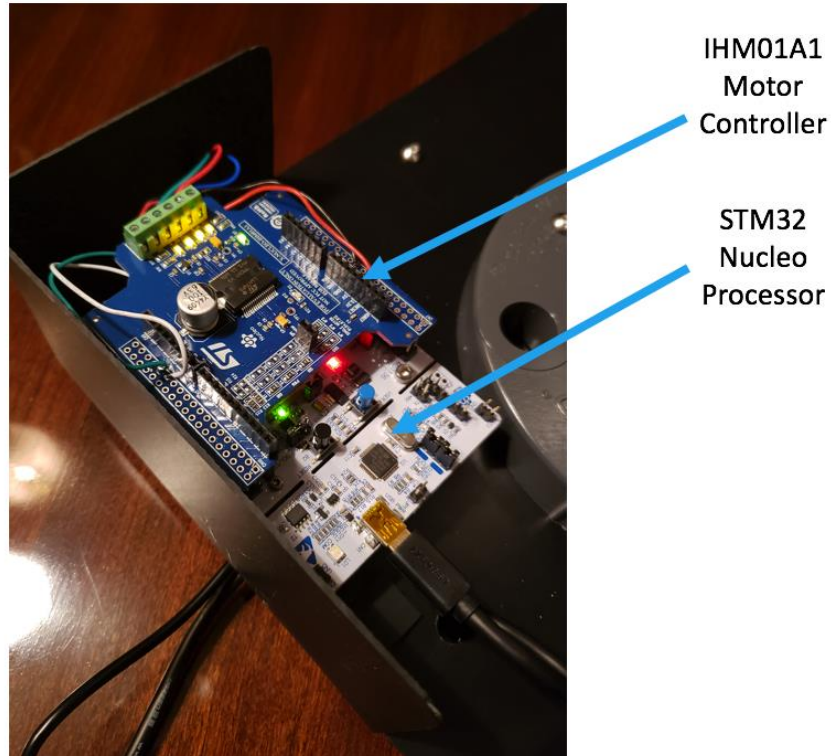


Figure 4. IHM01A1 Motor Controller and the Rotary Inverted Pendulum system processor.

3. Integrated Rotary Inverted Pendulum Characteristics

Table 2 describes system characteristics of the Integrated Rotary Inverted Pendulum. The Rotor actuator is based on a NEMA-17 Stepper Motor controlled by the L6474 – IHM01A1. Each incremental step command to the motor controller produces an effective 1/16th microstep for a 200 step per rotation motor. This results in an angular displacement of 9.817×10^{-4} radians per step command or 0.0563 degrees per step and a Rotor Angle Control Gain of 17.778 step commands per degree. This gain is applicable for steady state, DC response. Motor control dynamics at high control frequency is described in Section 4.

This is configured to operate at an adjustable step rate M_{Speed} . The value of M_{Speed} are set to 200 steps per second and also to 100 steps per second in the examples in this review.

Each incremental change in stepper motor position is read with a factor of two greater gain for an effective 1/16th microstep for a 200 step per rotation. This results in angular displacement measurement of 1.963×10^{-3} radians per step measured or 0.1126 degrees per step and a Rotor Angle Measurement Gain of 8.889 steps measured per degree.

Pendulum Angle, θ , is measured with a quadrature optical encoder (LPD3806-600BM-G5-24C) providing a resolution of 2400 step count values per revolution equal to 6.667 step counts per degree.

<i>System Characteristic</i>	<i>System Characteristic Description</i>	<i>System Characteristic Value</i>
l	Pendulum Length measured as vertical separation from Rotor Arm to Pendulum Mass	0.235 m
r	Rotor Arm Length	0.14 m
ϕ	Angle of Rotor relative to initial angle reference.	
θ	Angle of Pendulum relative to gravity vector	
Rotor Angle Measurement Gain	Measurement gain of rotor angle provided by the motor and motor control interface	8.889 Steps per Degree
Rotor Angle Control Gain	Rotor angle actuation gain provided by the motor and motor control interface	17.778 Steps per Degree
Pendulum Angle Measurement Gain	Measurement gain of Pendulum Angle provided by the optical encoder and its interface	6.667 Steps per Degree

Table 2. The Integrated Rotary Inverted Pendulum System Characteristics

4. Integrated Rotary Inverted Pendulum: Rotor System Model

1) Motor Control Overview

Motor control systems appearing in the previous generation of actuators and robotic systems relied on simplified control and measurement. For example, analog methods for control of motor current resulted in control of motor torque only. Measurement of motor shaft angle relied on separate angle encoder systems that were often limited in resolution.

State of the art motor control systems are based on integrated systems combining high speed current switching devices and circuits with current sensing to provide precise motor control. This enables the replacement of torque control of the motor system with direct control of motor operation schedule.

An example is an integrated Stepper Motor control system that provides control of motor speed, acceleration, and deceleration. In addition, an integrated Stepper Motor controller includes direct detection of motor position.

Also, most importantly, the Stepper Motor enables a precise control of motion at a fixed speed, M_{Speed} , rather than a control of torque with a resulting response dependent on instantaneous system state and associated inertial and gravitational forces. The Stepper Motor control system initiates motion of the Stepper Motor rotor towards a target angle at the speed, M_{Speed} . Motion continues at M_{Speed} until the target is reached or the motor control system receives a new target value.

Previous inverted pendulum research and available inverted pendulum systems were based on analog motor control. The Integrated Rotary Inverted Pendulum includes a Stepper Motor Controller based on the STMicroelectronics L6474 integrated motor interface. This is supported by open source software systems developed for the Integrated Rotary Inverted Pendulum.

The powerful motor control systems available require operation models as was required for simple motor control systems in the past.

Multiple motor configurations and corresponding models have been developed. This offers an ideal opportunity for instruction since instructors and students may now select a motor configuration and its dynamic response and implement new control systems adapted to each motor characteristic.

2) Motor Controller Response Model

Development of control systems first requires development of a model for the Stepper Motor system providing Rotor control of Rotor Angle, ϕ , in response to Rotor Angle Control input, ϕ_{RC} .

The Stepper Motor controller provides multiple configuration values for design of motor response meeting specific objectives. The Stepper Motor interface is provided with configuration of settings prior to initiation of control. Control proceeds with multiple motor command modes. One used for the Integrated Rotary Inverted Pendulum is target position.

Here, a new angle target, measured in steps of rotation, is supplied to the interface. The Stepper Motor Control initiates motion towards the target and will cease motion if the target angle is reached.

During each cycle of control system operation for the Integrated Rotary Inverted Pendulum, new target angles are supplied. In general, the target angle updates occur at time intervals that are much shorter than a target travel time for the motor. Thus, the motor controller target angle is updated at each control cycle thus changing direction of motor rotation.

Motor control characteristics applied in the Integrated Rotary Inverted Pendulum and that are adjustable are described in Table 3.

<i>Stepper Motor Configuration Parameter</i>	<i>Definition</i>
Maximum Speed	The maximum speed in step rate (in units of steps per second) of Stepper Motor reached by the motor after a time determined by Maximum Acceleration.
Minimum Speed	The minimum speed in step rate (in units of steps per second) of the Stepper Motor for any motion. The motion of the Stepper Motor for any motion initiates at the rate of Minimum Speed and may accelerate to greater speed if the Motor Control Target is not changed or reached.
Maximum Acceleration	The maximum acceleration rate (in units of steps per second per second) of Stepper Motor operation in motion towards a target angle.
Maximum Deceleration	The maximum deceleration rate (in units of steps per second per second) of Stepper Motor operation in motion towards a target angle.

Table 3. Stepper Motor Control configuration definitions.

It is important to note that the Motor Control system enables a diverse set of Rotor Response characteristics. These can be applied for optimization of performance and energy demand. Also, the Motor Controller integrates both precise motion control and angular position measurement.

It is also important to note that this deterministic Motor Control system response to Rotor Angle control input is nonlinear. However, control system design and experimental development may avoid influence by this nonlinear response that is exhibited for large amplitude and high frequency motion.

The inverted pendulum control system operates in a limit of small signals and small angle variation. Thus, a linear model of Rotor Angle, ϕ , to Rotor Angle Control, ϕ_{RC} , may be developed.

This is based on direct measurement of system response under control. This is also based on an approach that matches both DC gain for the Stepper Motor Controller, that will be unity, with the frequency response of the Stepper Motor Controller system for a specified configuration.

A Rotor Angle Response Transfer Function, G_{Rotor} , model was developed by introducing a second order response function:

$$G_{Rotor} = \frac{\phi}{\phi_{RC}} = \frac{a}{s^2 + bs + c} \quad (1)$$

Model development was based on the measurement of **both** ϕ and ϕ_{RC} time series during system operation under PID control.

Determination of the values of coefficients, a , and b , was developed by supplying the recorded Rotor Angle Control, ϕ_{RC} , time series as an input to the resulting model, yielding computation of a simulated Rotor Angle, ϕ , time series. Coefficients a and c are equal since G_{Rotor} has unity gain at zero frequency. The simulated signal may then be compared directly to that of the experimentally measured ϕ time series.

The selection of coefficients is based on comparison of the of simulated and experimentally measured response of Rotor Angle, ϕ .

Model development is based on direct comparison of experimental and model-simulated time domain response for an operating, closed loop system. The Integrated Rotary Inverted Pendulum was operated in closed loop for each of the High, Medium, and Low Speed configurations of Table 4. The correlation between experimental and simulated characteristics was then computed. A simple grid search over the values of coefficients, α and β was performed to find maximum correlation. Correlation coefficients at maximum, best fit, were greater than 0.999 for each configuration.

Three Motor Configurations are described in Table 4. The results of linear model development for each of these configurations are summarized in Table 5. In the Integrated Rotary Inverted Pendulum physical system, due to definitions for the primary angles, a positive control system rotor control signal induces a negative excursion in rotor angle. The transfer function, therefore shows negative polarity as noted in the polarity of the numerator coefficient, a .

<i>Stepper Motor Configuration Parameter</i>	<i>Symbol</i>	<i>High Speed System Example</i>	<i>Medium Speed System Example</i>	<i>Low Speed System Example</i>
Maximum Speed	Max_{Speed}	1000	1000	200
Minimum Speed	Min_{Speed}	300	200	200
Maximum Acceleration	$Max_{Acceleration}$	3000	3000	3000
Maximum Deceleration	$Max_{Deceleration}$	3000	3000	3000

Table 4. Stepper Motor Control configurations for three motor control models described here. These correspond to two values for Max_{Speed} with both operating at Min_{Speed} of 200 steps per second. These are examples of the many optimization choices available

<i>Stepper Motor Configuration Example</i>	<i>Stepper Motor Configuration</i>	<i>Coefficient A</i>	<i>Coefficient b</i>	<i>Coefficient c</i>
High Speed	Maximum Speed = 1000 Minimum Speed = 300	0.22	0.90	0.44
Medium Speed	Maximum Speed = 1000 Minimum Speed = 200	0.245	1.12	0.49
Low Speed	Maximum Speed = 200 Minimum Speed = 200	0.275	1.89	0.55

Table 5. Rotor Angle Response Transfer Function, G_{Rotor} , coefficients for the three example motor speed configurations.

The comparison of simulated and measured Rotor Angle, ϕ , power spectral density characteristics are shown in Figure 5. for the High Speed System Example of $Min_{Speed} = 300$ and $Max_{Speed} = 1000$ steps per second parameters, Figure 6 for the Medium Speed System Example $Min_{Speed} = 200$ and $Max_{Speed} = 1000$ steps per second parameters and Figure 7 for the Low Speed System Example $Min_{Speed} = 200$ and $Max_{Speed} = 200$ steps per second,

Figure 5 through Figure 7 show the comparison between simulate response and experimental measurements for each speed configuration. Agreement between model and data is accurate. The

Rotor Angle Response Transfer Function model for this motor configuration is then applied for control system design. Direct measurement of full system control system performance relative to simulation of full system performance, will be applied to confirm the validity of this model.

Figure 8 compares the Bode response for each Rotor Response transfer function.

Finally, an important confirmation of the applicability of this modeling method is its application to design of controllers by the optimizing LQR method for each configuration. Section 10 includes the comparison of experimental and simulated response of Rotor and Pendulum for each of three controllers designed for each configuration. The agreement between experimental and simulated response for each example where no other adjustable parameters appear provides confirmation of these models.

It is important also to note that other configurations may also be modeled. Higher order models may also be developed. Configurations may also be adjusted in real time to characterize robust control, compliant to motor system variability due to manufacturing variability, system aging, and many other characteristics. Finally, the development of novel, real time adaptive motor response methods integrated with new adaptive controllers creates a valuable future opportunity.

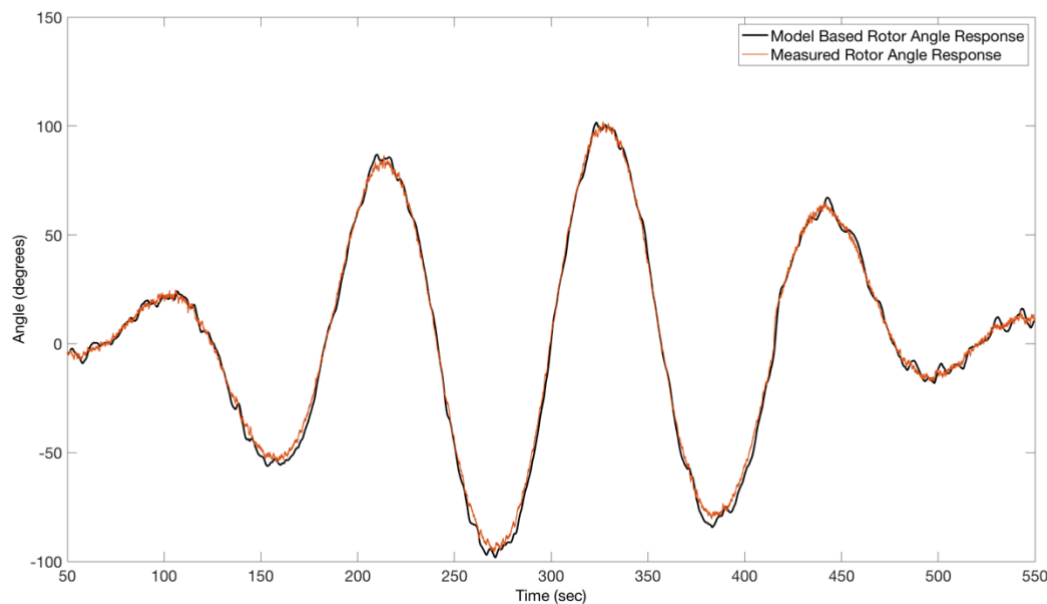


Figure 5. Comparison of model-based Rotor Angle response and measured Rotor Angle response for the Rotary Inverted Pendulum under closed loop operation with a modulated amplitude sinusoidal rotor angle tracking input signal. This characteristic response corresponds to values of $\text{Min}_{\text{Speed}} = 300$ and $\text{Max}_{\text{Speed}} = 1000$ steps per second..

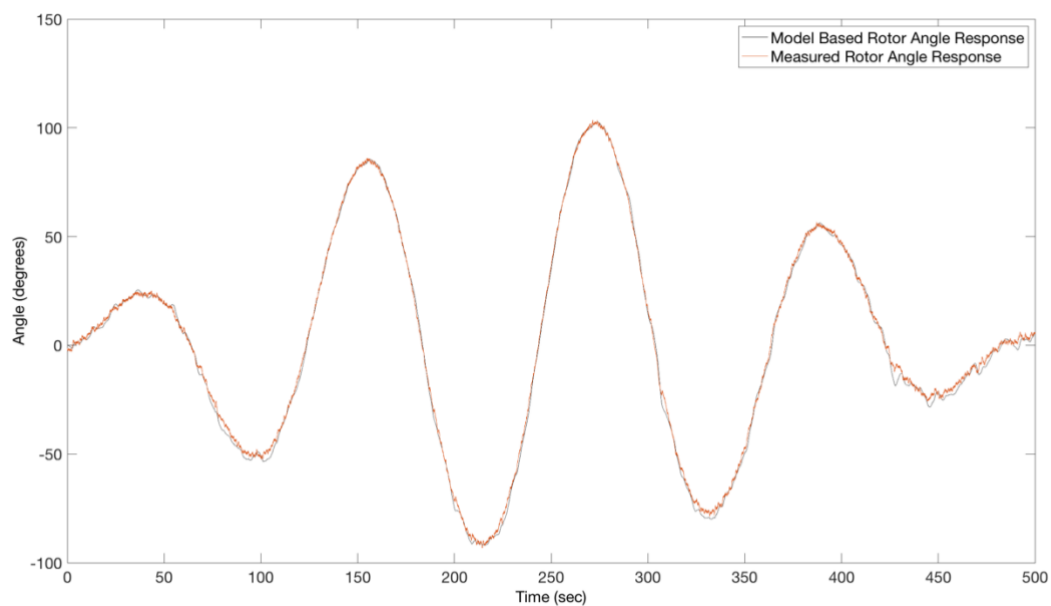


Figure 6. Comparison of model-based Rotor Angle response and measured Rotor Angle response for the Rotary Inverted Pendulum under closed loop operation with a modulated amplitude sinusoidal rotor angle tracking input signal. This characteristic response corresponds to values of $\text{Min}_{\text{Speed}} = 200$ and $\text{Max}_{\text{Speed}} = 1000$ steps per second.

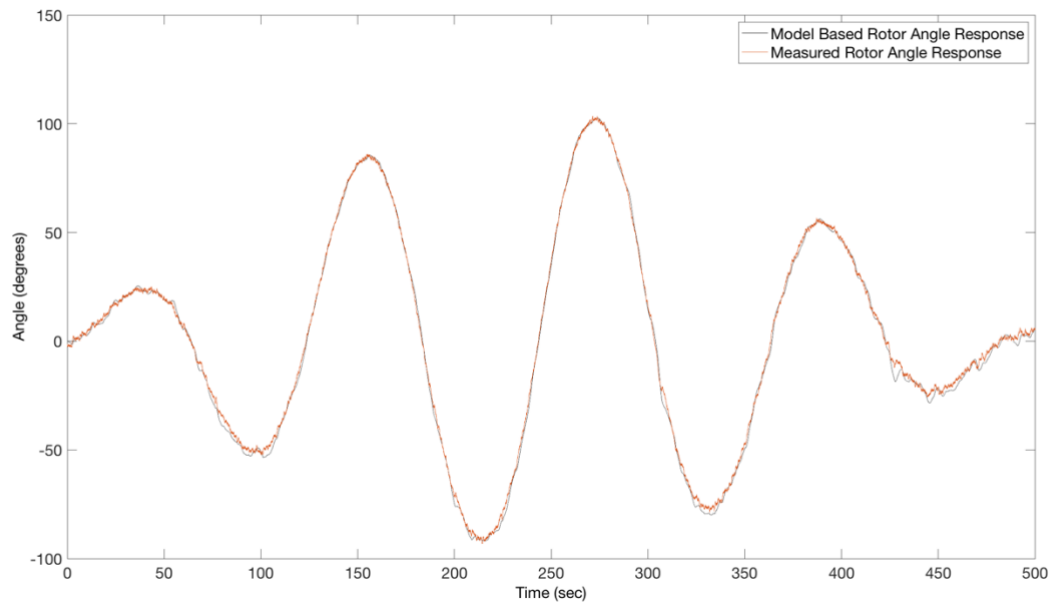


Figure 7. Comparison of model-based Rotor Angle response and measured Rotor Angle response for the Rotary Inverted Pendulum under closed loop operation with a modulated amplitude sinusoidal rotor angle tracking input signal. This characteristic response corresponds to values of $\text{Min}_{\text{Speed}} = 200$ and $\text{Max}_{\text{Speed}} = 200$ steps per second.

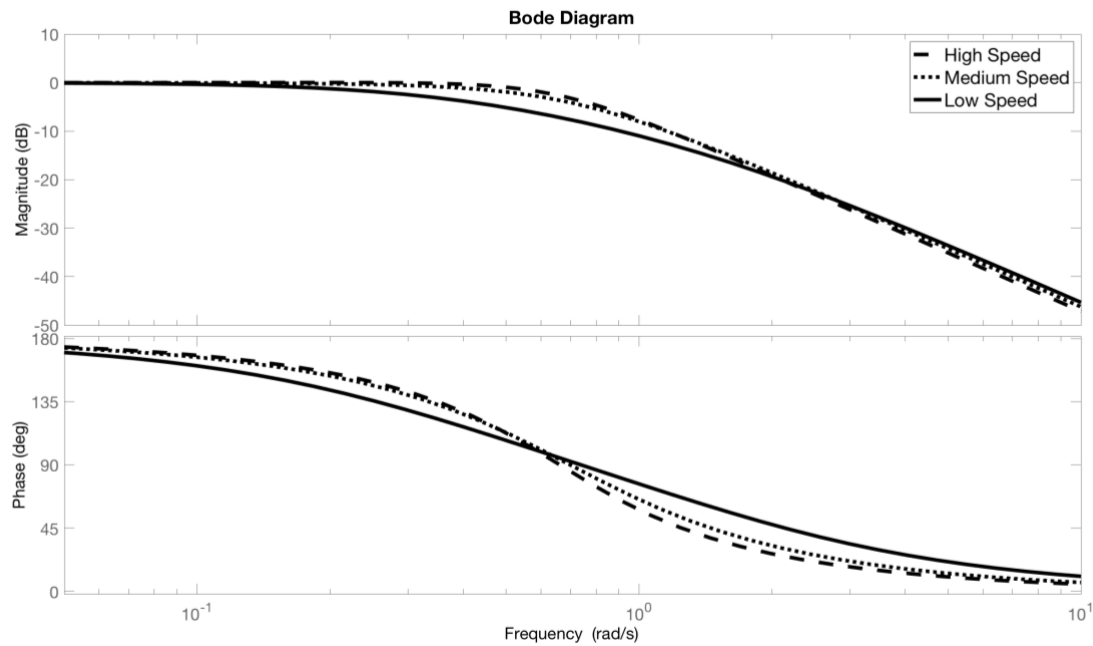


Figure 8. Comparison of Bode response for each of the Low Speed, Medium Speed, and High Speed Rotor Angle response configurations.

5. Suspended Pendulum Dynamic Response

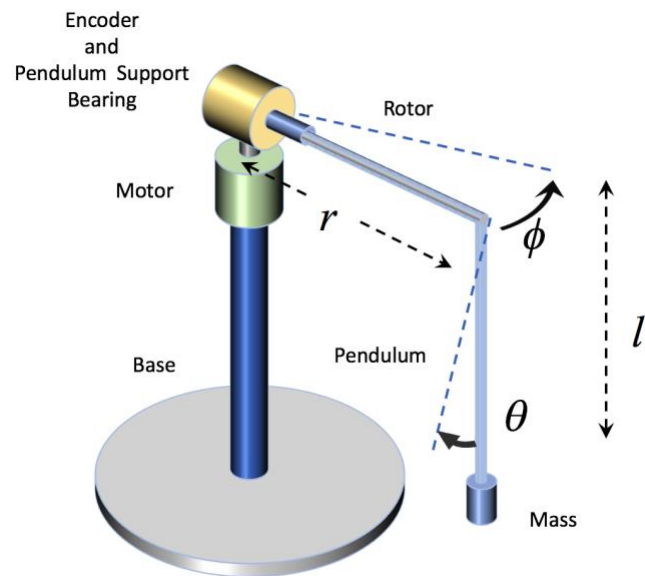


Figure 9. The Integrated Rotary Inverted Pendulum System shown with pendulum suspended. The definitions of dimensions and rotation angles defining pendulum position are also shown.

The suspended pendulum configuration is shown in Figure 9. This is a stable system where Pendulum angle, θ remains zero in the absence of a control input of rotor angle, ϕ .

The response of the suspended pendulum is determined by rotor angle, ϕ , gravitational acceleration, and friction force. Pendulum mass, m , is dominated by the presence of the suspended mass at the end of the pendulum structure since the pendulum arm mass is low. Referring to Figure 5, gravity acts on both the pendulum mass, m , suspended at angle, θ , as well as friction force proportional to velocity, $\gamma\dot{\theta}$, to induce an acceleration on the pendulum mass. The result of summing forces acting on the pendulum is

$$m\ddot{\theta}_{gravitational} + \gamma\dot{\theta} = -\frac{mg}{l}\sin\theta \quad (2)$$

Further, the rotor rotation induces an acceleration of the pendulum mass of

$$\ddot{\theta}_{rotor} = \frac{(r)\sin\ddot{\phi}}{l}\cos\theta \quad (3)$$

Then acceleration of the pendulum mass is the sum of these contributions

$$\ddot{\theta} = -\frac{g}{l}\sin\theta + \frac{(r)\sin\ddot{\phi}}{l}\cos\theta - \frac{\gamma}{m}\dot{\theta} \quad (4)$$

Considering small angles,

$$\ddot{\theta} = -\frac{g}{l}\theta + \frac{r}{l}\ddot{\phi} - \frac{\gamma}{m}\dot{\theta} \quad (5)$$

or

$$l\ddot{\theta} + \frac{\gamma}{m}\dot{\theta} + g\theta = r\ddot{\phi} \quad (6)$$

Then the Pendulum plant transfer function is

$$G_{pendulum}(s) = \frac{\theta(s)}{\phi(s)} = \frac{rs^2}{ls^2 + \frac{\gamma}{m}s + g} = \frac{(r/l)s^2}{s^2 + (\gamma/m_l)s + (g/l)} \quad (7)$$

$$G_{pendulum}(s) = \frac{\theta(s)}{\phi(s)} = \frac{(r/l)s^2}{s^2 + (\omega_o/Q)s + \omega_o^2} \quad (8)$$

where $\omega_o = g/l$ and $Q = \omega_o(m/l\gamma)$

Now, Q will be found by direct experimental characterization of the pendulum by a process of system identification.

The value of Q = 10 applies to all discussion below.

6. Suspended Pendulum Single PID Controller: Root Locus Design

The control system design results presented here, are intended as examples. Each engineer, each student and instructor may select many different valuable design methods.

This section describes the development of a Single Input Single Output (SISO) PID Controller controlling only Pendulum Angle. This is followed by Sections that describes a Dual PID Controller architecture that combines two SISO systems. Both systems will be designed using Root Locus methods.

This design and development provides valuable background in PID control and its limitations associated with design guidance. Later Sections introduce Multiple Input Multiple Output (MIMO) Control based on the Linear Quadratic Regulator. This permits development of optimal control for parameters including a specified cost function.

The Suspended Mode feedback control system supplies an output to Rotor Control, ϕ , to control the difference between Pendulum angle, θ , and a reference tracking command, $\theta_{reference}$, as shown in Figure 10.

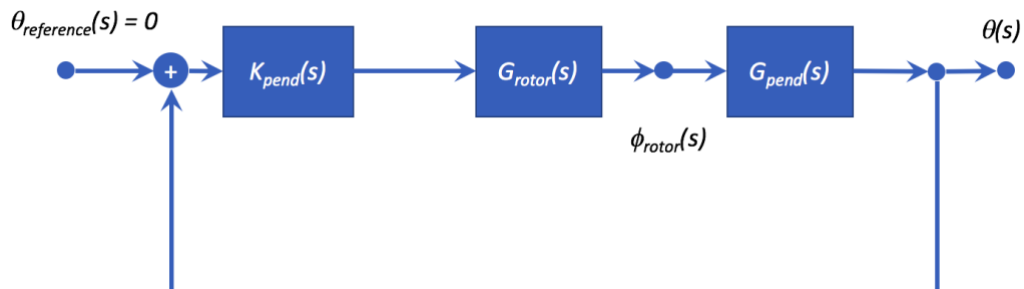


Figure 10. Pendulum Angle stabilization control system for Suspended Mode Pendulum operation.

Examining, Figure 10, the transfer function from $\theta_{reference}$ to θ is

$$\frac{\theta(s)}{\theta_{reference}(s)} = \frac{G_{rotor}(s)G_{pendulum}(s)K_{pendulum}(s)}{1 + G_{rotor}(s)G_{pendulum}(s)K_{pendulum}(s)}$$

As described in Section 4, development of the PID control system first requires development of a model for the Stepper Motor system providing Rotor control of Rotor Angle, ϕ , in response to Rotor Angle Control input, ϕ_{RC} . The Medium Speed System example of Table 2 is applied to the system in this section.

Thus, the Rotor response transfer function of Figure 10 is defined as in Equation 1,

$$G_{Rotor}(s) = \frac{\phi(s)}{\phi_{RC}(s)} = \frac{a}{s^2 + bs + c}$$

with

$$a = 0.245$$

$$b = 1.12$$

$$c = 0.49$$

First, the stability of the plant including the Pendulum and Rotor response transfer functions is evaluated. The response of the Pendulum, $G_{pendulum}$, is shown in the Bode plot of Figure 11. The resonance in its response at $\omega_o = g/l$ is observed.

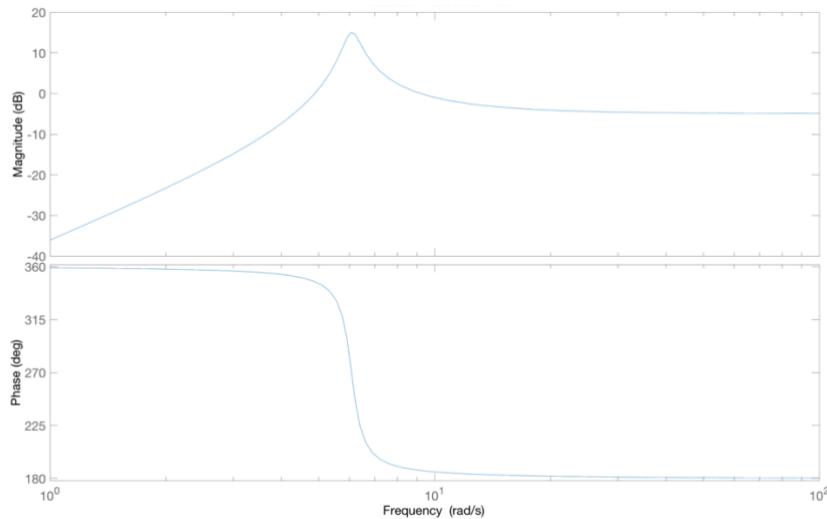


Figure 11. The Bode plot of the Pendulum transfer function between Pendulum Angle and Rotor Angle is shown. The resonance appears at $\omega_o = g/l$.

The product of the transfer functions, $G_{pendulum}$ and G_{rotor} , forms the control system plant. The Bode plot for the open loop plant, $G_{pendulum}G_{rotor}$, is shown in *Figure 12*.

The step response for this plant for an input of Rotor Angle, and an output of Pendulum Angle is shown in Figure 13. The underdamped response, is clear.

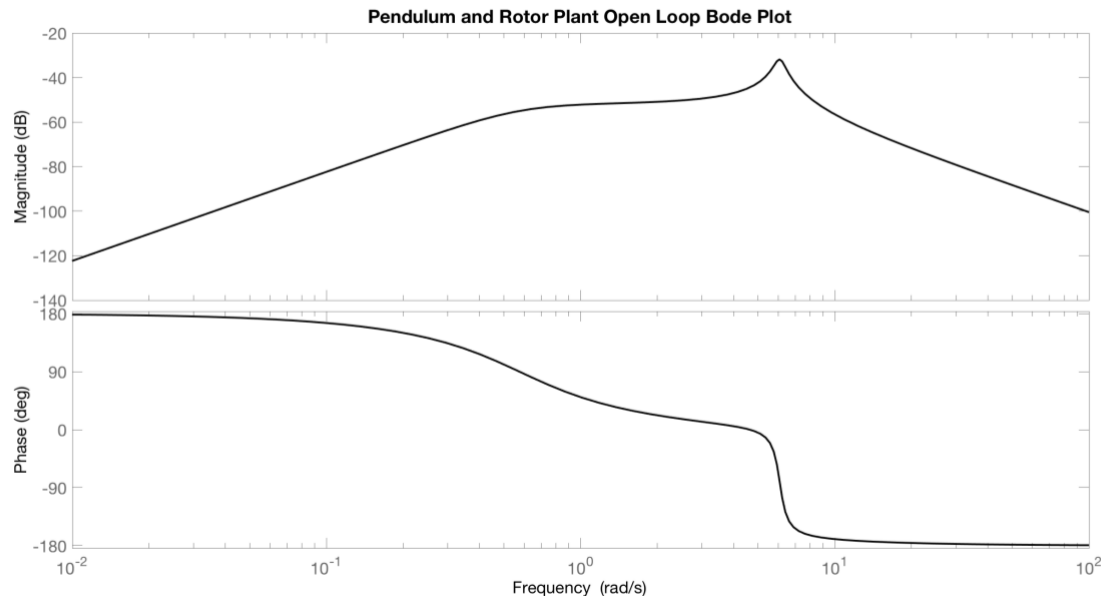


Figure 12. The Bode plot of the open loop Pendulum and Rotor Plant is shown. The resonance appears at $\omega_o = g/l$.

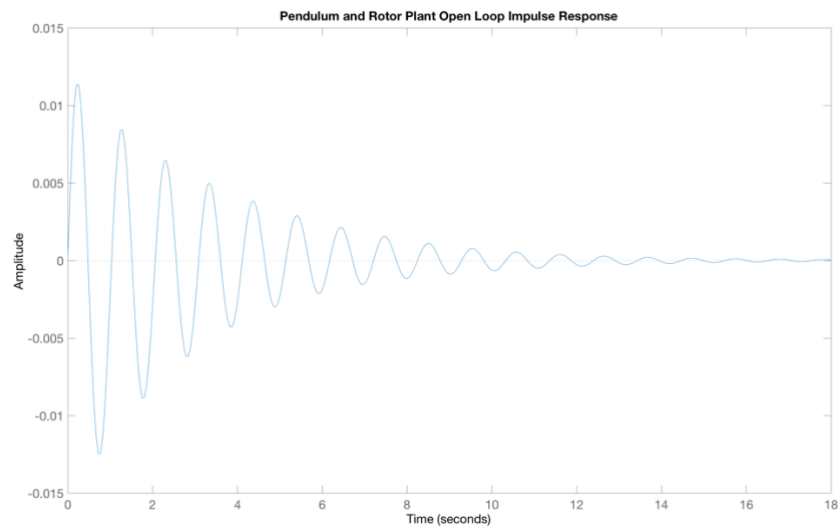


Figure 13. The step response of the open loop plant corresponding to the product of Pendulum Angle and Rotor Angle transfer functions is shown. The resonance, “ringing” behavior appears at $\omega_o = g/l$

It is clear that proportional and derivative control will be required to provide properly damped control of pendulum angle. Integral control is also added to ensure accurate settling of pendulum angle at DC.

The design of a PID controller proceeds first with selection of Integral Frequency and Derivative Frequency values. Then, system gain will be determined by Root Locus design methods for selected damping and natural frequency values.

The poles appearing for the open loop plant are

$$\begin{aligned} & -0.3264 + 6.5194i \\ & -0.3264 - 6.5194i \\ & -0.4173 + 0.4008i \\ & -0.4173 - 0.4008i \end{aligned}$$

The two zeroes appearing for the open loop plant are both at the origin.

Design of a SISO PID controller proceeds using root locus methods. The design objectives for this example will include:

- 1) A damping defined by a Maximum Overshoot, $M_p = 0.1$
- 2) A natural frequency defined by a Time to First Peak, T_p , of 0.1

First, a PID controller is selected. Second, for this controller integral and derivative time constants are selected.

Design proceeds with selection of PID controller Integral and Derivative times. An Integral Time, T_i , of 5 seconds is selected. A Derivative Time, T_d , of 0.15 seconds is selected.

These values are:

$$T_i = 5.0 \text{ sec} \text{ and } T_d = 0.15 \text{ sec}$$

This form a controller with this structure:

$$K_{pend} = K \left(1 + \frac{1}{T_i s} + T_d s \right)$$

The Bode plot for this controller, K_{pend} , the Pendulum and Rotor Plant, $G_{pendulum}G_{rotor}$, and for the open loop combined plant and controller, $K_{pend}G_{pendulum}G_{rotor}$, is shown in Figure 14 for $K = 1$.

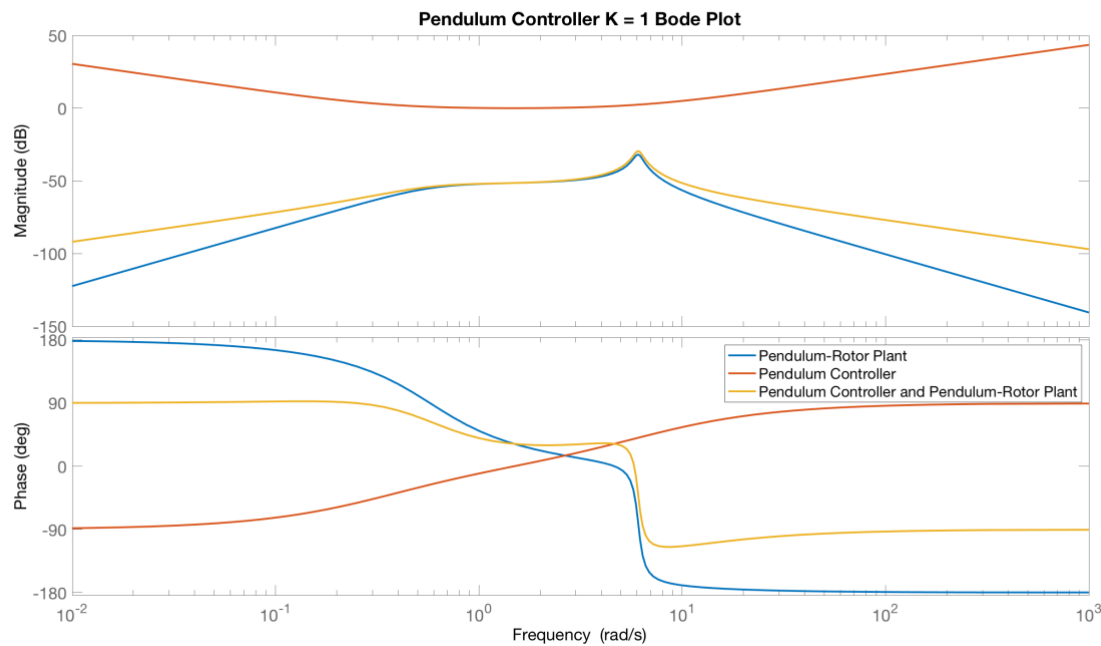


Figure 14. The Bode plot of the Pendulum and Rotor plant, Pendulum controller, and the open loop controller – plant product transfer function is shown for gain, K , of unity.

The Bode plot shows that this suspended pendulum system is stable since phase remains greater than 180 degrees.

The gain, K , may now be determined by root locus design.

The controller closed loop response will approximate a second order response and therefore the properties of second order systems can be applied to determine its Natural Frequency, ω_N , and Damping Ratio, ζ , by specifying a Maximum Overshoot, $M_p = 0.1$. [Astrom_2008]

A Damping Ratio is selected based on the criteria for a maximum overshoot. [Nise_2015]

$$\text{Damping Ratio} = \sqrt{\frac{\ln^2(M_p)}{\pi^2 + \ln^2(M_p)}}$$

This produces a Damping Ratio, ζ , of 0.59.

Then, we will select a target Time to First Peak, T_p , of 10 seconds and estimate a corresponding natural frequency. This can be estimated with [Nise_2015]

$$\omega_N = \frac{\pi}{T_p \sqrt{1 - \zeta^2}}$$

This produces a Natural Frequency, ω_N , of 0.369 rad/sec or 0.11 Hz.

A Root Locus plot for this system and with these Damping Ratio and Natural Frequency values is shown in Figure 15.

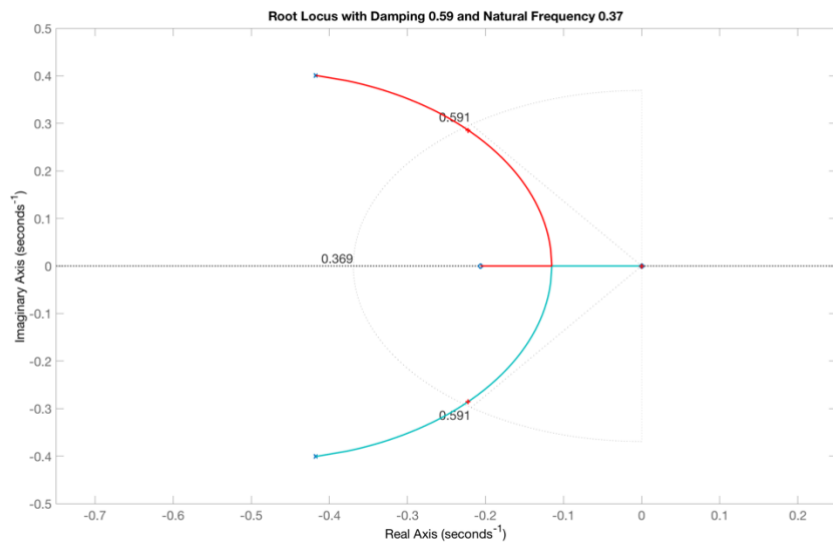


Figure 15. The Root Locus plot of the open loop control system including controller and plant product transfer function is shown. The Matlab rlocfind method has been used to select a point on where the arc of constant natural frequency intersects the root locus.

The Root Locus plot shows an arc of constant natural frequency of $\omega_N = 0.369$ rad/sec. Also, the lines emanating at the origin are lines of constant Damping Ratio such that points between these lines correspond to solutions with Damping Ratio, ζ , greater than 0.59.

Thus, using Matlab rlocfind, we select a point on the real axis at the intersection of the real axis and the arc of constant natural frequency. This point is indicated by the crosshair symbol on the negative real axis near the arc of $\omega_N = 0.369$. This yields a K value of 667.3

This yields these gain values:

$$K_p = 667.3, \quad K_i = \frac{K}{T_i} = 133.5, \quad Kd = KT_d = 100.1$$

Now, the Pendulum step response is not defined for this system since the Pendulum cannot take on a DC steady state angle other than zero. However, pendulum impulse response may be measured.

First, these gain values are applied to the experimental system. Its control algorithm is hosted on the Nucleo platform and operates as a real-time C code implementation.

This control system also includes an impulse generation method. This method acts to suspend control for a short interval, $\tau_{impulse}$. During this period, the controller does not supply an output to the rotor control system. Also, during this period, the rotor control system is deflected through a small angle, $\phi_{impulse}$. Figure 16 shows the response of the closed loop Integrated Rotary Inverted Pendulum of $\tau_{impulse} = 0.22$ seconds for $\phi_{impulse} = 5$ degrees. Control was then restored and pendulum position was measured at each control cycle of 4 milliseconds.

Figure 17 shows the simulated response for a Matlab model of this same control system and the Integrated Rotary Inverted Pendulum structure.

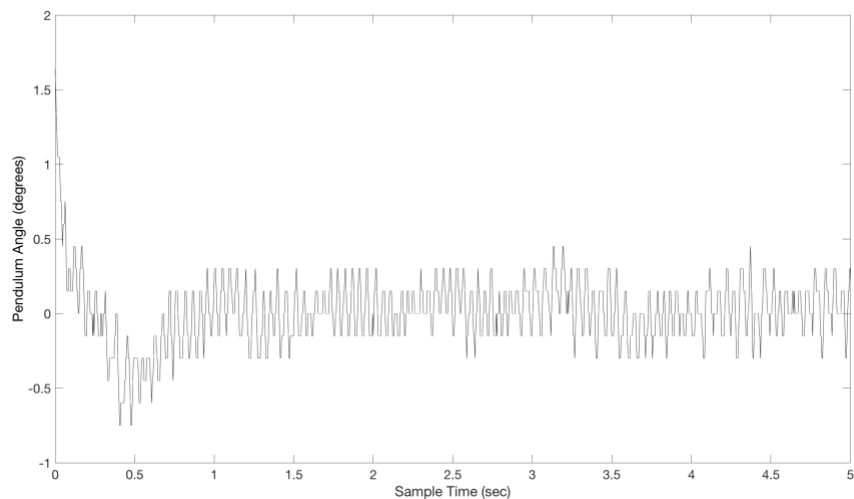


Figure 16. Impulse response of Pendulum angle for an impulse of a 5 degree step angle change in rotor angle at $t = 0$ measured with the Integrated Rotary Inverted Pendulum. Note that the individual steps in Pendulum angle due to finite encoder resolution are revealed. Each step corresponds to 0.15 degrees.

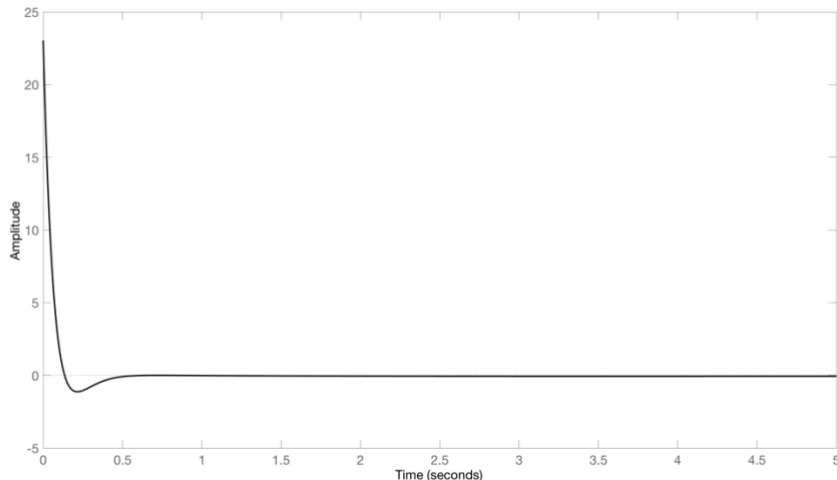


Figure 17. Impulse response of Pendulum angle for a step change in rotor angle at $t = 0$ computed by simulation of the Integrated Rotary Inverted Pendulum.

Note that the discrete steps in the output of the digital rotary encoder are visible. These introduce a switching noise that is removed by the control system low pass filter. Each step corresponds to 0.15 degrees of rotation.

An important limitation of this Single Input Single Output (SISO) controller appears. Specifically, while the controller stabilizes Pendulum Angle, Rotor Angle does not appear as an input and is not stabilized. Thus, a disturbance in Rotor position is not compensated for by this controller.

The limitations of SISO control may be characterized directly. The response of Rotor Angle, ϕ_{rotor} , to a signal applied to $\theta_{reference}$ may be computed. Examining Figure 10, the transfer function from $\theta_{reference}(s)$ to $\phi_{rotor}(s)$ is

$$T_{Rotor-Response} = \frac{\phi_{rotor}(s)}{\theta_{reference}(s)} = \frac{G_{rotor}K_{pend}}{1 + G_{pend}G_{rotor}K_{pend}}$$

The computed response of Rotor Angle, ϕ_{rotor} , to an impulse applied to Pendulum references angle, is $\theta_{reference}$, is shown in Figure 18. Pendulum angle remains near zero, as shown in Figure 17 after the impulse. However, the response of Rotor Angle shown in Figure 18 confirms that the Rotor Angle is not controlled by this SISO system.

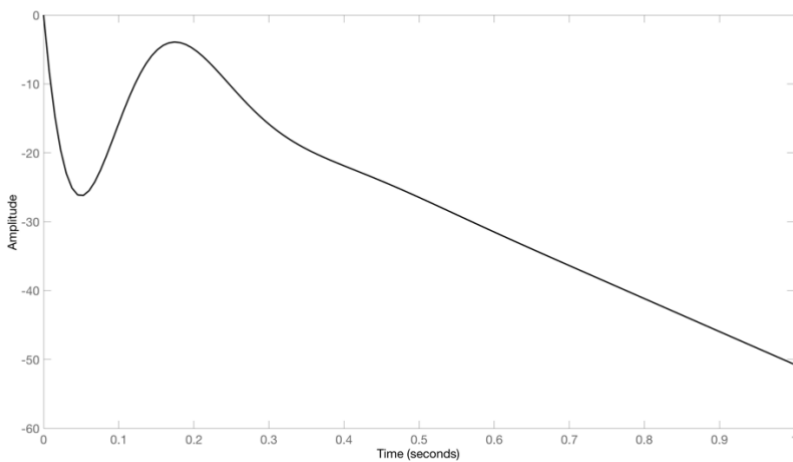


Figure 18. Response of Rotor Angle, ϕ_{rotor} , to an impulse signal applied to Pendulum angle reference, $\theta_{\text{reference}}$, at $t = 0$ computed by simulation of the Integrated Rotary Inverted Pendulum. Note the drift in Rotor Angle. During this period, Pendulum Angle remains constant and near zero.

As an experimental example, the Pendulum position for the Integrated Rotary Inverted Pendulum was disturbed, leading to a drift in Rotor position shown in Figure 19.

The next section describes the addition of a second PID controller that provides Rotor Angle stabilization relative to a tracking command.

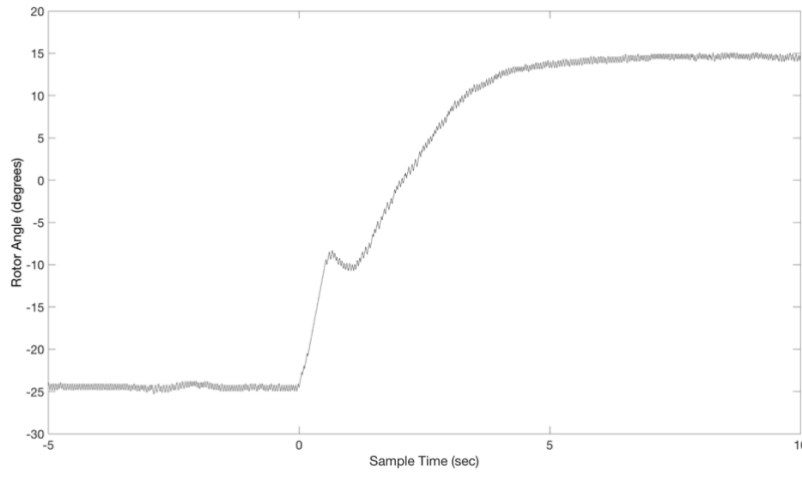


Figure 19. Response of Rotor Angle of the Integrated Rotary Inverted Pendulum as a result of a disturbance applied at $t = 0$. The drift observed is the result of the limitation of this Single Input Single Output controller that stabilizes Pendulum Angle but not Rotor Angle.

7. Suspended Pendulum Dual PID Controller: Root Locus Design

The introduction of a second PID controller may enable stabilization of Rotor Angle. This will be accomplished by introducing an Inner Loop and Outer Loop.

The design process will include the steps of:

- 1) Design of Single PID Controller, $K_{pend}(s)$
- 2) Definition of Inner Control Loop including $K_{pend}(s)$
- 3) Definition of Outer Control Loop integrating the Inner Control Loop and a new controller, $K_{rotor}(s)$
- 4) Design of the Rotor Control system, $K_{rotor}(s)$.

The Inner Loop controller will depend on the design of $K_{pend}(s)$ in section 0. This will be held constant while a new Outer Loop controller of Rotor Angle, $K_{rotor}(s)$, is added.

The Inner Loop Controller defines a transfer function from a Rotor Angle Control signal, $\phi_{rotor-control}(s)$ to the Rotor Angle, ϕ_{rotor} . The Outer Loop Controller provides control of Rotor Angle, Rotor Angle, ϕ_{rotor} to a Rotor Angle Tracking Command, $\phi_{rotor-tracking}$.

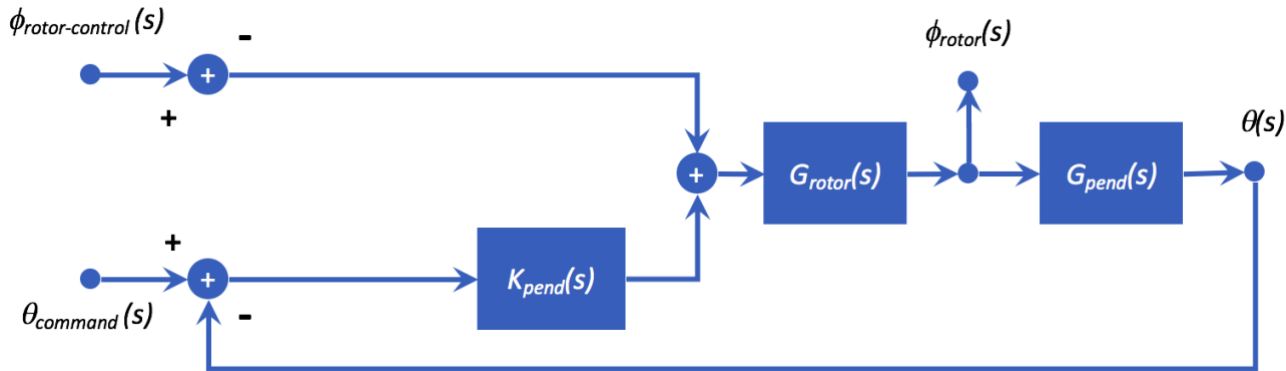


Figure 20. Dual PID Control System Inner Control Loop

The SISO Pendulum Angle control system architecture of *Figure 10* will be now modified to create an Inner Loop controller. This will be accomplished by adding a feedback signal from Rotor Angle, ϕ_{rotor} .

This Rotor Angle Control system also introduces a first order low-pass filter operating on Rotor Angle, ϕ_{rotor} . The difference between the output of this filter and the Rotor Angle tracking command,

$\phi_{rotor-control}$ is supplied as an error signal and summed with the output of the Pendulum Angle Controller, $K_{pendulum}$ as shown in the Inner Loop Controller of *Figure 20*.

Now, the Rotor Angle Control transfer function, $T_{rotor-angle}(s)$ between $\phi_{rotor-control}$ and ϕ_{rotor} will be determined. The input signal, $\theta_{command}(s)$, will be held zero.

$$\phi_{rotor}(s) = (\phi_{rotor-control}(s) - \phi_{rotor}(s)G_{pendulum}(s)K_{pendulum}) G_{rotor}(s)$$

$$T_{rotor-angle}(s) = \frac{\phi_{rotor}(s)}{\phi_{rotor-command}(s)}$$

and

$$T_{rotor-angle}(s) = \frac{G_{rotor}(s)}{1 + G_{pend}(s)K_{pend}(s) G_{rotor}(s)}$$

This Rotor Angle Control system now introduces the Outer Loop controller to enable control of Rotor Angle. Here, the difference between a Rotor Angle tracking command, $\phi_{rotor-tracking}(s)$ and Rotor Angle, $\phi_{rotor}(s)$, is supplied as an error signal to a new controller, K_{rotor} , and summed with the output of the Pendulum Angle Controller, $K_{pendulum}$ as shown in

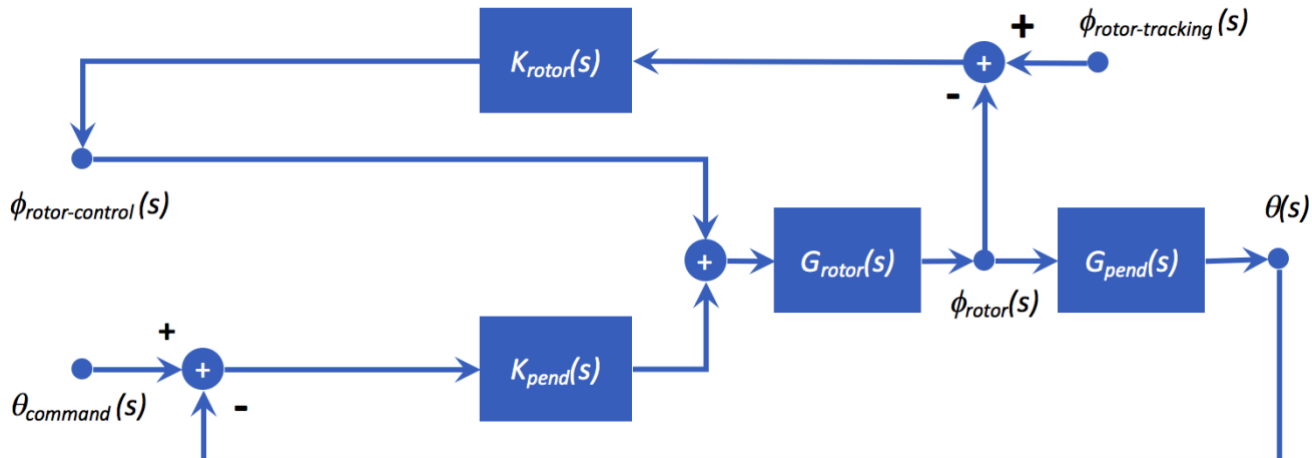


Figure 21.

During subsequent design steps, the configuration of $K_{pendulum}(s)$ will remain fixed.

The Outer Loop controls ϕ_{rotor} with the goal of tracking the input, $\phi_{rotor-tracking}$.

By definition

$$\phi_{rotor} = \phi_{rotor-command}(s)T_{rotor-angle}(s)$$

Thus, the transfer function from $\phi_{rotor-tracking}$ to ϕ_{rotor} is

$$T_{rotor-tracking}(s) = \frac{\phi_{rotor}(s)}{\phi_{rotor-tracking}(s)} = \frac{1}{1 + T_{rotor-angle}(s)K_{rotor}(s)}$$

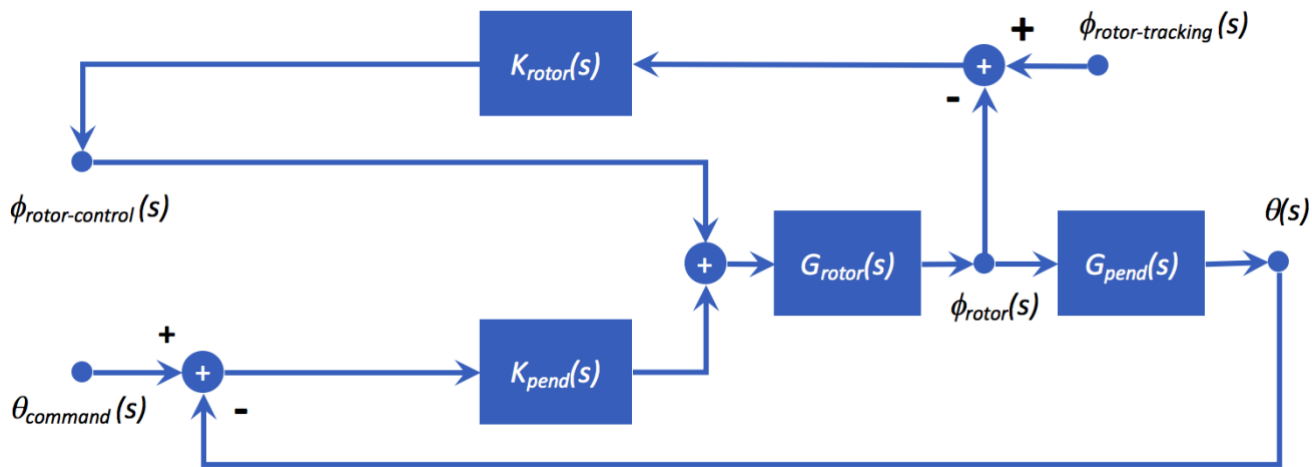


Figure 21. Dual PID Control System Inner and Outer Control Loop

Design of K_{rotor} begins with selection of integral time constant, T_{i-r} , and derivative time constant, T_{d-r} . This is followed by selection of controller gain, K . The form of this controller is:

$$K_{rotor}(s) = K \left(1 + \frac{1}{T_{i-r}s} + T_{d-r}s \right)$$

The selection of optimal values for T_{i-r} , T_{d-r} and K , can also include selection of values for T_i , T_d and K for the Pendulum Angle control PID loop.

To review the characteristics of the Single PID Inverted Mode Pendulum controller of section 0, the closed loop poles, zeroes of $1 + G_{rotor}G_{pend}K_{pend}(s)$ were determined to be:

$$\begin{aligned}
 & 0.0000 + 0.0000i \\
 & -17.0222 + 0.0000i \\
 & -7.7119 + 11.5106i \\
 & -7.7119 - 11.5106i \\
 & -0.2251 + 0.2890i \\
 & -0.2251 - 0.2890i
 \end{aligned}$$

Thus, the integral time constant, T_{i-r} , is then set at the value of 5 seconds. The derivative time constant, T_{d-r} , is set at 1.5 second. The selected values are.

$$T_{i-r} = 5.0s$$

$$T_{d-r} = 1.5s$$

The controller closed loop response will approximate a second order response and therefore the properties of second order systems can be applied to determine its Natural Frequency, ω_N , and Damping Ratio, ζ , by specifying a Maximum Overshoot, $M_p = 0.1$. [Astrom_2008]

A Damping Ratio is selected based on the criteria for a maximum overshoot. [Nise_2015]

$$\text{Damping Ratio} = \sqrt{\frac{\ln^2(M_p)}{\pi^2 + \ln^2(M_p)}}$$

This produces a Damping Ratio, ζ , of 0.59.

Then, we will select a target Time to First Peak, T_p , of 5.0 seconds and estimate a corresponding natural frequency. This can be estimated with [Nise_2015]

$$\omega_N = \frac{\pi}{T_p \sqrt{1 - \zeta^2}}$$

This produces a Natural Frequency, ω_N , of 0.74 rad/sec.

Thus, using Matlab rlocfind as shown in *Figure 22*, we select a point on the real axis at the intersection of the real axis and the arc of constant natural frequency. This point is indicated by the crosshair symbol on the negative real axis near the arc of $\omega_N = 0.37$.

This yields a value of gain of $K = 11.8$ Using this gain scale factor value, the PID controller becomes

$$K_{rotor}(s) = K_{p-rotor} + \frac{K_{i-rotor}}{s} + K_{d-rotor}s$$

with

$$K_{p-rotor} = 11.8, \quad K_{i-rotor} = K/T_{i-r} = 2.4, \quad K_{d-rotor} = KT_{d-r} = 17.6$$

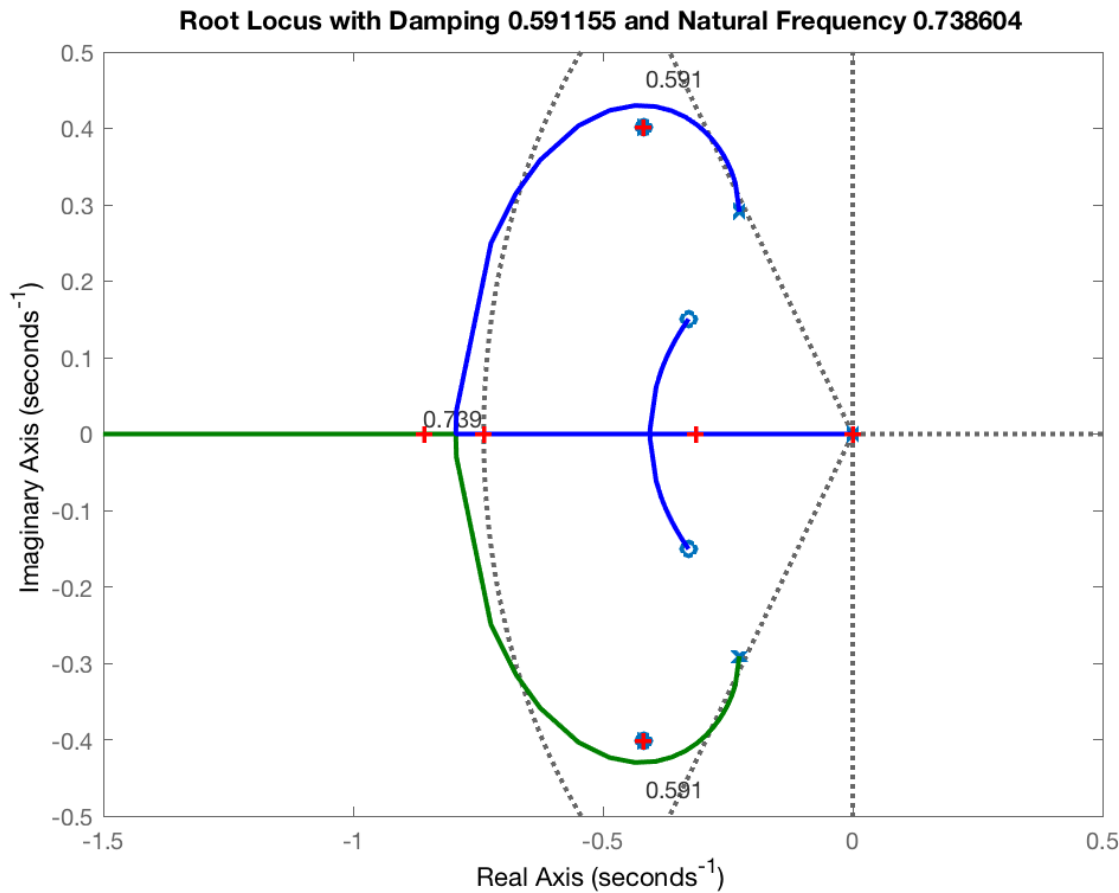


Figure 22. The Root Locus plot of the open loop control system including controller and plant product transfer function is shown. The Matlab rlocfind method has been used to select a point where the arc of constant natural frequency intersects the negative real axis.

Simulated system response to a step input to $\phi_{rotor-command}$, shown in Figure 23 displays stable operation.

Experimentally measured system response to a step input to $\phi_{rotor-command}$, shown in Figure 24, also displays stable operation with a Maximum Overshoot and Time to First Peak value similar to that of the simulated response.

Finally, experimentally measured system response of Pendulum Angle to a step input to $\phi_{rotor-command}$, shown in Figure 25, also displays stable operation

Further development of Dual PID design may continue. However, the challenge for optimizing this MIMO system are clear. Later sections introduce Modern Control methods that enable direct

optimization of controller design for this system. This produces a dramatic performance advance in overshoot and response time characteristics.

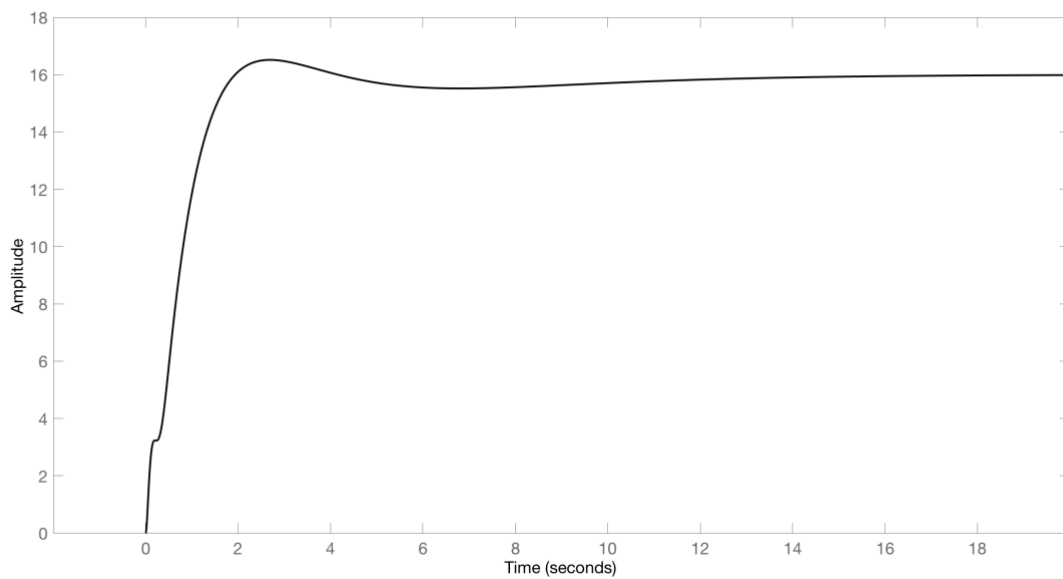


Figure 23. Simulated Rotor Angle response of the Dual PID Control System response for a step input of amplitude 16 degrees to the Rotor Angle command input applied at $t = 0$.

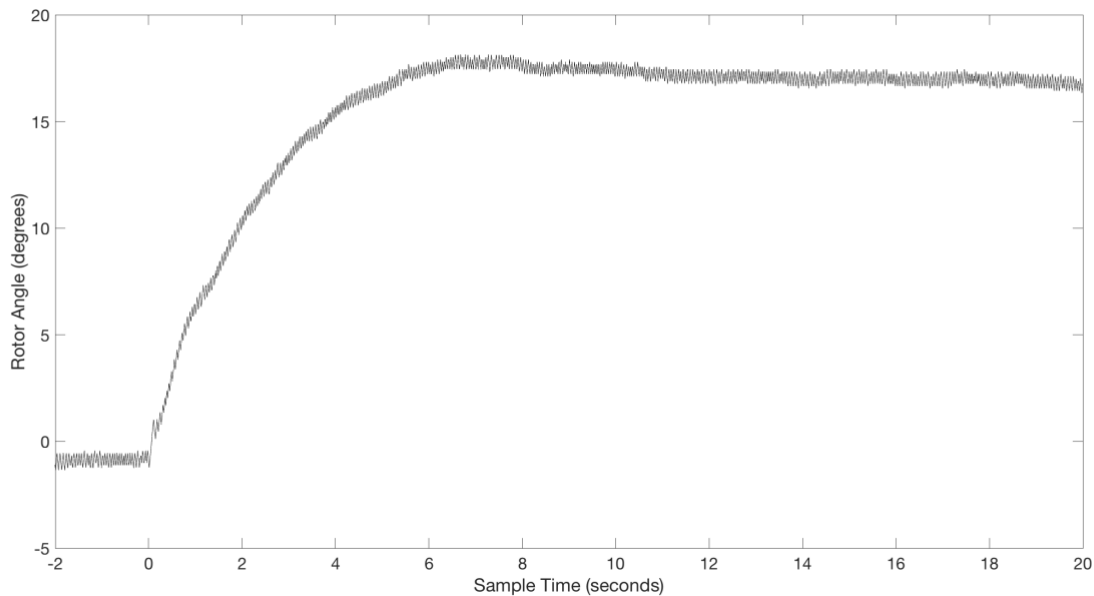


Figure 24. Experimental measurement of Rotor Angle response of the Dual PID Control System response for a step input of amplitude 16 degrees to the Rotor Angle command input applied at $t = 0$.

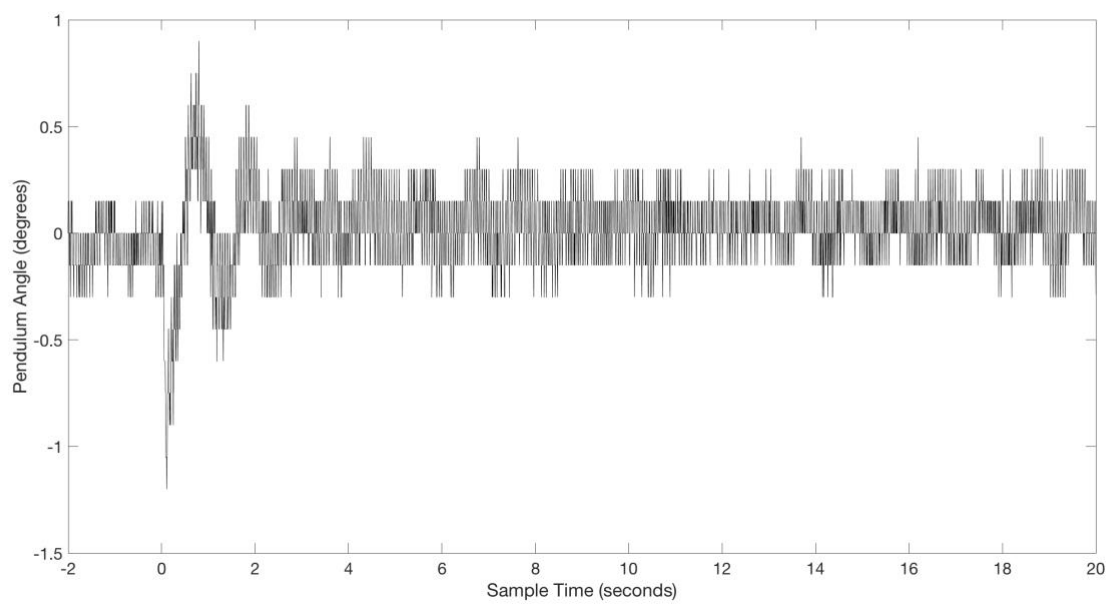


Figure 25. Experimental measurement of Pendulum Angle response of the Dual PID Control System response for a step input of amplitude 16 degrees to the Rotor Angle command input applied at $t = 0$. The discrete values associated with Pendulum Angle measurement resolution (0.16 degrees) are observed.

8. Suspended Pendulum Single PID Controller: Frequency Response Design

This section also describes the development of a Single Input Single Output (SISO) PID Controller controlling only Pendulum Angle. This is followed by Sections that describes a Dual PID Controller architecture that combines two SISO systems. Both systems will be designed using Frequency Response methods in contrast to the previous sections relying on Root Locus design methods.

This design and development provides valuable background in PID control and its limitations associated with design guidance. Later Sections introduce Multiple Input Multiple Output (MIMO) Control based on the Linear Quadratic Regulator. This permits development of optimal control for parameters including a specified cost function.

The Suspended Mode feedback control system supplies an output to Rotor Control, ϕ , to control the difference between Pendulum angle, θ , and a reference tracking command, $\theta_{reference}$, as shown in *Figure 26*.

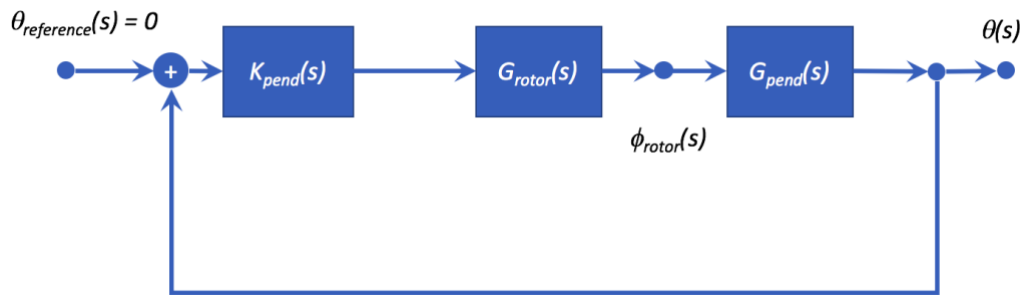


Figure 26. Pendulum Angle stabilization control system for Suspended Mode Pendulum operation.

Examining, *Figure 26*, the transfer function from $\theta_{reference}$ to θ is

$$\frac{\theta(s)}{\theta_{reference}(s)} = \frac{G_{rotor}(s)G_{pendulum}(s)K_{pendulum}(s)}{1 + G_{rotor}(s)G_{pendulum}(s)K_{pendulum}(s)}$$

As described in Section 4, development of the PID control system first requires development of a model for the Stepper Motor system providing Rotor control of Rotor Angle, ϕ , in response to Rotor Angle Control input, ϕ_{RC} . The Medium Speed System example of Table 2 is applied to the system in this section.

Thus, the Rotor response transfer function of *Figure 26* is defined as in Equation 1,

$$G_{Rotor}(s) = \frac{\phi(s)}{\phi_{RC}(s)} = \frac{a}{s^2 + bs + c}$$

with

$$\begin{aligned}a &= 0.245 \\b &= 1.12 \\c &= 0.49\end{aligned}$$

First, the stability of the plant including the Pendulum and Rotor response transfer functions is evaluated. The response of the Pendulum, $G_{pendulum}$, is shown in the Bode plot of *Figure 27*. The resonance in its response at $\omega_o = g/l$ is observed.

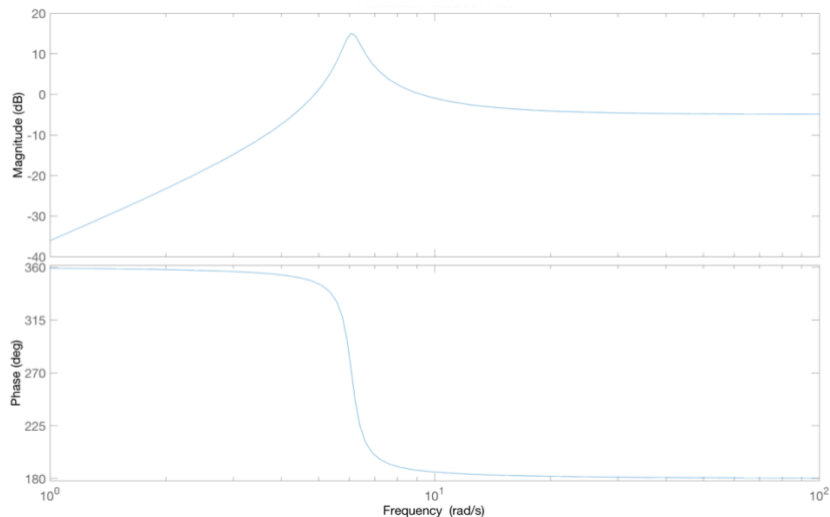


Figure 27. The Bode plot of the Pendulum transfer function between Pendulum Angle and Rotor Angle is shown. The resonance appears at $\omega_o = g/l$.

The product of the transfer functions, $G_{pendulum}$ and G_{rotor} , forms the control system plant. The Bode plot for the open loop plant, $G_{pendulum}G_{rotor}$, is shown in *Figure 28*.

The step response for this plant for an input of Rotor Angle, and an output of Pendulum Angle is shown in *Figure 29*. The underdamped response, is clear.

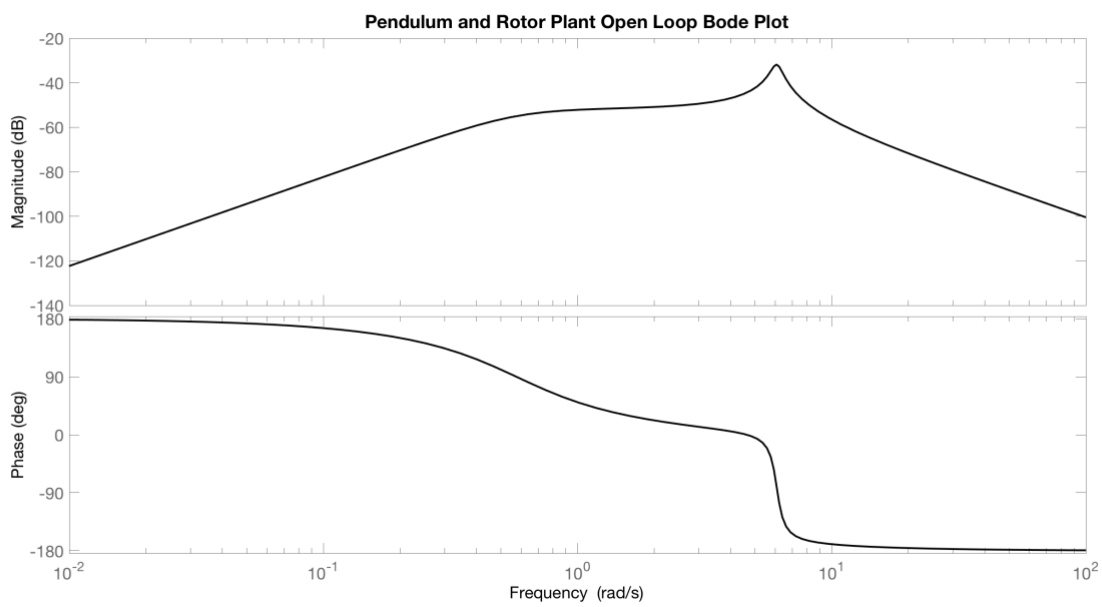


Figure 28. The Bode plot of the open loop Pendulum and Rotor Plant is shown. The resonance appears at $\omega_o = g/l$.

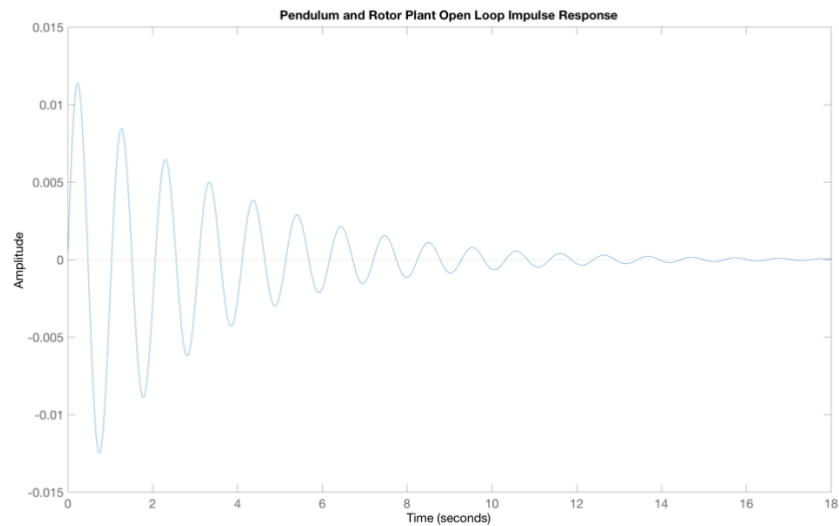


Figure 29. The step response of the open loop plant corresponding to the product of Pendulum Angle and Rotor Angle transfer functions is shown. The resonance, “ringing” behavior appears at $\omega_o = g/l$.

It is clear that proportional and derivative control will be required to provide properly damped control of pendulum angle. Integral control is also added to ensure accurate settling of pendulum angle at DC.

The design of a PID controller proceeds first with selection of Integral Frequency and Derivative Frequency values. Then, system gain will be determined by Frequency Response design methods subject to stability and performance constraints.

The poles appearing for the open loop plant are

$$\begin{aligned} &-0.3229 + 6.4496i \\ &-0.3229 - 6.4496i \\ &-0.5600 + 0.4200i \\ &-0.5600 - 0.4200i \end{aligned}$$

The two zeroes appearing for the open loop plant are both at the origin.

Design of a SISO PID controller proceeds using frequency response methods. The design objectives for this example will include:

- 1) Phase margin is greater than 30 degrees [Seborg_1989]

An additional constraint is to meet maximum bandwidth requirements. The Integrated Rotary Inverted Pendulum includes a first order low pass filter in its computation of derivative. This well-known method is required to reduce the influence of noise in this computation.[Astrom_2008] The Integrated Rotary Inverted Pendulum may be adjusted. However, its default value is 5 Hz or 31.4 rad/sec. This means that the maximum bandwidth for the controller should also be set to a fraction of this value, or approximately 15 rad/sec. This finally leads to one more requirement on the Phase Cross-Over Frequency (the frequency where phase crosses -180 degrees).

- 2) Phase Cross-Over Frequency is less than 15 rad/sec.

Subsequent to design, stability for this example will be determined by examination of both Bode and Nyquist characteristics.

Design proceeds with selection of PID controller Integral and Derivative times. An Integral Time, T_i , of 5 seconds is selected. A Derivative Time, T_d , of 0.15 seconds is selected.

These values are:

$$T_i = 5.0 \text{ sec} \text{ and } T_d = 0.15 \text{ sec}$$

The form of this PID controller is then,

$$K_{pend}(s) = K \left(1 + \frac{1}{T_i s} + T_d s \right)$$

where K will be found via Frequency Response design methods.

The open loop system is

$$G_{open-loop} = G_{rotor}G_{pend}K_{pend}(s)$$

The Bode plot for this controller, K_{pend} , the Pendulum and Rotor Plant, $G_{pendulum}G_{rotor}$, and for the open loop combined plant and controller, $K_{pend}G_{pendulum}G_{rotor}$, is shown in *Figure 30* for $K = 1$.

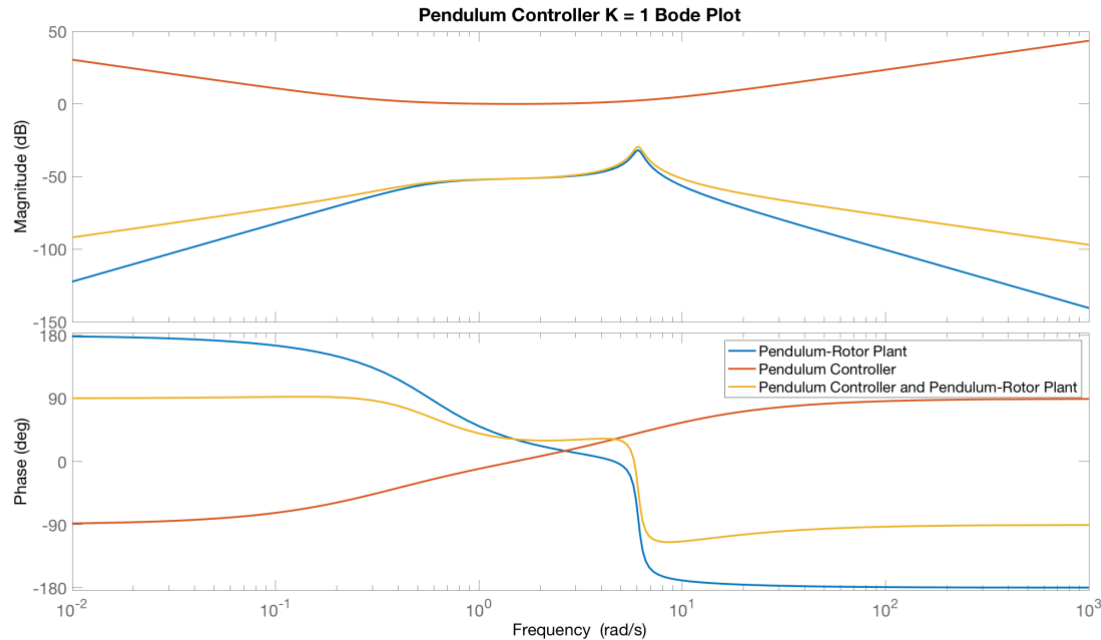


Figure 30. The Bode plot of the Pendulum and Rotor plant, Pendulum controller, and the open loop controller – plant product transfer function is shown for gain, K , of unity.

Figure 31 displays the Bode plot for $K = 1$ with Gain and Phase margins. These are clearly excessive and will result in slow system response.

Figure 32 displays the Bode plot for $K = 500$ with Gain and Phase margins. The Phase margin is greater than the design objective and the Phase Cross Over Frequency is less than the objective.

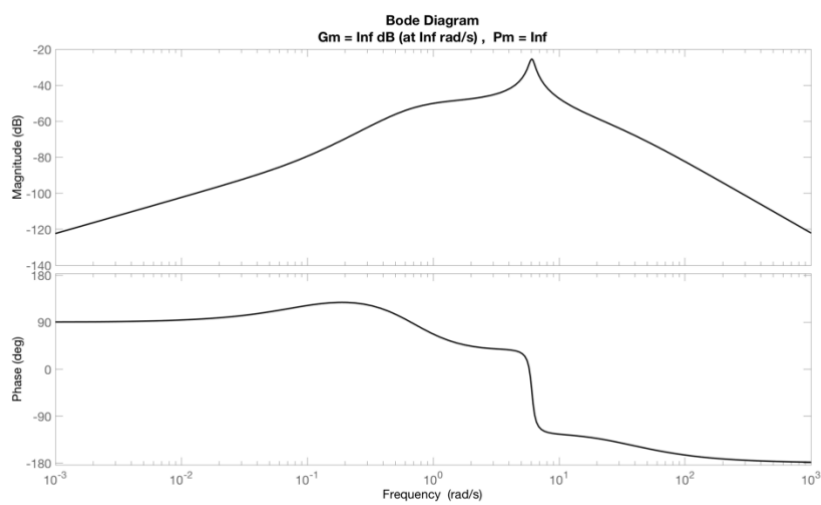


Figure 31. The Bode plot of $G_{open-loop}$ with gain and phase margin is shown for gain, K , of unity.

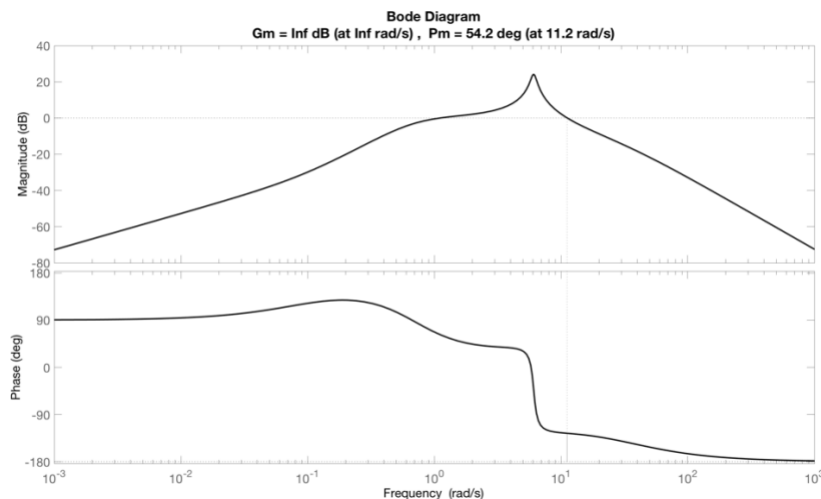


Figure 32. The Bode plot of $G_{open-loop}$ with gain and phase margin is shown for gain, K , of 500.

Finally, as another example, Figure 33 displays the Bode plot for $K = 1000$ with Gain and Phase margins. The Phase margin is greater than the design objective and the Phase Cross Over Frequency is less than the objective.

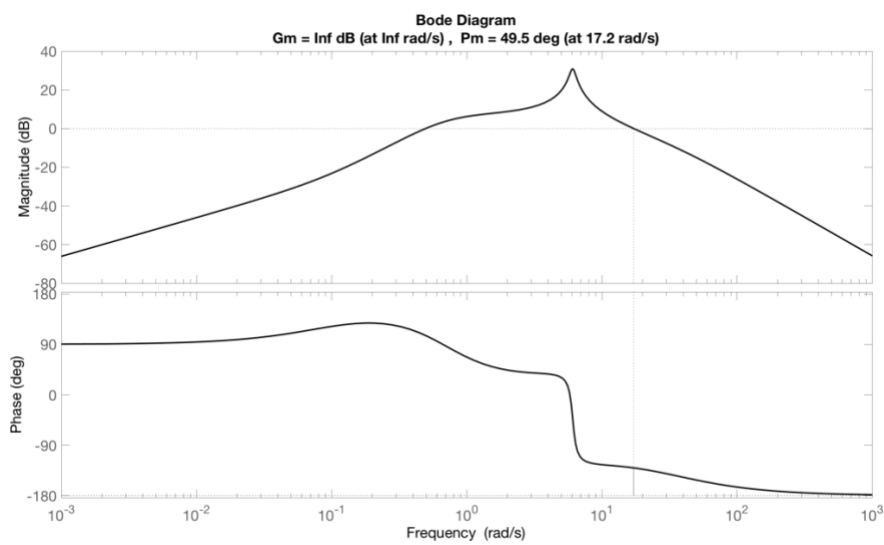


Figure 33. The Bode plot of $G_{\text{open-loop}}$ with gain and phase margin is shown for gain, K , of 650.

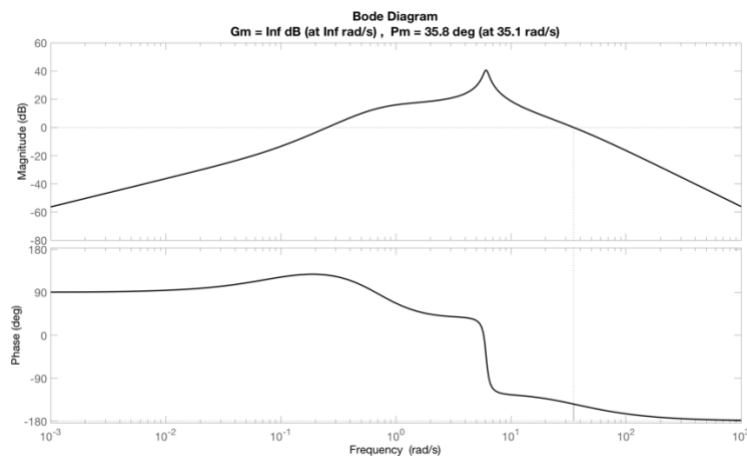


Figure 34. The Bode plot of $G_{\text{open-loop}}$ with gain and phase margin is shown for gain, K , of 2000.

Figure 34 displays the Bode plot for $K = 2000$ with Gain and Phase margins. The Phase margin is less than the design objective and the Phase Cross Over Frequency is greater than the design objective.

Each gain configuration meets the stability requirements evaluated by analysis of Gain and Phase Margins.

The Nyquist Criterion may also be tested for indication of stability. First, for $K = 1000$, the poles of the closed loop system, zeroes of $1 + G_{rotor}G_{pend}K_{pend}(s)$ are

$$\begin{aligned} & 0.0000 + 0.0000i \\ & -11.1389 + 16.3738i \\ & -11.1389 - 16.3738i \\ & -10.4152 + 0.0000i \\ & -0.2443 + 0.3122i \\ & -0.2443 - 0.3122i \end{aligned}$$

Then, the poles of $G_{rotor}G_{pend}K_{pend}(s)$ are

$$\begin{aligned} & 0.0000 + 0.0000i \\ & -31.4159 + 0.0000i \\ & -0.3229 + 6.4496i \\ & -0.3229 - 6.4496i \\ & -0.5600 + 0.4200i \\ & -0.5600 - 0.4200i \end{aligned}$$

There are no RHP poles, confirming stability. The number of zeroes of $1 + G_{rotor}G_{pend}K_{pend}(s)$ in the right half plane, $Z = 1$. Also, the number of poles, of $G_{rotor}G_{pend}K_{pend}(s)$ in the right half plane, $P = 1$. Then, the number of clockwise encirclements of the point, $s = -1$, is zero.

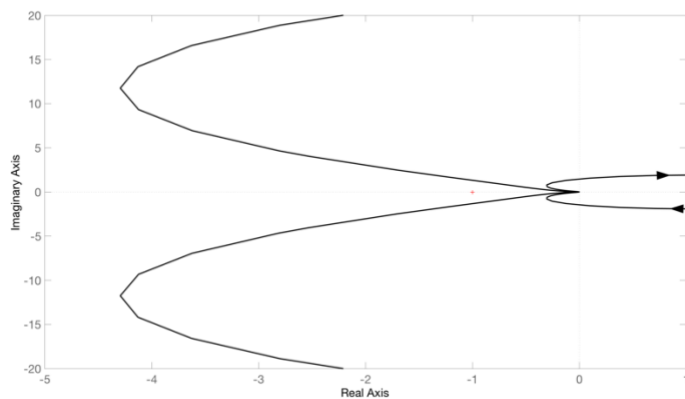


Figure 35. The Nyquist plot of $G_{open-loop}$ for gain, K , of 650.

Figure 35 displays the Nyquist plot for $K = 650$. This behavior is consistent with stability since no encirclement of the $s = -1$ point occur.

Control system design must also consider the selection of parameters that reduce sensitivity of the control system to variation in plant characteristics as well as to noise present in a control system. [Astrom_2008]

The next step in design is the selection of the gain K. This will be subject to the following objectives:

- 1) The Nyquist Criterion will be met for the plant.
- 2) The Bode characteristic of the plant displays a Phase Margin greater than 30 degrees.
- 3) The maximum values of both the Sensitivity Function and Complimentary Sensitivity Function will be minimized.
- 4) The maximum value of the Noise Sensitivity Function will also be minimized.

The latter requirement relies on the Sensitivity Function defined as

$$S(s) = \frac{1}{1 + T_{rotor-angle}(s)K_{rotor}(s)}$$

$$T(s) = \frac{T_{rotor-angle}(s)K_{rotor}(s)}{1 + T_{rotor-angle}(s)K_{rotor}(s)}$$

The maximum value for the range of $s = 0$ to $s = \infty$ will be computed for each with

$$M_S = \max_{0 \leq \omega < \infty} |S(j\omega)|$$

and

$$M_T = \max_{0 \leq \omega < \infty} |T(j\omega)|$$

These values measure the robustness of the control system to variations in plant characteristics.

The third important metric is the Noise Sensitivity function that determines the susceptibility of the control system to errors introduced by measurement noise.

The Noise Sensitivity Function is

$$NS(s) = \frac{K_{rotor}(s)}{1 + T_{rotor-angle}(s)K_{rotor}(s)}$$

The maximum value for the range of $s = 0$ to $s = \infty$ will be computed with

$$M_{NS} = \max_{0 \leq \omega < \infty} |NS(j\omega)|$$

The dependence of M_S , M_T , and M_{NS} on selection of Gain K will can be evaluated. The values of each is listed below in Table 6 along with the values of Phase Margin, and Phase Cross Over

Frequency.

Gain	M_s	M_T	M_{NS}	Phase Margin (degrees)	Phase Cross Over Frequency (rad/sec)
500	1.37	1.23	10013.4	51.2	14.3
650	1.43	1.26	13018.0	49	17.9
2000	1.89	1.67	40061.5	35	36.3

Table 6. Values of M_s , M_T , and M_{NS} Phase Margin, and Phase Cross Over Frequency for selections of Gain, K.

The value of K = 500 produces a low Cross Over Frequency and therefore reduced bandwidth. The value of K = 2000 produces enhanced bandwidth, but also large sensitivity to noise. The increase in values of M_s and M_T also indicate an undesired greater sensitivity to variation in plant characteristics.

The value of K = 650 is selected for the next step in design. However, it is important to note that this gain value may be adjusted and corresponding change in system characteristics may be characterized with the Integrated Rotary Inverted Pendulum physical system.

This yields these gain values:

$$K_p = 650.0, \quad K_i = K/T_i = 65.0, \quad Kd = KT_d = 97.5$$

Now, the Pendulum step response is not defined for this system since the Pendulum cannot take on a DC steady state angle other than zero. However, pendulum impulse response may be measured.

First, these gain values are applied to the experimental system. Its control algorithm is hosted on the Nucleo platform and operates as a real-time C code implementation.

This control system also includes an impulse generation method. This method acts to suspend control for a short interval, $\tau_{impulse}$. During this period, the controller does not supply an output to the rotor control system. Also, during this period, the rotor control system is deflected through a small angle, $\phi_{impulse}$. Figure 16 shows the response of the closed loop Integrated Rotary Inverted Pendulum of $\tau_{impulse} = 0.22$ seconds for $\phi_{impulse} = 5$ degrees. Control was then restored and pendulum position was measured at each control cycle of 4 milliseconds.

Figure 17 shows the simulated response for a Matlab model of this same control system and the Integrated Rotary Inverted Pendulum structure.

Note that the discrete steps in the output of the digital rotary encoder are visible. These introduce a switching noise that is removed by the control system low pass filter. Each step corresponds to 0.15 degrees of rotation.

An important limitation of this Single Input Single Output (SISO) controller appears. Specifically, while the controller stabilizes Pendulum Angle, Rotor Angle does not appear as an input and is not stabilized. Thus, a disturbance in Rotor position is not compensated for by this controller.

The limitations of SISO control may be characterized directly. The response of Rotor Angle, ϕ_{rotor} , to a signal applied to $\theta_{reference}$ may be computed. Examining Figure 10, the transfer function from $\theta_{reference}(s)$ to $\phi_{rotor}(s)$ is

$$T_{Rotor-Response} = \frac{\phi_{rotor}(s)}{\theta_{reference}(s)} = \frac{G_{rotor}K_{pend}}{1 + G_{pend}G_{rotor}K_{pend}}$$

The computed response of Rotor Angle, ϕ_{rotor} , to an impulse applied to Pendulum references angle, is $\theta_{reference}$, is shown in *Figure 36*. Pendulum angle remains near zero, as shown in *Figure 36* after the impulse. However, the response of Rotor Angle shown in *Figure 38* confirms that the Rotor Angle is not controlled by this SISO system.

As an experimental example, the Pendulum position for the Integrated Rotary Inverted Pendulum was disturbed, leading to a drift in Rotor position shown in *Figure 38*.

The next section describes the addition of a second PID controller that provides Rotor Angle stabilization relative to a tracking command.

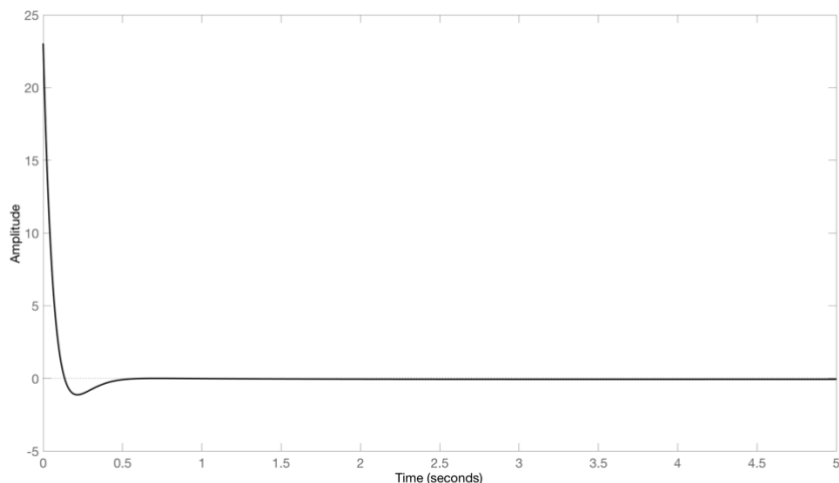


Figure 36. Impulse response of Pendulum angle for a step change in rotor angle at t = 0 computed by simulation of the Integrated Rotary Inverted Pendulum.

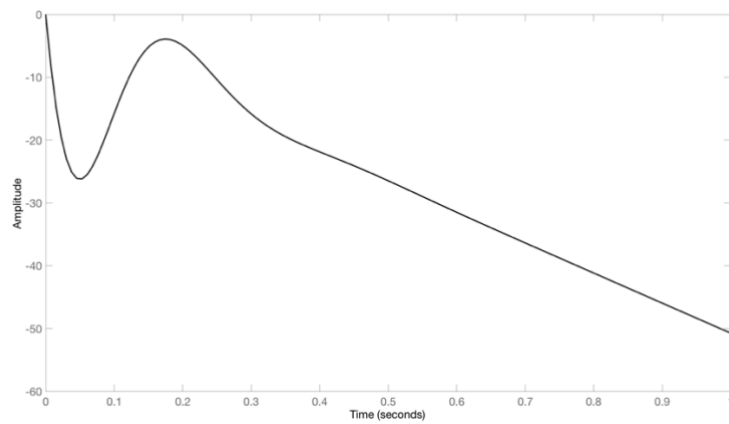


Figure 37. Response of Rotor Angle, ϕ_{rotor} , to an impulse signal applied to Pendulum angle reference, $\theta_{\text{reference}}$, at $t = 0$ computed by simulation of the Integrated Rotary Inverted Pendulum. Note the drift in Rotor Angle. During this period, Pendulum Angle remains constant and near zero.

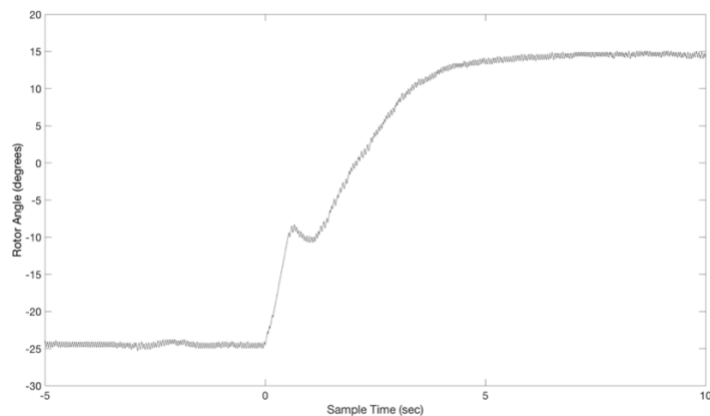


Figure 38. Response of Rotor Angle of the Integrated Rotary Inverted Pendulum as a result of a disturbance applied at $t = 0$. The drift observed is the result of the limitation of this Single Input Single Output controller that stabilizes Pendulum Angle but not Rotor Angle.

9. Suspended Pendulum Dual PID Controller: Frequency Response Design

The introduction of a second PID controller may enable stabilization of Rotor Angle. This will be accomplished by introducing an Inner Loop and Outer Loop.

The design process will include the steps of:

- 1) Design of Single PID Controller, $K_{pend}(s)$
- 2) Definition of Inner Control Loop including $K_{pend}(s)$
- 3) Definition of Outer Control Loop integrating the Inner Control Loop and a new controller, $K_{rotor}(s)$
- 4) Design of the Rotor Control system, $K_{rotor}(s)$.

The Inner Loop controller will depend on the design of $K_{pend}(s)$ in section 0. This will be held constant while a new Outer Loop controller of Rotor Angle, $K_{rotor}(s)$, is added.

The Inner Loop Controller defines a transfer function from a Rotor Angle Control signal, $\phi_{rotor-control}$ to the Rotor Angle, ϕ_{rotor} . The Outer Loop Controller provides control of Rotor Angle, Rotor Angle, ϕ_{rotor} to a Rotor Angle Tracking Command, $\phi_{rotor-tracking}$.

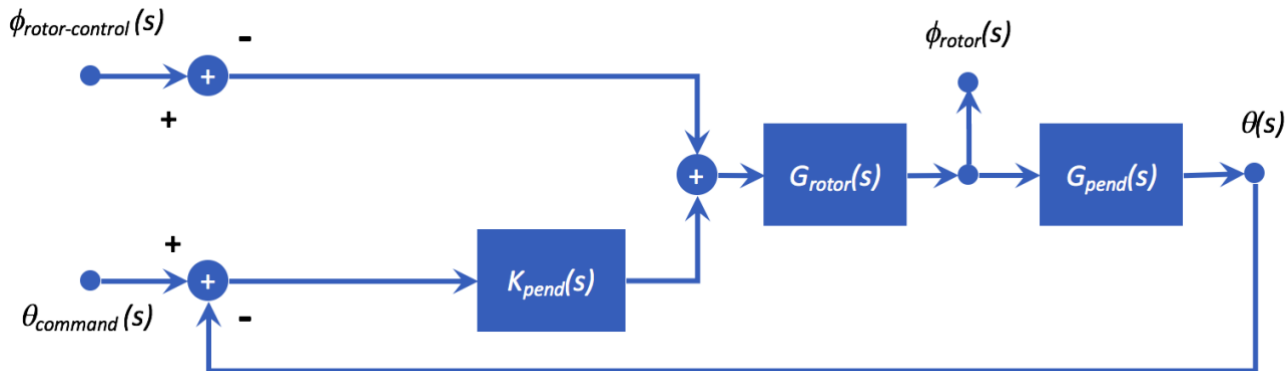


Figure 39. Dual PID Control System Inner Control Loop

The SISO Pendulum Angle control system architecture of *Figure 10* will be now modified to create an Inner Loop controller. This will be accomplished by adding a feedback signal from Rotor Angle, ϕ_{rotor} .

This Rotor Angle Control system also introduces a first order low-pass filter operating on Rotor Angle, ϕ_{rotor} . The difference between the output of this filter and the Rotor Angle tracking command, $\phi_{rotor-control}$ is supplied as an error signal and summed with the output of the Pendulum Angle Controller, $K_{pendulum}$ as shown in the Inner Loop Controller of *Figure 39*.

Now, the Rotor Angle Control transfer function, $T_{rotor-angle}(s)$ between $\phi_{rotor-control}$ and ϕ_{rotor} will be determined. The input signal, $\theta_{command}(s)$, will be held zero.

$$\phi_{rotor}(s) = (\phi_{rotor-control}(s) - \phi_{rotor}(s)G_{pendulum}(s)K_{pendulum}) G_{rotor}(s)$$

$$T_{rotor-angle}(s) = \frac{\phi_{rotor}(s)}{\phi_{rotor-command}(s)}$$

and

$$T_{rotor-angle}(s) = \frac{G_{rotor}(s)}{1 + G_{pend}(s)K_{pend}(s) G_{rotor}(s)}$$

This Rotor Angle Control system now introduces the Outer Loop controller to enable control of Rotor Angle. Here, the difference between a Rotor Angle tracking command, $\phi_{rotor-tracking}(s)$ and Rotor Angle, $\phi_{rotor}(s)$, is supplied as an error signal to a new controller, K_{rotor} , and summed with the output of the Pendulum Angle Controller, $K_{pendulum}$ as shown in *Figure 40*.

During subsequent design steps, the configuration of $K_{pend}(s)$ will remain fixed.

The Outer Loop controls ϕ_{rotor} with the goal of tracking the input, $\phi_{rotor-tracking}$.

By definition

$$\phi_{rotor} = \phi_{rotor-command}(s)T_{rotor-angle}(s)$$

Thus, the transfer function from $\phi_{rotor-tracking}$ to ϕ_{rotor} is

$$T_{rotor-tracking}(s) = \frac{\phi_{rotor}(s)}{\phi_{rotor-command}(s)} = \frac{1}{1 + T_{rotor-angle}(s)K_{rotor}(s)}$$

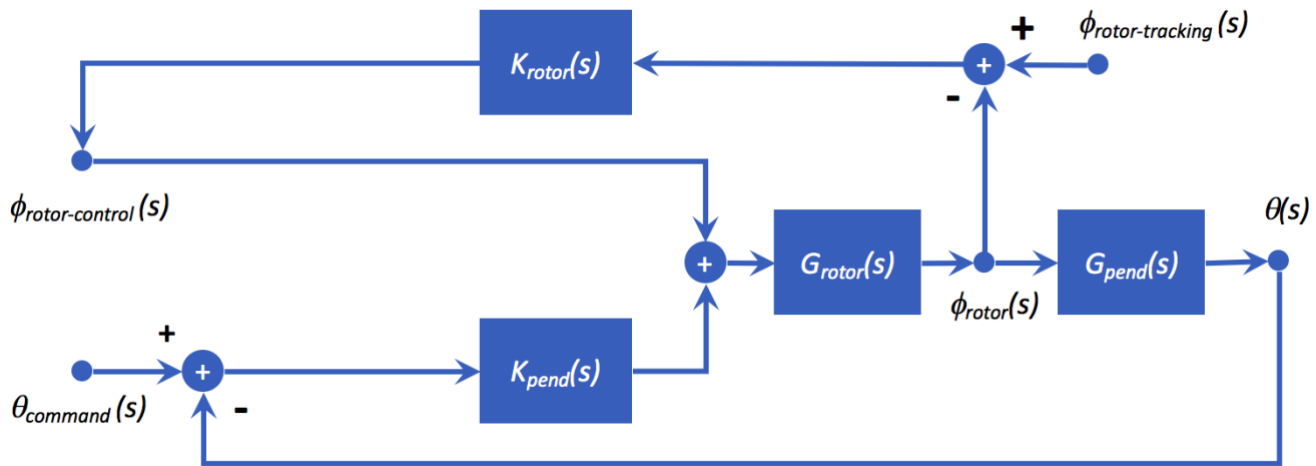


Figure 40. Dual PID Control System Inner and Outer Control Loop

Design of K_{rotor} begins with selection of integral time constant, T_{i-r} , and derivative time constant, T_{d-r} . This is followed by selection of controller gain, K . The form of this controller is:

$$K_{rotor}(s) = K \left(1 + \frac{1}{T_{i-r}s} + T_{d-r}s \right)$$

The selection of optimal values for T_{i-r} , T_{d-r} and K , can also include selection of values for T_i , T_d and K for the Pendulum Angle control PID loop.

To review the characteristics of the Single PID Inverted Mode Pendulum controller of section 0, the closed loop poles, zeroes of $1 + G_{rotor}G_{pend}K_{pend}(s)$ were determined to be

$$\begin{aligned} & 0.0000 + 0.0000i \\ & -11.1389 + 16.3738i \\ & -11.1389 - 16.3738i \\ & -10.4152 + 0.0000i \\ & -0.2443 + 0.3122i \\ & -0.2443 - 0.3122i \end{aligned}$$

Thus, the integral time constant, T_{i-r} , is then set at the value of 5 seconds. The derivative time constant, T_{d-r} , is set at 1.5 seconds. The selected values are.

$$\begin{aligned} T_{i-r} &= 5.0s \\ T_{d-r} &= 1.5s \end{aligned}$$

The next step in design is the selection of the gain K. This will be subject to the following objectives:

- 1) The Nyquist Criterion will be met for the plant.
- 2) The Bode characteristic of the plant displays a Phase Margin greater than 30 degrees.
- 3) The maximum values of both the Sensitivity Function and Complimentary Sensitivity Function will be minimized.
- 4) The maximum value of the Noise Sensitivity Function will also be minimized.

The latter requirement relies on the Sensitivity Function defined as

$$S(s) = \frac{1}{1 + T_{rotor-angle}(s)K_{rotor}(s)}$$

$$T(s) = \frac{T_{rotor-angle}(s)K_{rotor}(s)}{1 + T_{rotor-angle}(s)K_{rotor}(s)}$$

The maximum value for the range of $s = 0$ to $s = \infty$ will be computed for each with

$$M_s = \max_{0 \leq \omega < \infty} |S(j\omega)|$$

and

$$M_T = \max_{0 \leq \omega < \infty} |T(j\omega)|$$

These values measure the robustness of the control system to variations in plant characteristics.

The third important metric is the Noise Sensitivity function that determines the susceptibility of the control system to errors introduced by measurement noise.

The Noise Sensitivity Function is

$$NS(s) = \frac{K_{rotor}(s)}{1 + T_{rotor-angle}(s)K_{rotor}(s)}$$

The maximum value for the range of $s = 0$ to $s = \infty$ will be computed with

$$M_{NS} = \max_{0 \leq \omega < \infty} |NS(j\omega)|$$

As a first example, the value of $K = 12$ is selected. The Bode plot, Nyquist characteristic, and Sensitivity Function plot are shown in *Figure 41*.

The values of M_s , M_T , and M_{NS} are shown in Table 7 Table 6 along with the values of Phase Margin, and Phase Cross Over Frequency.

The Bode plot indicates a Phase Margin of 73 degrees meeting the design requirement.

Also, for this gain value, the closed loop poles, zeroes of $1 + T_{rotor-angle}(s)K_{rotor}(s)$ are:

$$\begin{aligned} & 0.0000 + 0.0000i \\ & -31.4159 + 0.0000i \\ & -12.9514 + 20.2968i \\ & -12.9514 - 20.2968i \\ & -4.7539 + 0.0000i \\ & -1.6943 + 0.0000i \\ & -0.5600 + 0.4200i \\ & -0.5600 - 0.4200i \\ & -0.5023 + 0.0000i \\ & -0.3285 + 0.0000i \end{aligned}$$

Then, the poles of $T_{rotor-angle}(s)K_{rotor}(s)$ are:

$$\begin{aligned} & 0.0000 + 0.0000i \\ & 0.0000 + 0.0000i \\ & -31.4159 + 0.0000i \\ & -11.1389 + 16.3738i \\ & -11.1389 - 16.3738i \\ & -10.4152 + 0.0000i \\ & -0.5600 + 0.4200i \\ & -0.5600 - 0.4200i \\ & -0.2443 + 0.3122i \\ & -0.2443 - 0.3122i \end{aligned}$$

Then, the number of zeroes of $1 + G_{rotor}G_{pend}K_{pend}(s)$ in the right half plane, $Z = 0$. Also, the number of poles, of $G_{rotor}G_{pend}K_{pend}(s)$ in the right half plane is also zero, $P = 0$. Then, there will be no encirclements of the point, $s = -1$ required to meet the Nyquist Criterion. This is indeed observed in *Figure 41*, meeting the design requirement.

The dependence of M_s , M_T , and M_{NS} on selection of Gain K will can be evaluated. The values of each is listed below in Table 7 along with the values of Phase Margin, and Phase Cross Over Frequency.

Gain	M_s	M_T	M_{NS}	Phase Margin (degrees)	Phase Cross Over Frequency (rad/sec)
8	1.09	1.00	384.8	75.0	1.04
12	1.11	1.00	577.3	73.0	1.44
14	1.12	1.01	673.5	72.0	1.63

Table 7. Values of M_s , M_T , and M_{NS} Phase Margin, and Phase Cross Over Frequency for selections of Gain, K.

The gain value of 11 is selected as meeting objectives for Phase Margin with relative low values of M_s and M_T , and also yielding an intermediate value of Noise Sensitivity, M_{NS} .

Using this gain, the PID controller becomes

$$K_{rotor}(s) = K_{p-rotor} + \frac{K_{i-rotor}}{s} + K_{d-rotor}s$$

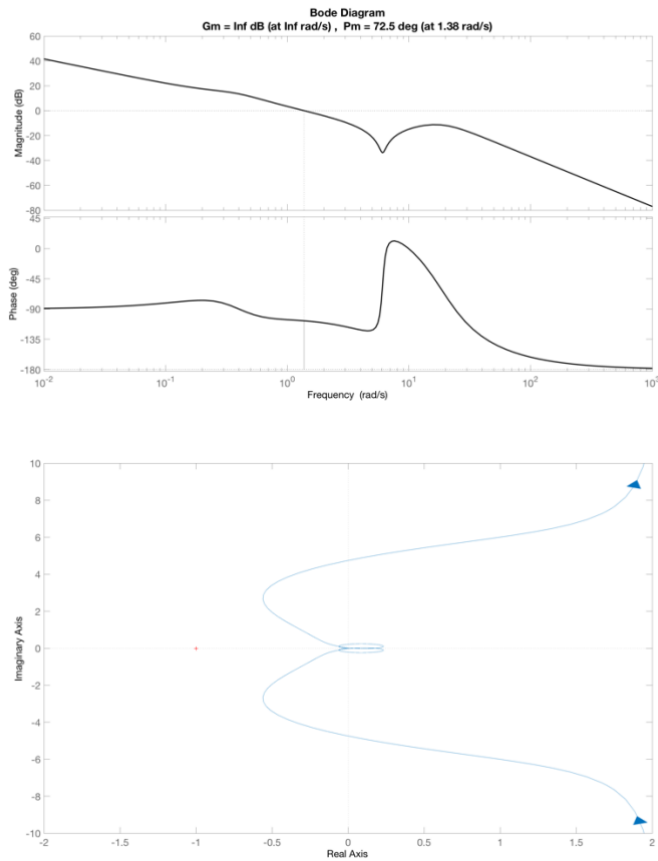
with

$$K_{p-rotor} = 12.00, \quad K_{i-rotor} = K/T_{i-r} = 2.40, \quad K_{d-rotor} = KT_{d-r} = 18.0$$

Simulated system response to a step input to $\phi_{rotor-command}$, shown in *Figure 42* displays stable operation.

Experimentally measured system response to a step input to $\phi_{rotor-command}$, shown in *Figure 43*, also displays stable operation. Finally, experimentally measured system response of Pendulum Angle to a step input to $\phi_{rotor-command}$, shown in *Figure 44*, also displays stable operation

Further development of Dual PID design may continue. However, the challenge for optimizing this MIMO system are clear. Later sections introduce Modern Control methods that enable direct



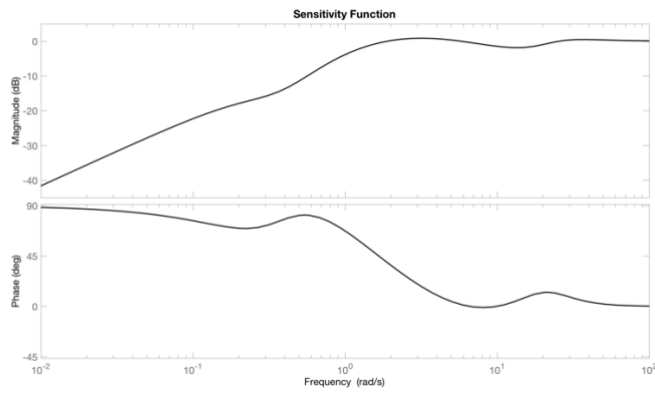


Figure 41. The Bode plot (upper panel), Nyquist characteristic (middle panel), and Sensitivity Function (lower panel) for $K = 12$.

optimization of controller design for this system. This produces a dramatic performance advance in overshoot and response time characteristics.

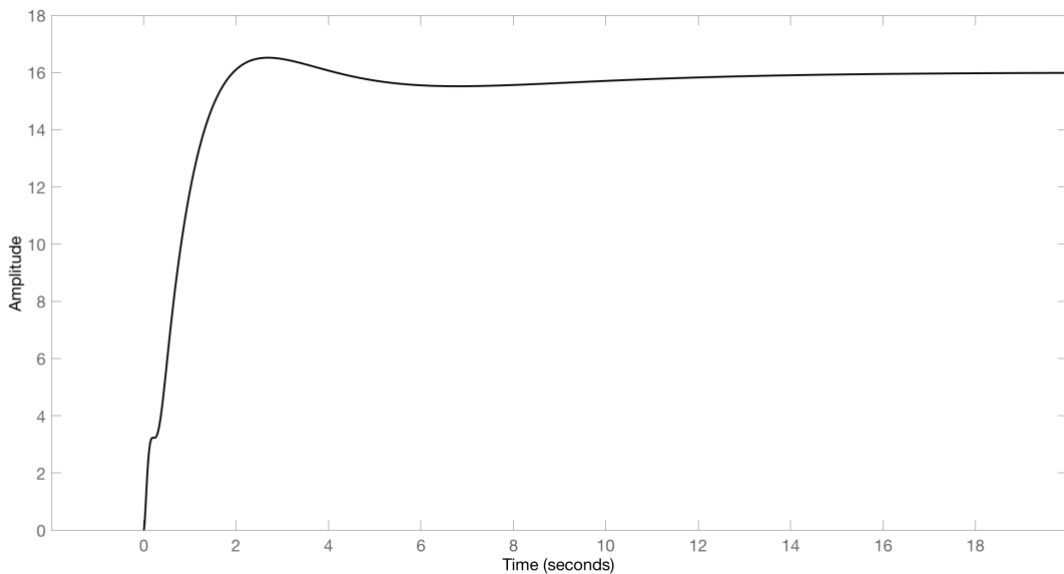


Figure 42. Simulated Rotor Angle response of the Dual PID Control System response for a step input of amplitude 16 degrees to the Rotor Angle command input applied at $t = 0$.

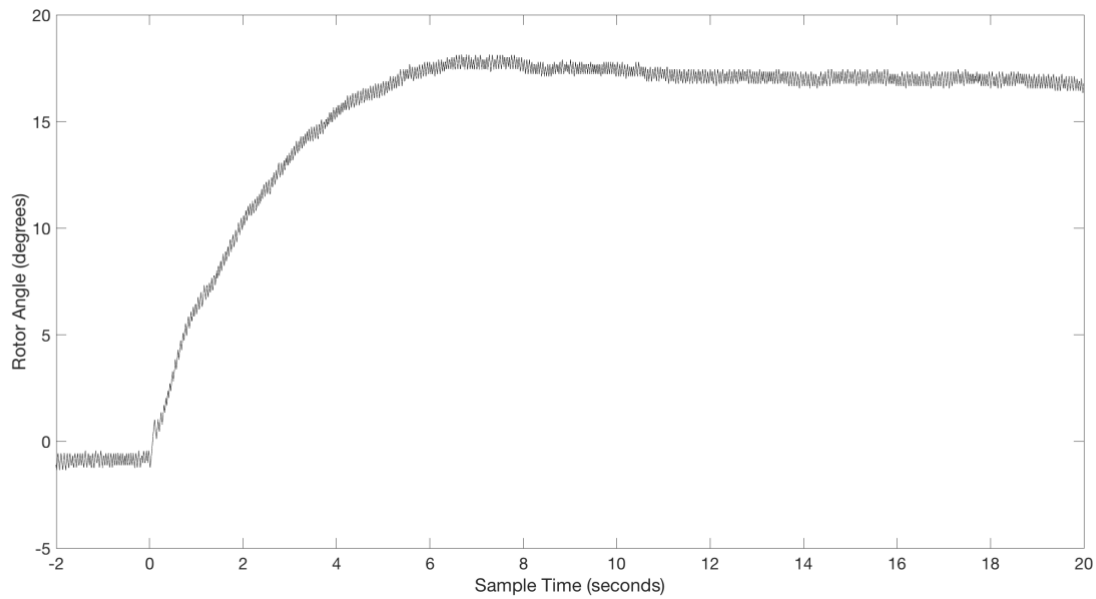


Figure 43. Experimental measurement of Rotor Angle response of the Dual PID Control System response for a step input of amplitude 20 degrees to the Rotor Angle command input applied at $t = 0$.

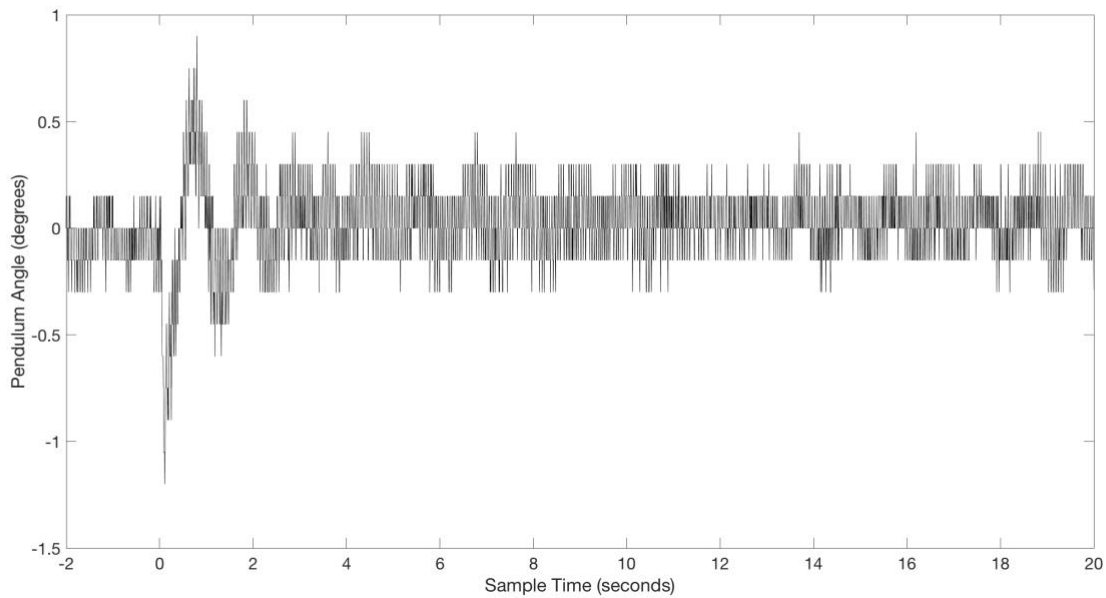


Figure 44. Experimental measurement of Pendulum Angle response of the Dual PID Control System response for a step input of amplitude 16 degrees to the Rotor Angle command input applied at $t = 0$. The discrete values associated with Pendulum Angle measurement resolution (0.16 degrees) are observed.

10. Inverted Pendulum Single PID Controller: Root Locus Design

This section describes the development of a Single Input Single Output (SISO) PID Controller controlling only Pendulum Angle. This is followed by Section 9 that describes a Dual PID Controller architecture that combines two SISO systems. This design and development provides valuable background in PID control and its limitations associated with design guidance.

It is important to note that control of the Rotary Inverted Pendulum requires sensing and control of *both* Pendulum Angle and Rotor Angle. This section introduces control of Pendulum Angle. However, such a system, is not an effective control system since Rotor Angle is not controlled relative to a tracking reference.

The next section will introduce a Dual PID structure that enables both control of Pendulum and Rotor Angles.

Section 10 introduces Multiple Input Multiple Output (MIMO) Control based on the Linear Quadratic Regulator. This permits development of optimal control for parameters including a specified cost function.

The Inverted Pendulum Mode feedback control system supplies an output to Rotor Control, ϕ , to control the difference between Pendulum angle, θ , and a reference tracking command, $\theta_{reference}$, as shown in *Figure 45*.

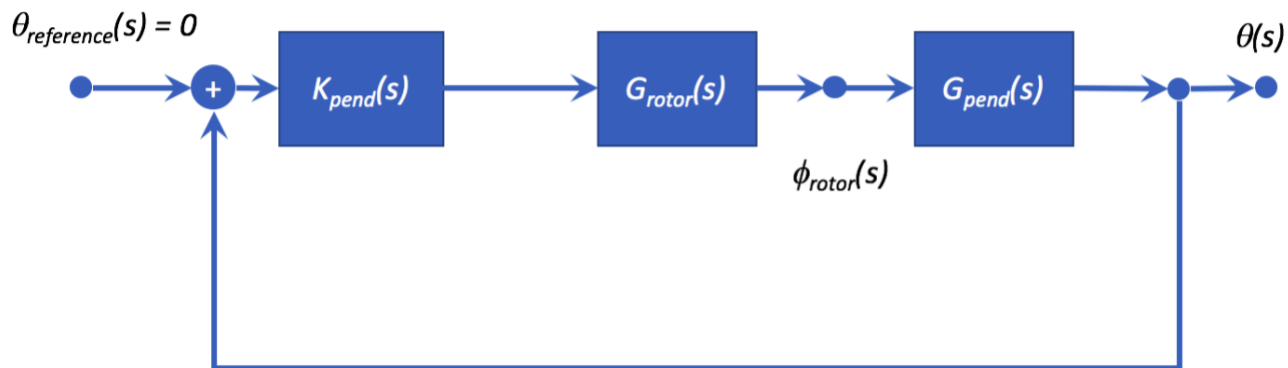


Figure 45. Pendulum Orientation PID Control System

First, the dynamic response of the inverted pendulum is computed. The Integrated Rotary Inverted Pendulum operation in an Inverted Pendulum configuration is shown in Figure 1. The development of the pendulum dynamic response follows directly by accounting for gravitational force, pendulum angle θ , and rotor angle, ϕ .

Now, referring to Figure 1, gravity induces an acceleration on the pendulum mass of

$$\ddot{\theta}_{gravitational} = \frac{g}{l} \sin\theta$$

Further, the rotor rotation induces an acceleration of the pendulum angle of

$$\ddot{\theta}_{rotor} = \frac{(r)sin\dot{\phi}}{l}cos\theta$$

Then acceleration of the pendulum mass is

$$\ddot{\theta} = \frac{g}{l}sin\theta + \frac{(r)sin\dot{\phi}}{l}cos\theta$$

Considering small angles,

$$\ddot{\theta} = \frac{g}{l}\theta + \frac{r}{l}\ddot{\phi}$$

or

$$l\ddot{\theta} - g\theta = r\ddot{\phi}$$

Then the Pendulum plant transfer function is

$$G_{pendulum}(s) = \frac{\theta(s)}{\phi(s)} = \frac{(r/g)s^2}{ls^2 - g} = \frac{r/l}{1 - \frac{(g/l)}{s^2}} = \frac{r/l}{1 - 1/(\tau_L^2 s^2)}$$

where $\tau_L = \sqrt{l/g}$.

As described in Section 4, development of the PID control system first requires development of a model for the Stepper Motor system providing Rotor control of Rotor Angle, ϕ , in response to Rotor Angle Control input, ϕ_{RC} . The Medium Speed System example of Table 2 is applied to the system in this section.

Thus, the transfer functions of *Figure 45* are defined:

$$G_{Rotor}(s) = \frac{\phi(s)}{\phi_{RC}(s)} = \frac{a}{s^2 + bs + c}$$

with

$$\begin{aligned} a &= 0.245 \\ b &= 1.12 \\ c &= 0.49 \end{aligned}$$

$$G_{pend}(s) = \frac{\theta(s)}{\phi(s)} = \frac{(r/g)s^2}{ls^2 - g} = \frac{r/l}{1 - \frac{(g/l)}{s^2}} = \frac{r/l}{1 - 1/(\tau_L^2 s^2)}$$

The reference signal, $\theta_{reference}(s)$ is set to zero in this control stage.

Note that the polarity of both $G_{pend}(s)$ and $G_{Rotor}(s)$ are opposite that for the suspended pendulum configuration due to the definition of angles θ and ϕ for each configuration as well as the direction of gravitational acceleration acting on the pendulum.

Therefore, the resulting relationship between rotor angle and reference angle is.

$$\theta(s) = (\theta_{reference}(s) - \theta(s)) K_{pendulum}(s) G_{rotor}(s) G_{pendulum}(s)$$

The transfer function from $\theta_{reference}$ to θ is

$$\frac{\theta(s)}{\theta_{reference}(s)} = \frac{G_{rotor}(s) G_{pendulum}(s) K_{pendulum}(s)}{1 + G_{rotor}(s) G_{pendulum}(s) K_{pendulum}(s)}$$

Now, the open loop plant is

$$G_{pend-rotor} = G_{pend}(s) G_{rotor}(s) = \frac{\phi_{rotor}(s)}{\phi_{rotor-control}(s)} \frac{\theta(s)}{\phi_{rotor}(s)}$$

$$G_{pend-rotor} = \left(\frac{-(r/l)s^2}{s^2 - (g/l)} \right) \left(\frac{a}{s^2 + bs + c} \right) = \frac{-a(r/l)s^2}{s^4 + bs^3 + (c - (g/l))s^2 - b(g/l)s - c(g/l)}$$

For the identified parameters for a, b, c, r, and l, the root locus characteristic for the pendulum plant is shown in *Figure 46*.

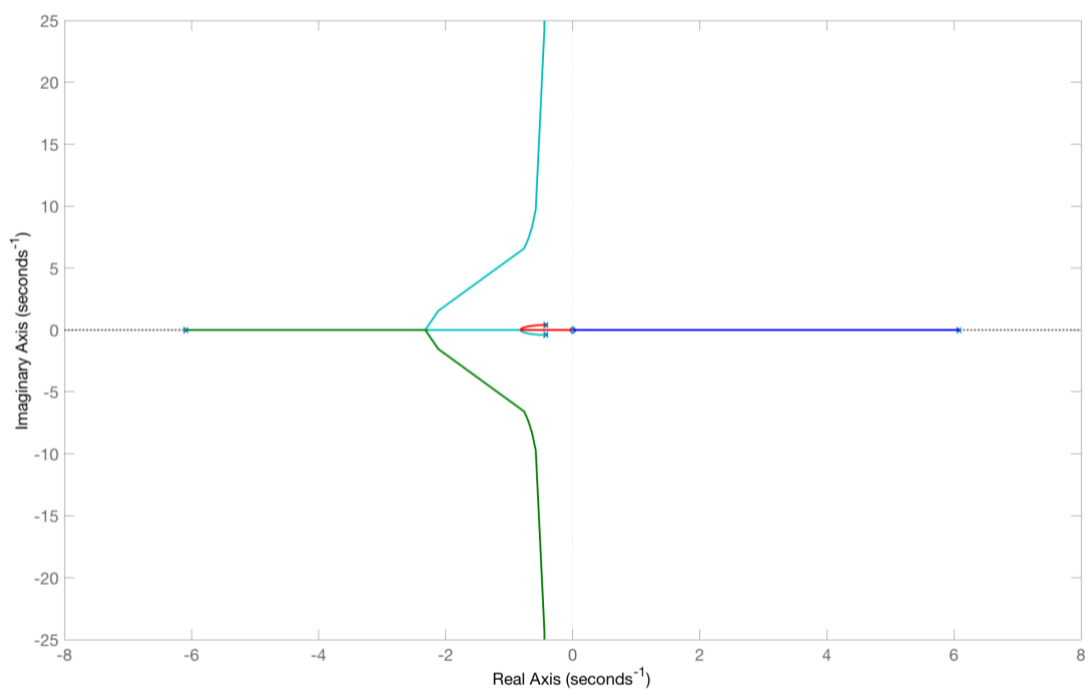


Figure 46. The Root Locus plot of Pendulum-Rotor plant, $G_{\text{pend-rotor}}$, is shown.

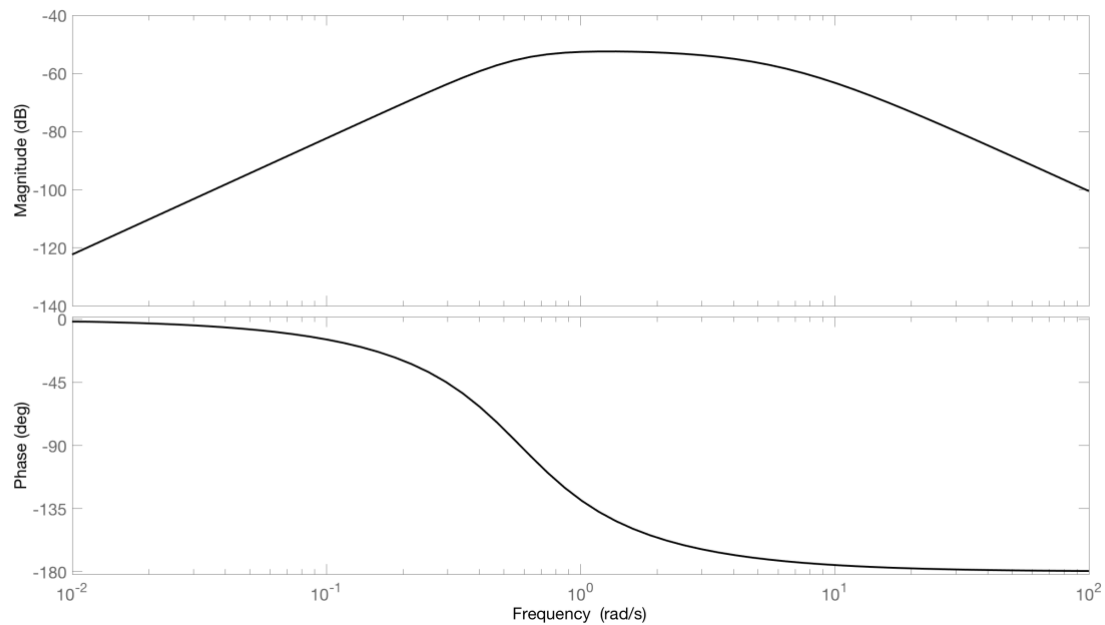


Figure 47. The Bode plot of Pendulum-Rotor plant, $G_{\text{pend-rotor}}$, is shown.

The poles appearing for $G_{pend-rotor}$ are

$$\begin{aligned} & 6.4577 + 0.0000i \\ & -6.4577 + 0.0000i \\ & -0.5600 + 0.4200i \\ & -0.5600 - 0.4200i \end{aligned}$$

The two zeroes appearing for $G_{pend-rotor}$ are both at the origin.

Design of a SISO PID controller proceeds using root locus methods. The design objectives for this example will include:

- 3) A damping defined by a Maximum Overshoot, $M_p = 0.1$
- 4) A natural frequency defined by a Time to First Peak, T_p , of 0.1

Subsequent to design, stability for this example will be determined by ensuring that

- 1) Phase margin is greater than 30 degrees [Seborg_1989]

First, a PID controller is selected. Second, for this controller integral and derivative time constants are selected. The Bode plot of the Pendulum-Rotor plant is shown in *Figure 47*. The influence of poles near 6.46 rad/sec and 0.56 rad/sec is observed.

As a first design choice, the integral time constant is set to the conservative value of 5.0 seconds corresponding to one third of the frequency of the pole at 0.56 rad/sec. The derivative time constant is set at 0.15 seconds, corresponding to the frequency of the pole at 6.46 rad/sec. These values are:

$$T_i = 5.0 \text{ sec and } T_d = 0.15 \text{ sec}$$

The form of this PID controller is then,

$$K_{pend}(s) = K \left(1 + \frac{1}{T_i s} + T_d s \right)$$

where K will be found via Root Locus design methods.

The Bode plot for this controller, K_{pend} , the Pendulum and Rotor Plant, $G_{pendulum}G_{rotor}$, and for the open loop combined plant and controller, $K_{pend}G_{pendulum}G_{rotor}$, is shown in *Figure 48* for $K = 1$.

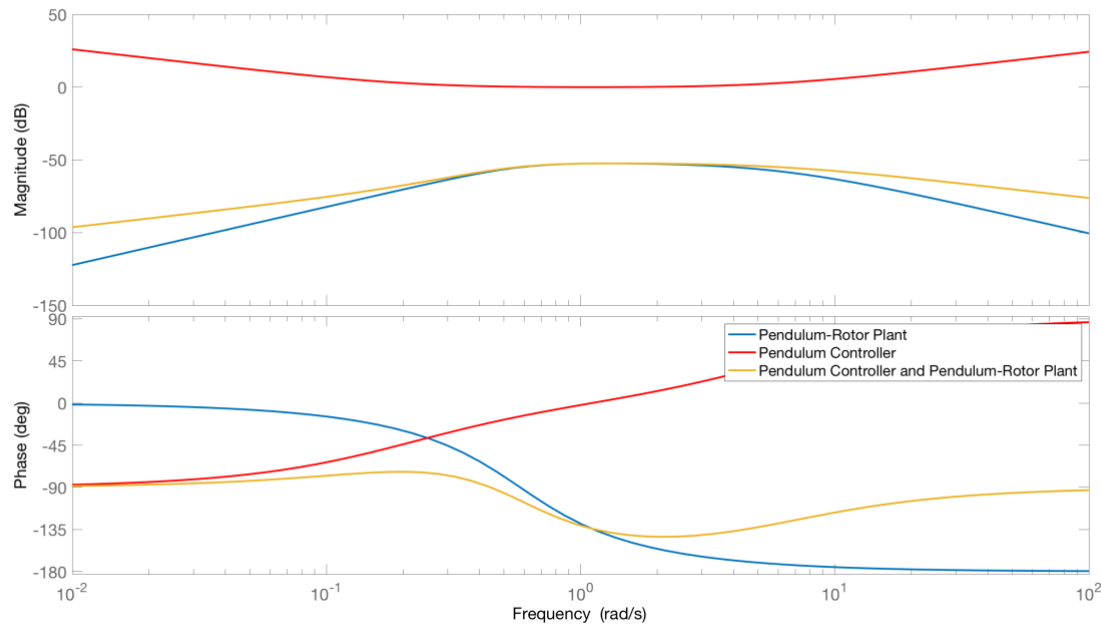


Figure 48. The Bode plot of the Pendulum and Rotor plant, Pendulum controller, and the open loop controller – plant product transfer function is shown for gain, K, of unity.

The gain, K, may now be determined by root locus design.

The controller closed loop response will approximate a second order response and therefore the properties of second order systems can be applied to determine its Natural Frequency, ω_N , and Damping Ratio, ζ , by specifying a Maximum Overshoot, $M_p = 0.1$. [Astrom_2008]

A Damping Ratio is selected based on the criteria for a maximum overshoot. [Nise_2015]

$$\text{Damping Ratio} = \sqrt{\frac{\ln^2(M_p)}{\pi^2 + \ln^2(M_p)}}$$

This produces a Damping Ratio, ζ , of 0.69.

Then, we will select a target Time to First Peak, T_p , of 0.10 seconds and estimate a corresponding natural frequency. This can be estimated with [Nise_2015]

$$\omega_N = \frac{\pi}{T_p \sqrt{1 - \zeta^2}}$$

This produces a Natural Frequency, ω_N , of 36.9 rad/sec or 5.9 Hz.

The open loop system is

$$G_{open-loop} = G_{rotor}G_{pend}K_{pend}(s)$$

The Root Locus plot for this system is shown in *Figure 49*.

The Root Locus plot shows an arc of constant natural frequency of $\omega_N = 36.9$. Also, the lines emanating at the origin are lines of constant Damping Ratio such that points between these lines correspond to solutions with Damping Ratio, ζ , greater than 0.59.

Thus, using Matlab rlocfind, we select a point on the real axis at the intersection of the real axis and the arc of constant natural frequency. This point is indicated by the crosshair symbol on the negative real axis near the arc of $\omega_N = 36.9$.

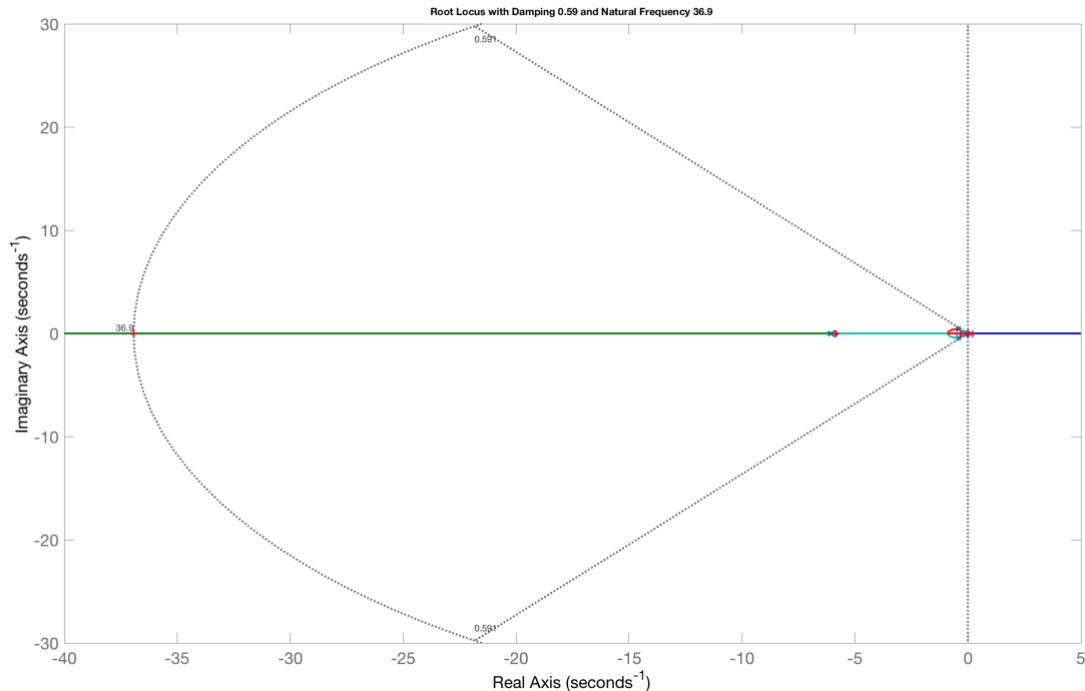


Figure 49. The Root Locus plot of the open loop control system including controller and plant product transfer function is shown. The Matlab rlocfind method has been used to select a point where the arc of constant natural frequency intersects the negative real axis.

This yields a value of gain of $K = 2719.1$. Using this gain scale factor value, the PID controller becomes

$$K_{pend}(s) = K_{p-pend} + \frac{K_{i-pend}}{s} + K_{d-pend}s$$

with

$$K_{p-pend} = 1924.5, \quad K_{i-pend} = K/T_i = 384.9, \quad K_{d-pend} = KT_d = 288.7$$

The poles appearing for the open loop transfer function, $G_{rotor}G_{pend}K_{pend}(s)$ are:

$$\begin{aligned} & 0.0000 + 0.0000i \\ & -31.4159 + 0.0000i \\ & 6.4577 + 0.0000i \\ & -6.4577 + 0.0000i \\ & -0.5600 + 0.4200i \\ & -0.5600 - 0.4200i \end{aligned}$$

The closed loop poles, zeroes of $1 + G_{rotor}G_{pend}K_{pend}(s)$ are

$$\begin{aligned} & 0.0000 + 0.0000i \\ & -13.6816 + 35.6853i \\ & -13.6816 - 35.6853i \\ & -5.1167 + 0.0000i \\ & -0.3224 + 0.0000i \\ & 0.2664 + 0.0000i \end{aligned}$$

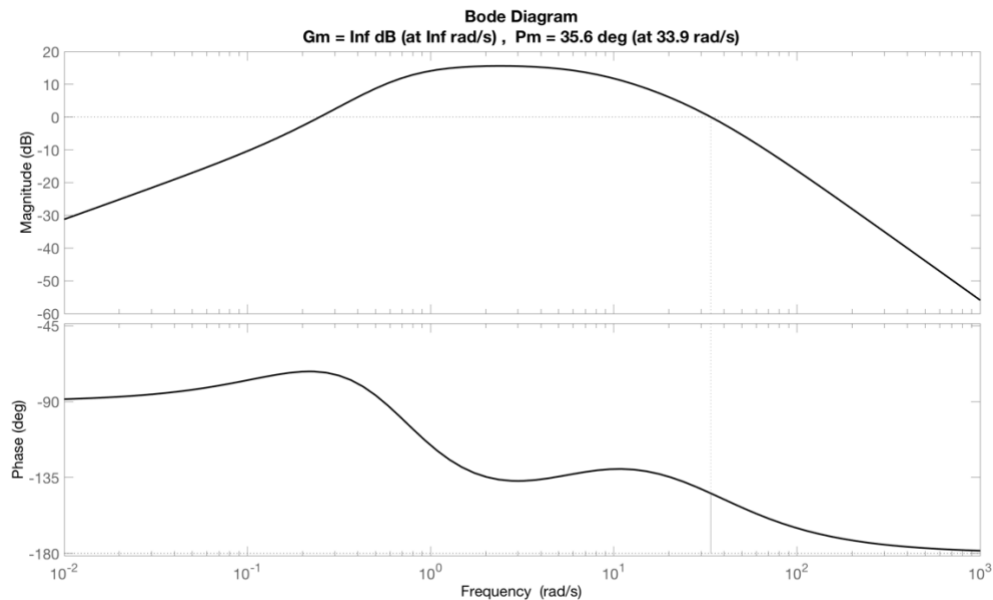


Figure 50. The Bode plot of the open loop control system including controller and plant product transfer function. The gain and phase margins indicate stability with Phase Margin and Phase Cross Over Frequency equaling design objectives.

An evaluation of stability is provided by the Bode plot of $G_{open-loop}$ with the above gains as shown in Figure 50.

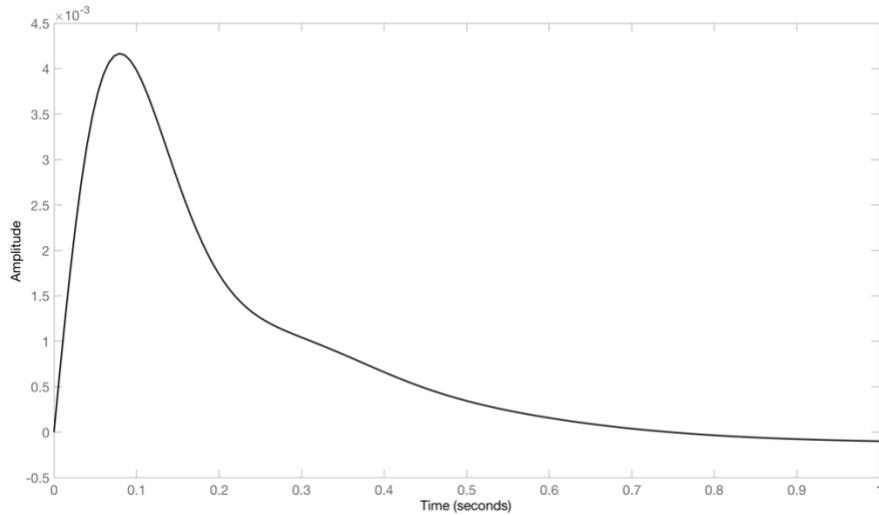


Figure 51. Simulated impulse response of Pendulum angle for the closed loop control system is shown. This system is stable through the interval shown. However, the lack of constraint on Rotor Angle leads to instability for extended periods.

Also, the impulse response of Pendulum angle is shown in *Figure 51*. Note that impulse response characteristic indicates stability. However, this SISO system does not control Rotor Angle. The impulse here induces a drift in Rotor Angle and ultimately unstable behavior. This requires a second controller as described further below and in the next section.

The Integrated Rotary Inverted Pendulum system may be configured with these PID controller values. Suppression of noise resulting from finite resolution and decimation of rotor and encoder angle is provided by a first order filter at corner frequency 5 Hz applied to the derivative computation.

Figure 52 shows experimental system response. It is noted that Pendulum Angle is maintained near zero as required by the system design. Note that the discrete steps associated with the finite resolution of the Pendulum Angle sensor is revealed in this data.

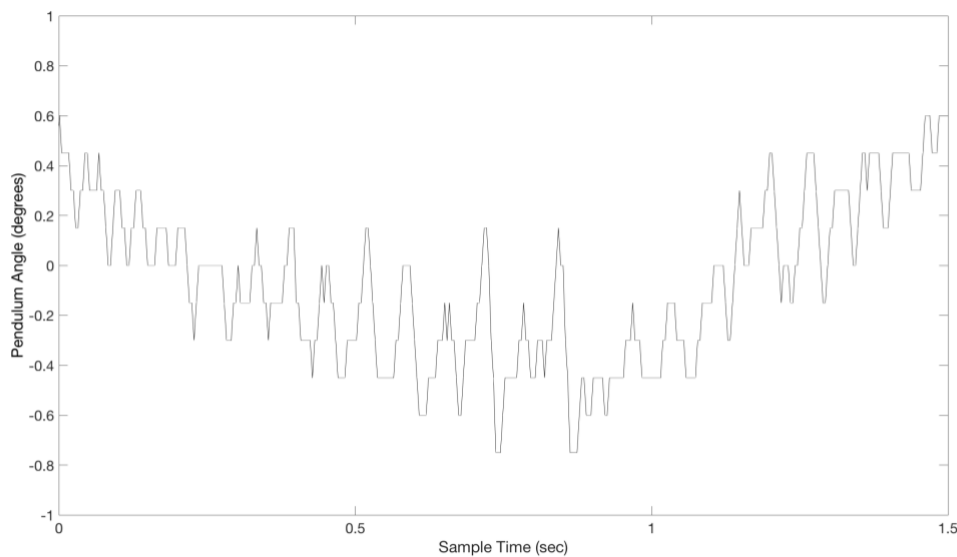


Figure 52. Experimental closed loop operation of the Single Input Single Output PID control system showing Pendulum angle variation. Stable operation is demonstrated. The individual steps observed in this time series data corresponds to the discrete steps in angle measurement by the digital optical encoder.

As noted previously, an important limitation of this Single Input Single Output (SISO) controller appears. Specifically, while the controller stabilizes Pendulum Angle, Rotor Angle does not appear as an input and is not stabilized. Thus, a disturbance in Rotor position is not compensated for by this controller.

The limitations of SISO control may be characterized directly. The response of Rotor Angle, ϕ_{rotor} , to a signal applied to $\theta_{reference}$ may be computed. Examining *Figure 45*, the transfer function from $\theta_{reference}(s)$ to $\phi_{rotor}(s)$ is

$$T_{Rotor-Response} = \frac{\phi_{rotor}(s)}{\theta_{reference}(s)} = \frac{G_{rotor}K_{pend}}{1 + G_{pend}G_{rotor}K_{pend}}$$

The computed response of Rotor Angle, ϕ_{rotor} , to an impulse applied to Pendulum references angle, is $\theta_{reference}$, is shown in

Figure 53.. Pendulum angle remains near zero, as shown in *Figure 17* after the impulse. However, the response of Rotor Angle shown in

Figure 53 confirms that the Rotor Angle is not controlled by this SISO system.

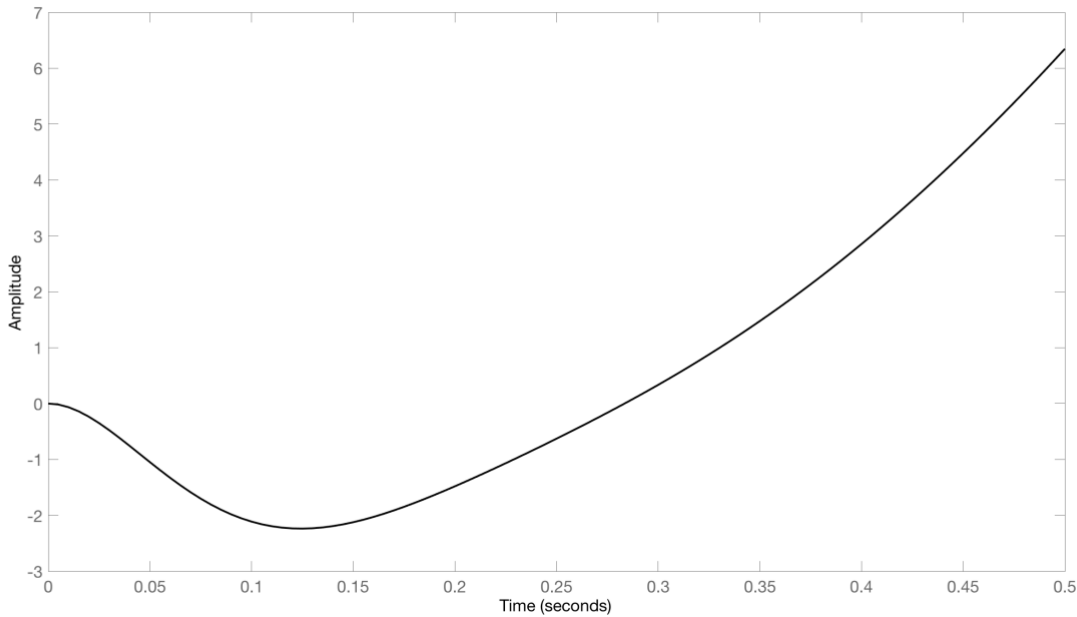


Figure 53. Simulated response of Rotor Angle, ϕ_{rotor} , to an impulse signal applied to Pendulum angle reference, $\theta_{reference}$, at $t = 0$ computed by simulation of the Integrated Rotary Inverted Pendulum. Note the drift in Rotor Angle. During this period, Pendulum Angle remains constant and near zero.

As an experimental example, the Pendulum position for the Integrated Rotary Inverted Pendulum was disturbed, leading to a drift in Rotor position shown in *Figure 55*.

The next section describes the addition of a second PID controller that provides Rotor Angle stabilization relative to a tracking command.

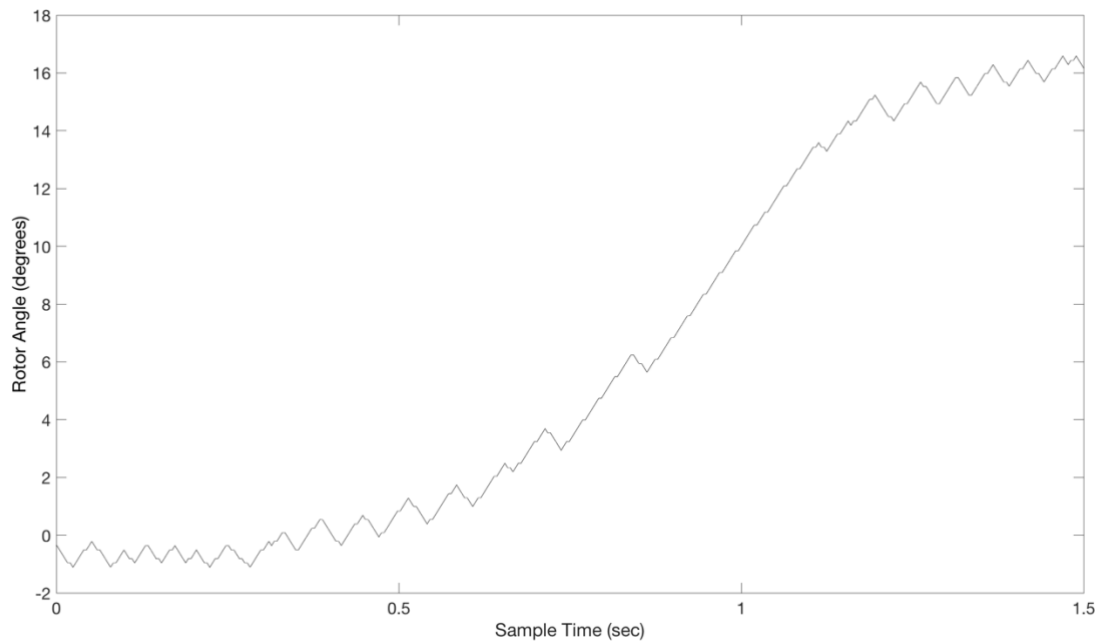


Figure 54. Response of Rotor Angle of the Integrated Rotary Inverted Pendulum as a result of a disturbance applied at $t = 0$. The drift observed is the result of the limitation of this Single Input Single Output controller that stabilizes Pendulum Angle but not Rotor Angle.

Now, as noted, this SISO system controls only Pendulum Angle by providing control input to the Rotor Angle motor actuator. Rotor Angle relative to a tracking reference is not controlled by this SISO system. Thus, Rotor Angle drifts as shown in *Figure 54*.

Instead a second PID control system is introduced in the next Section that applies rotor angle control input to stabilize rotor angle and enable tracking of a rotor angle command input.

11. Inverted Pendulum Dual PID Controller: Root Locus Design

The introduction of a second PID controller may enable stabilization of Rotor Angle. This will be accomplished by introducing an Inner Loop and Outer Loop.

The design process will include the steps of:

- 5) Design of Single PID Controller, $K_{pend}(s)$
- 6) Definition of Inner Control Loop including $K_{pend}(s)$
- 7) Definition of Outer Control Loop integrating the Inner Control Loop and a new controller, $K_{rotor}(s)$
- 8) Design of the Rotor Control system, $K_{rotor}(s)$.

The Inner Loop controller will depend on the design of $K_{pend}(s)$ in section 0. This will be held constant while a new Outer Loop controller of Rotor Angle, $K_{rotor}(s)$, is added.

The Inner Loop Controller defines a transfer function from a Rotor Angle Control signal, $\phi_{rotor-control}$ to the Rotor Angle, ϕ_{rotor} . The Outer Loop Controller provides control of Rotor Angle, Rotor Angle, ϕ_{rotor} to a Rotor Angle Tracking Command, $\phi_{rotor-tracking}$.

The SISO Pendulum Angle control system architecture of *Figure 45* will be now modified to create an Inner Loop controller. This will be accomplished by adding a feedback signal from Rotor Angle, ϕ_{rotor} .

This Rotor Angle Control system also introduces a first order low-pass filter operating on Rotor Angle, ϕ_{rotor} . The difference between the output of this filter and the Rotor Angle tracking command, $\phi_{rotor-control}$ is supplied as an error signal and summed with the output of the Pendulum Angle Controller, $K_{pendulum}$ as shown in the Inner Loop Controller of *Figure 55*.

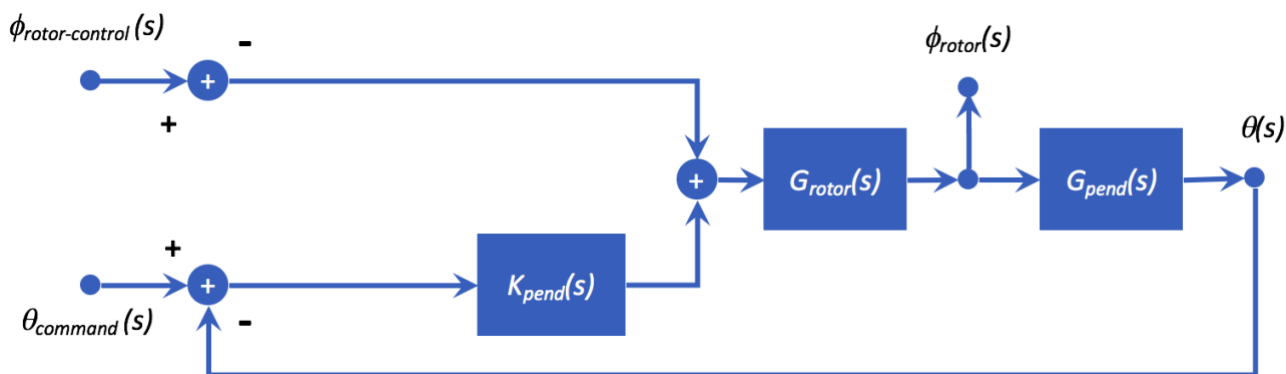


Figure 55. Dual PID Control System Inner Control Loop

Now, the Rotor Angle Control transfer function, $T_{rotor-angle}(s)$ between $\phi_{rotor-control}$ and ϕ_{rotor} will be determined. The input signal, $\theta_{command}(s)$, will be held zero. A summing junction appears at the input of the Pendulum transfer function, $G_{pendulum}$.

$$\phi_{rotor}(s) = (\phi_{rotor}(s)G_{pendulum}(s)K_{pendulum} - \phi_{rotor-control}(s)) G_{rotor}(s)$$

$$T_{rotor-angle}(s) = \frac{\phi_{rotor}(s)}{\phi_{rotor-command}(s)}$$

and

$$T_{rotor-angle}(s) = \frac{-G_{rotor}(s)}{1 + G_{pend}(s)K_{pend}(s) G_{rotor}(s)}$$

This Rotor Angle Control system now introduces the Outer Loop controller to enable control of Rotor Angle. Here, the difference between a Rotor Angle tracking command, $\phi_{rotor-tracking}(s)$ and Rotor Angle, $\phi_{rotor}(s)$, is supplied as an error signal to a new controller, K_{rotor} , and summed with the output of the Pendulum Angle Controller, $K_{pendulum}$ as shown in *Figure 56*.

During subsequent design steps, the configuration of $K_{pend}(s)$ will remain fixed.

The Outer Loop controls ϕ_{rotor} with the goal of tracking the input, $\phi_{rotor-tracking}$.

By definition

$$\phi_{rotor} = \phi_{rotor-command}(s)T_{rotor-angle}(s)$$

Thus, the transfer function from $\phi_{rotor-tracking}$ to ϕ_{rotor} is

$$T_{rotor-tracking}(s) = \frac{\phi_{rotor}(s)}{\phi_{rotor-command}(s)} = \frac{1}{1 + T_{rotor-angle}(s)K_{rotor}(s)}$$

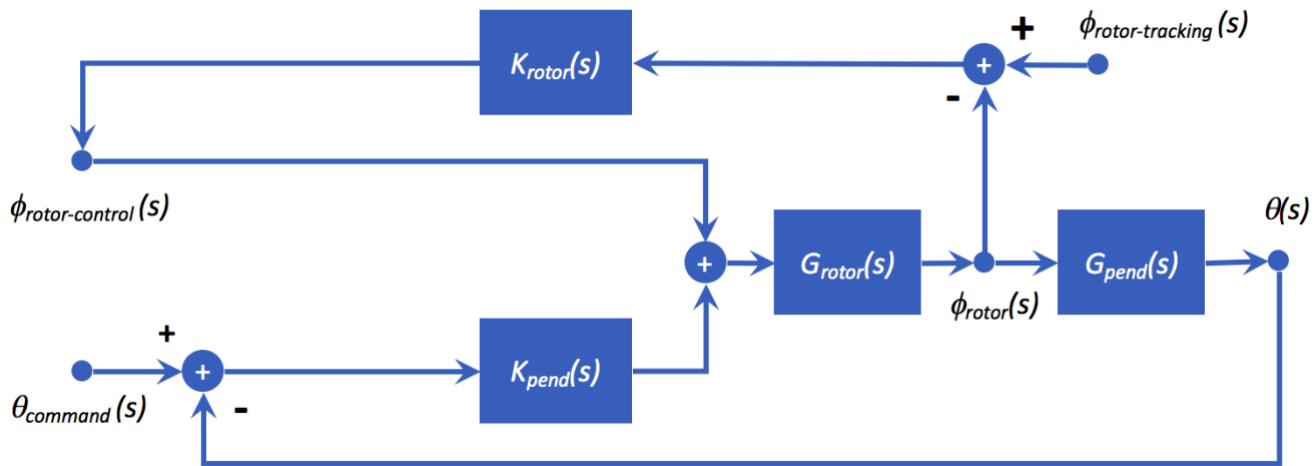


Figure 56. Dual PID Control System Inner and Outer Control Loop

Design of K_{rotor} begins with selection of integral time constant, T_{i-r} , and derivative time constant, T_{d-r} . This is followed by selection of controller gain, K . The form of this controller is:

$$K_{rotor}(s) = K \left(1 + \frac{1}{T_{i-r}s} + T_{d-r}s \right)$$

The selection of optimal values for T_{i-r} , T_{d-r} and K , can also include selection of values for T_i , T_d and K for the Pendulum Angle control PID loop.

To review the characteristics of the Single PID Inverted Mode Pendulum controller of section 0, the closed loop poles, zeroes of $1 + G_{rotor}G_{pend}K_{pend}(s)$ were determined to be:

$$\begin{aligned} & 0.0000 + 0.0000i \\ & -13.6816 + 35.6853i \\ & -13.6816 - 35.6853i \\ & -5.1167 + 0.0000i \\ & -0.3224 + 0.0000i \\ & 0.2664 + 0.0000i \end{aligned}$$

Thus, the integral time constant, T_{i-r} , is then set at the conservative value of 20 seconds. The derivative time constant, T_{d-r} , is set at 4 seconds corresponding to the dominant pole at 0.27 rad/sec. The selected values are.

$$\begin{aligned} T_{i-r} &= 20s \\ T_{d-r} &= 4s \end{aligned}$$

The controller closed loop response will approximate a second order response and therefore the properties of second order systems can be applied to determine its Natural Frequency, ω_N , and Damping Ratio, ζ , by specifying a Maximum Overshoot, $M_p = 0.1$. [Astrom_2008]

A Damping Ratio is selected based on the criteria for a maximum overshoot. [Nise_2015]

$$\text{Damping Ratio} = \sqrt{\frac{\ln^2(M_p)}{\pi^2 + \ln^2(M_p)}}$$

This produces a Damping Ratio, ζ , of 0.59.

Then, we will select a target Time to First Peak, T_p , of 5.0 seconds and estimate a corresponding natural frequency. This can be estimated with [Nise_2015]

$$\omega_N = \frac{\pi}{T_p \sqrt{1 - \zeta^2}}$$

This produces a Natural Frequency, ω_N , of 0.74 rad/sec.

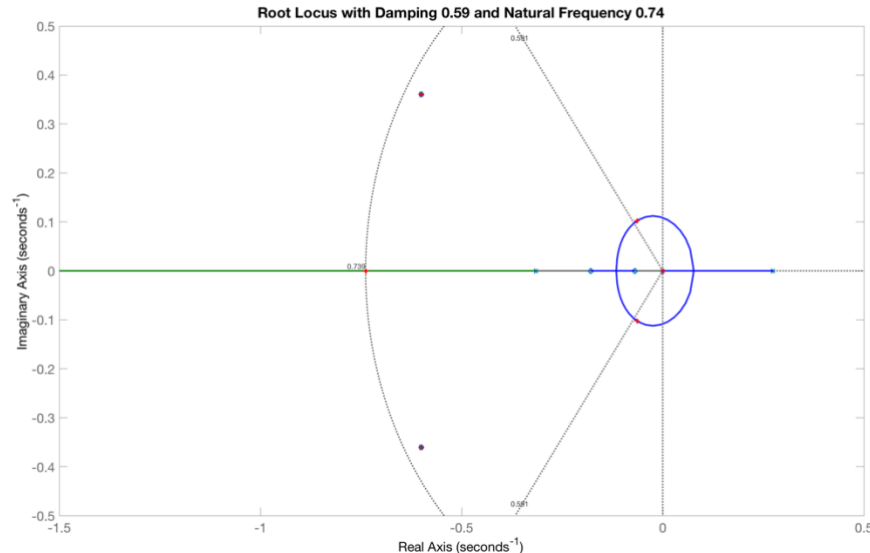


Figure 57. The Root Locus plot of the open loop control system including controller and plant product transfer function is shown. The Matlab rlocfind method has been used to select a point where the arc of constant natural frequency intersects the negative real axis.

Thus, using Matlab rlocfind, we select a point on the real axis at the intersection of the real axis and the arc of constant natural frequency. This point is indicated by the crosshair symbol on the negative real axis near the arc of $\omega_N = 0.74$.

This yields a value of gain of $K = 4.06$. Using this gain scale factor value, the PID controller becomes

$$K_{rotor}(s) = K_{p-rotor} + \frac{K_{i-rotor}}{s} + K_{d-rotor}s$$

with

$$K_{p-rotor} = 4.19, \quad K_{i-rotor} = K/T_{i-r} = 0.21, \quad K_{d-rotor} = KT_{d-r} = 16.5$$

Simulated system response to a step input to $\phi_{rotor-command}$, shown in *Figure 58* displays stable operation.

Experimentally measured system response to a step input to $\phi_{rotor-command}$, shown in *Figure 59*, also displays stable operation with a Maximum Overshoot and Time to First Peak value similar to that of the simulated response.

Further development of Dual PID design may continue. However, the challenge for optimizing this MIMO system are clear. The next section introduces Modern Control methods that enable direct optimization of controller design for this system. This produces a dramatic performance advance in overshoot and response time characteristics.

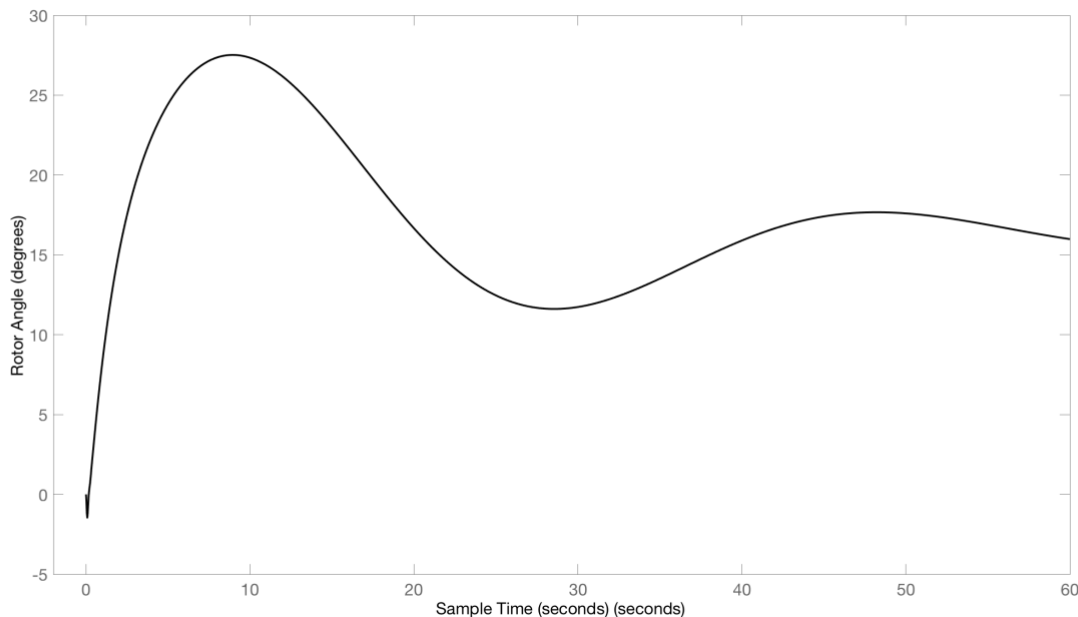


Figure 58. Simulated Rotor Angle response of the Dual PID Control System response for a step input of amplitude 16 degrees to the Rotor Angle command input applied at t = 0.

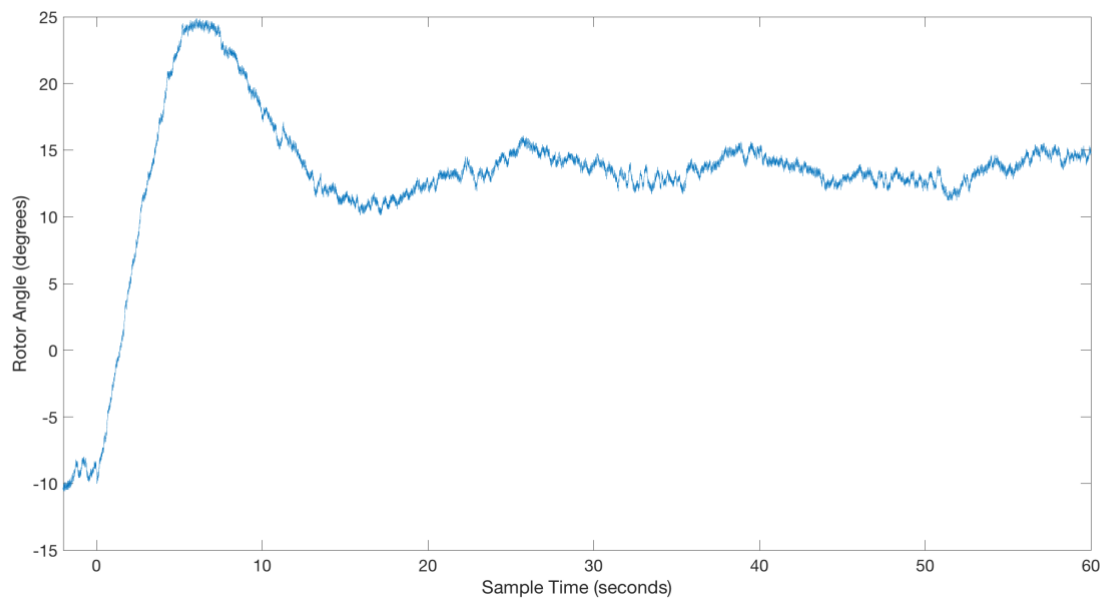


Figure 59. Experimental measurement of Rotor Angle response of the Dual PID Control System response for a step input of amplitude 16 degrees to the Rotor Angle command input applied at $t = 0$.

12. Inverted Pendulum Single PID Controller: Frequency Response Design

The previous sections have described design based on Root Locus Methods. This section and the section that follows presents design based on Frequency Response Methods. These can yield identical controllers through selection of virtually identical gain values.

This section describes the development of a Single Input Single Output (SISO) PID Controller controlling only Pendulum Angle. This is followed by Section 9 that describes a Dual PID Controller architecture that combines two SISO systems. This design and development provides valuable background in PID control and its limitations associated with design guidance.

It is important to note that control of the Rotary Inverted Pendulum requires sensing and control of *both* Pendulum Angle and Rotor Angle. This section introduces control of Pendulum Angle. However, such a system, is not an effective control system since Rotor Angle is not controlled relative to a tracking reference.

The next section will introduce a Dual PID structure that enables both control of Pendulum and Rotor Angles.

Section 10 introduces Multiple Input Multiple Output (MIMO) Control based on the Linear Quadratic Regulator. This permits development of optimal control for parameters including a specified cost function.

The Inverted Pendulum Mode feedback control system supplies an output to Rotor Control, ϕ , to control the difference between Pendulum angle, θ , and a reference tracking command, $\theta_{reference}$, as shown in *Figure 60*.

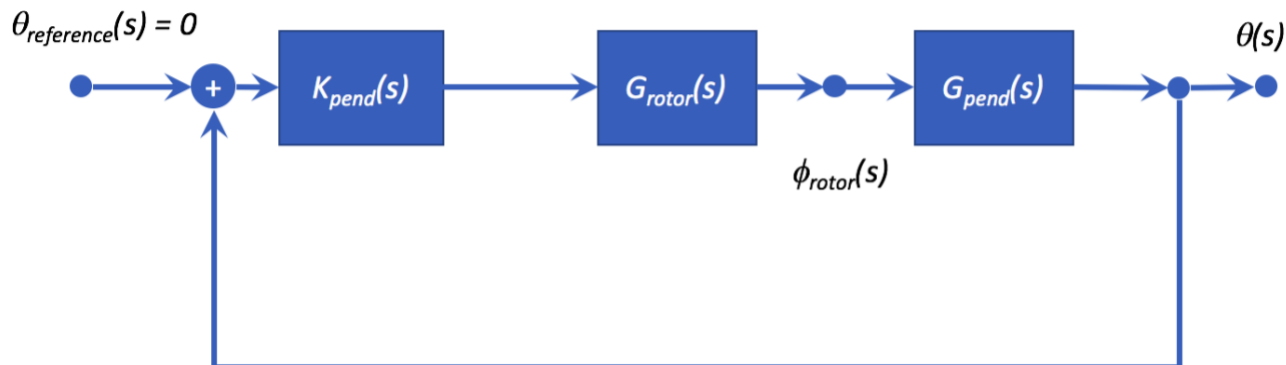


Figure 60. Pendulum Orientation PID Control System

First, the dynamic response of the inverted pendulum is computed. The Integrated Rotary Inverted Pendulum operation in an Inverted Pendulum configuration is shown in Figure 1. The development of the pendulum dynamic response follows directly by accounting for gravitational force, pendulum angle θ , and rotor angle, ϕ .

Now, referring to Figure 1, gravity induces an acceleration on the pendulum mass of

$$\ddot{\theta}_{gravitational} = \frac{g}{l} \sin\theta$$

Further, the rotor rotation induces an acceleration of the pendulum mass of

$$\ddot{\theta}_{rotor} = \frac{(r) \sin\dot{\phi}}{l} \cos\theta$$

Then acceleration of the pendulum mass is

$$\ddot{\theta} = \frac{g}{l} \sin\theta + \frac{(r) \sin\dot{\phi}}{l} \cos\theta$$

Considering small angles,

$$\ddot{\theta} = \frac{g}{l} \theta + \frac{r}{l} \ddot{\phi}$$

or

$$l\ddot{\theta} - g\theta = r\ddot{\phi}$$

Then the Pendulum plant transfer function is

$$G_{pendulum}(s) = \frac{\theta(s)}{\phi(s)} = \frac{(r/g)s^2}{ls^2 - g} = \frac{r/l}{1 - \frac{(g/l)}{s^2}} = \frac{r/l}{1 - 1/(\tau_L^2 s^2)}$$

where $\tau_L = \sqrt{l/g}$.

As described in Section 4, development of the PID control system first requires development of a model for the Stepper Motor system providing Rotor control of Rotor Angle, ϕ , in response to Rotor Angle Control input, ϕ_{RC} . The Medium Speed System example of Table 2 is applied to the system in this section.

Thus, the transfer functions of Figure 23 are defined:

$$G_{Rotor}(s) = \frac{\phi(s)}{\phi_{RC}(s)} = \frac{a}{s^2 + bs + c}$$

with

$$\begin{aligned}a &= 0.245 \\b &= 1.12 \\c &= 0.49\end{aligned}$$

$$G_{pend}(s) = \frac{\theta(s)}{\phi(s)} = \frac{(r/g)s^2}{ls^2 - g} = \frac{r/l}{1 - \frac{(g/l)}{s^2}} = \frac{r/l}{1 - 1/(\tau_L^2 s^2)}$$

The reference signal, $\theta_{reference}(s)$ is set to zero in this control stage.

Therefore, the resulting relationship between rotor angle and reference angle is.

$$\theta(s) = (\theta_{reference}(s) - \theta(s)) K_{pendulum}(s) G_{rotor}(s) G_{pendulum}(s)$$

The transfer function from $\theta_{reference}$ to θ is

$$\frac{\theta(s)}{\theta_{reference}(s)} = \frac{G_{rotor}(s) G_{pendulum}(s) K_{pendulum}(s)}{1 + G_{rotor}(s) G_{pendulum}(s) K_{pendulum}(s)}$$

Now, the open loop plant is

$$\begin{aligned}G_{pend-rotor} &= G_{pend}(s) G_{rotor}(s) = \frac{\phi_{rotor}(s)}{\phi_{rotor-control}(s)} \frac{\theta(s)}{\phi_{rotor}(s)} \\G_{pend-rotor} &= \left(\frac{-(r/l)s^2}{s^2 - (g/l)} \right) \left(\frac{a}{s^2 + bs + c} \right) = \frac{-a(r/l)s^2}{s^4 + bs^3 + (c - (g/l))s^2 - b(g/l)s - c(g/l)}\end{aligned}$$

For the identified parameters for a, b, c, r, and l, the root locus characteristic for the pendulum plant is shown in *Figure 61*.

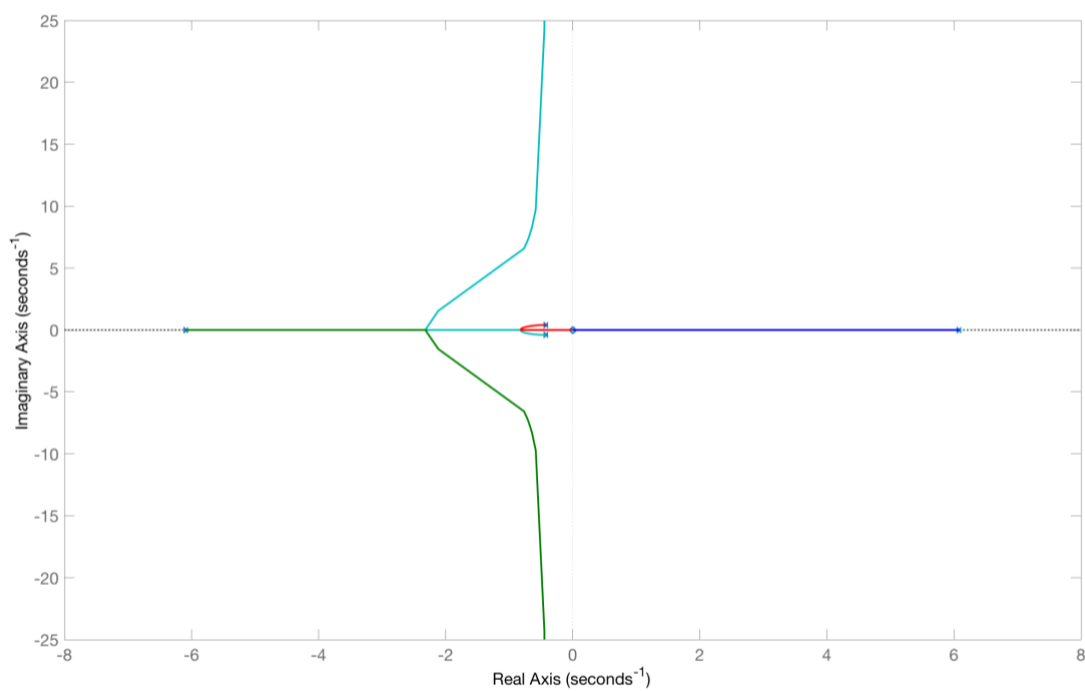


Figure 61. The Root Locus plot of Pendulum-Rotor plant, $G_{\text{pend-rotor}}$, is shown.

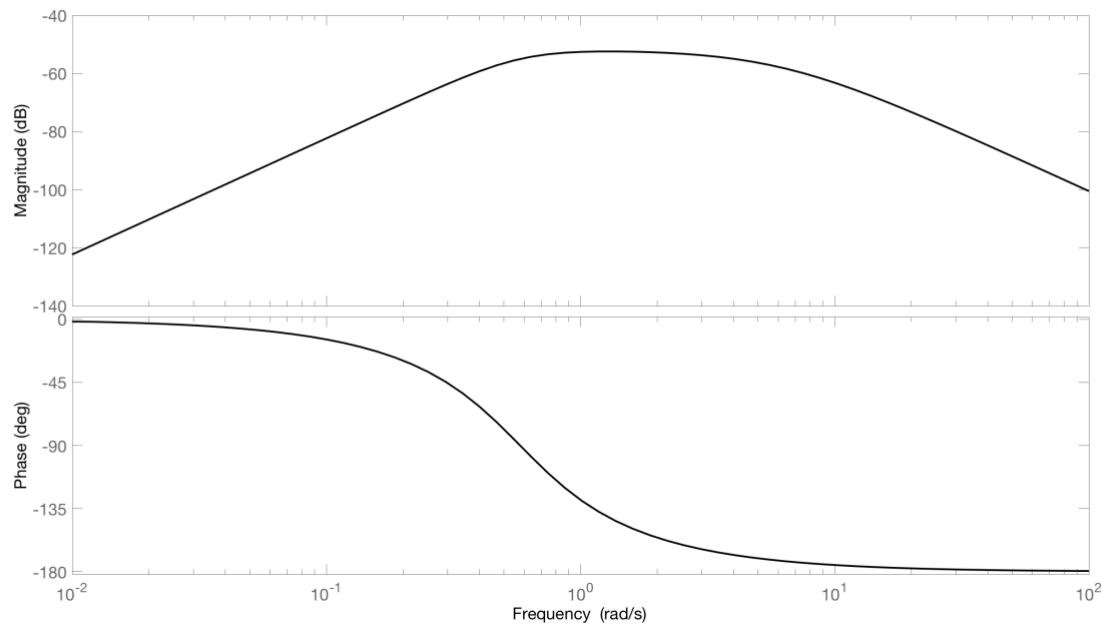


Figure 62. The Bode plot of Pendulum-Rotor plant, $G_{\text{pend-rotor}}$, is shown.

The poles appearing for $G_{pend\text{-}rotor}$ are

$$\begin{aligned} & 6.4577 + 0.0000i \\ & -6.4577 + 0.0000i \\ & -0.5600 + 0.4200i \\ & -0.5600 - 0.4200i \end{aligned}$$

The two zeroes appearing for $G_{pend\text{-}rotor}$ are both at the origin.

Design of a SISO PID controller proceeds using frequency response methods. The design objectives for this example will include:

- 3) Phase margin is greater than 30 degrees [Seborg_1989]

An additional constraint is to meet maximum bandwidth requirements. The Integrated Rotary Inverted Pendulum includes a first order low pass filter in its computation of derivative. This well-known method is required to reduce the influence of noise in this computation.[Astrom_2008] The Integrated Rotary Inverted Pendulum may be adjusted. However, its default value is 5 Hz or 31.4 rad/sec. This means that the maximum bandwidth for the controller should also be set to 31.4 rad/sec. This finally leads to one more requirement on the Phase Cross-Over Frequency (the frequency where phase crosses -180 degrees).

- 4) Phase Cross-Over Frequency is approximately 31 rad/sec.

Subsequent to design, stability for this example will be determined by examination of both Bode and Nyquist characteristics

First, a PID controller is selected. Second, for this controller integral and derivative time constants are selected. The Bode plot of the Pendulum-Rotor plant is shown in *Figure 62*. The influence of poles near 6.46 rad/sec and -0.6 rad/sec is observed.

As a first design choice, the integral time constant is selection is made to be 5.0 seconds corresponding to a value approximately one third that of the frequency of the pole at 0.56 rad/sec. The derivative time constant is set at 0.15 seconds, corresponding to the frequency of the pole at 6.46 rad/sec. These values are:

$$T_i = 5.0 \text{ sec} \text{ and } T_d = 0.15 \text{ sec}$$

The form of this PID controller is then,

$$K_{pend}(s) = K \left(1 + \frac{1}{T_i s} + T_d s \right)$$

where K will be found via Frequency Response design methods.

The open loop system is

$$G_{open-loop} = G_{rotor}G_{pend}K_{pend}(s)$$

The Bode plot for this controller, K_{pend} , the Pendulum and Rotor Plant, $G_{pendulum}G_{rotor}$, and for the open loop combined plant and controller, $K_{pend}G_{pendulum}G_{rotor}$, is shown in *Figure 63* for $K = 1$.

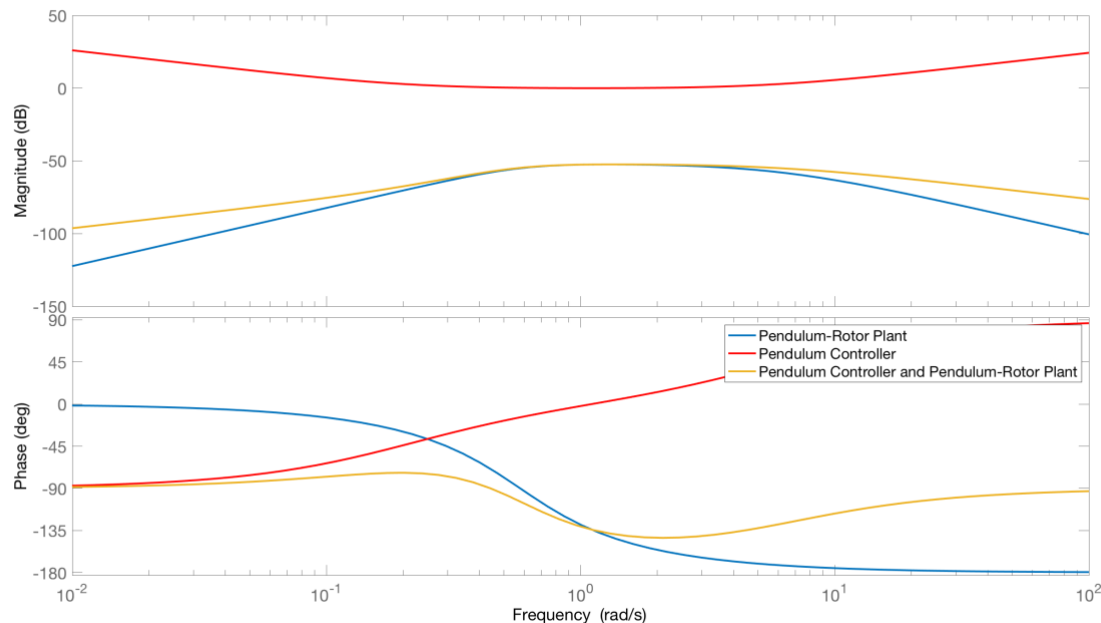


Figure 63. The Bode plot of the Pendulum and Rotor plant, Pendulum controller, and the open loop controller – plant product transfer function is shown for gain, K, of unity.

The next step in design is the selection of the gain K. This will be subject to the following objectives:

- 1) The Nyquist Criterion will be met for the plant.
- 2) The Bode characteristic of the plant displays a Phase Margin greater than 30 degrees.
- 3) The maximum values of both the Sensitivity Function and Complimentary Sensitivity Function will be minimized.
- 4) The maximum value of the Noise Sensitivity Function will also be minimized.

The latter requirement relies on the Sensitivity Function defined as

$$S(s) = \frac{1}{1 + T_{rotor-angle}(s)K_{rotor}(s)}$$

$$T(s) = \frac{T_{rotor-angle}(s)K_{rotor}(s)}{1 + T_{rotor-angle}(s)K_{rotor}(s)}$$

The maximum value for the range of $s = 0$ to $s = \infty$ will be computed for each with

$$M_S = \max_{0 \leq \omega < \infty} |S(j\omega)|$$

and

$$M_T = \max_{0 \leq \omega < \infty} |T(j\omega)|$$

These values measure the robustness of the control system to variations in plant characteristics.

The third important metric is the Noise Sensitivity function that determines the susceptibility of the control system to errors introduced by measurement noise.

The Noise Sensitivity Function is

$$NS(s) = \frac{K_{rotor}(s)}{1 + T_{rotor-angle}(s)K_{rotor}(s)}$$

The maximum value for the range of $s = 0$ to $s = \infty$ will be computed with

$$M_{NS} = \max_{0 \leq \omega < \infty} |NS(j\omega)|$$

The first choice of gain will be $K = 1$. *Figure 64* displays the Bode plot for $K = 1$ with Gain and Phase margins. These are clearly excessive and will result in slow system response.

The next choice of gain will be $K = 4000$. *Figure 65* displays the Bode plot for $K = 4000$ with Gain and Phase margins. The Phase margin is less than the design objective and the Phase Cross Over Frequency is greater than the objective.

The Nyquist Criterion may also be tested for indication of stability. First, for $K = 4000$, the poles of the closed loop system, zeroes of $1 + G_{rotor}G_{pend}K_{pend}(s)$ are

$$\begin{aligned} & 0.0000 + 0.0000i \\ & -13.5778 + 54.7503i \\ & -13.5778 - 54.7503i \\ & -5.1847 + 0.0000i \\ & -0.3180 + 0.0000i \\ & 0.1224 + 0.0000i \end{aligned}$$

Then, the poles of $G_{rotor}G_{pend}K_{pend}(s)$ are

$$\begin{aligned} & 0.0000 + 0.0000i \\ & -31.4159 + 0.0000i \\ & 6.4577 + 0.0000i \\ & -6.4577 + 0.0000i \\ & -0.5600 + 0.4200i \\ & -0.5600 - 0.4200i \end{aligned}$$

Then, the number of zeroes of $1 + G_{rotor}G_{pend}K_{pend}(s)$ in the right half plane, $Z = 1$. Also, the number of poles, of $G_{rotor}G_{pend}K_{pend}(s)$ in the right half plane, $P = 1$. Then, the number of clockwise encirclements of the point, $s = -1$, is zero.

Figure 66 displays the Nyquist plot for $K = 4000$. This behavior is consistent with stability since no encirclement of the $s = -1$ point occur.

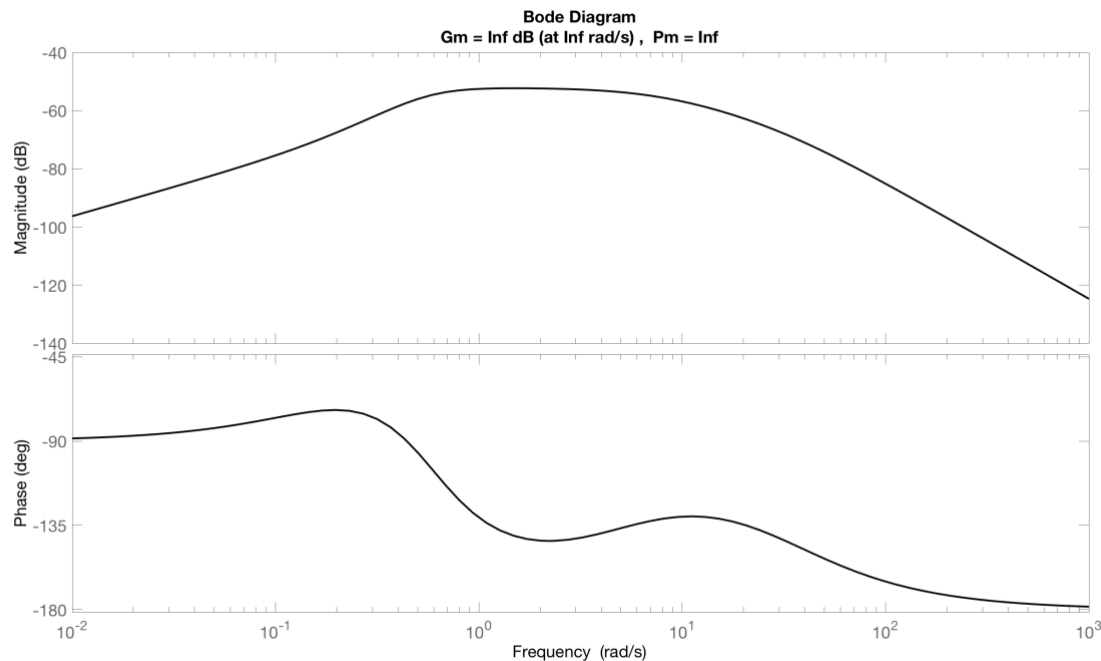


Figure 64. The Bode plot of the Pendulum and Rotor plant with gain and phase margin is shown for gain, K , of unity.

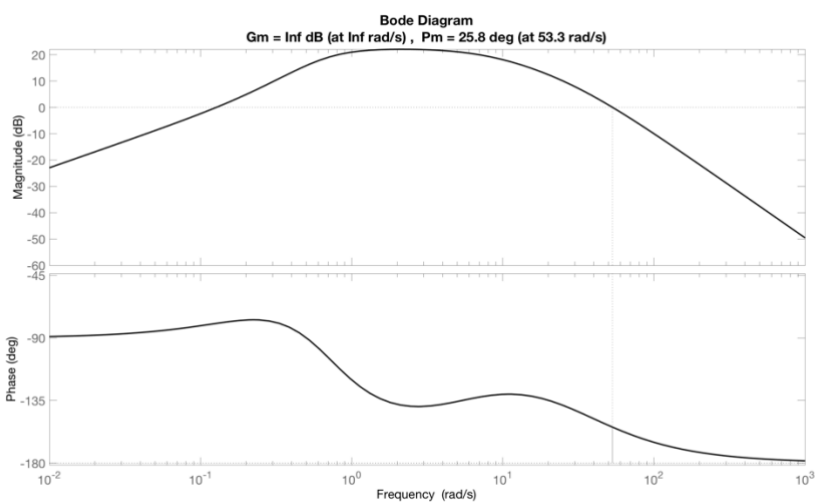


Figure 65. The Bode plot of the Pendulum and Rotor plant with gain and phase margin is shown for gain, K , of 4000.

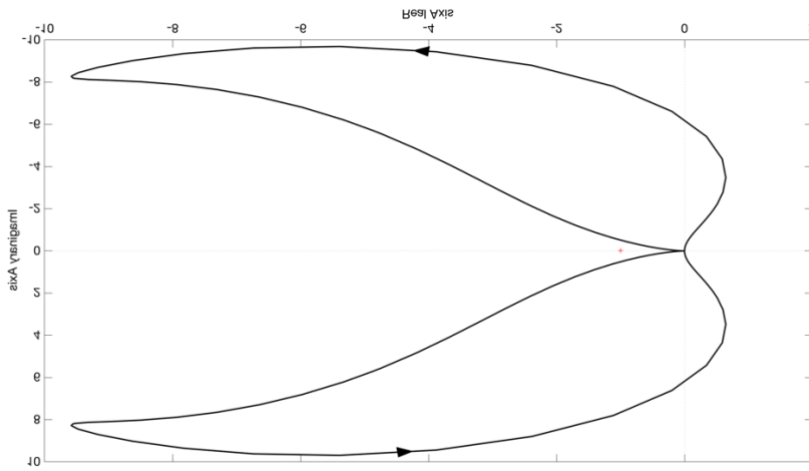


Figure 66. The Nyquist plot of the Pendulum and Rotor plant for gain, K , of 4000.

Now, adjustment of gain may continue. A selection of $K = 2000$ produces the Bode plot of Figure 67. The Phase Margin and Phase Cross-Over Frequency are consistent with design objectives.

The poles appearing for the open loop transfer function, $G_{rotor}G_{pend}K_{pend}(s)$ are:

$$\begin{aligned} & 0.0000 + 0.0000i \\ & -31.4159 + 0.0000i \\ & 6.4577 + 0.0000i \\ & -6.4577 + 0.0000i \\ & -0.5600 + 0.4200i \\ & -0.5600 - 0.4200i \end{aligned}$$

The closed loop poles, zeroes of $1 + G_{rotor}G_{pend}K_{pend}(s)$ are

$$\begin{aligned} & 0.0000 + 0.0000i \\ & -13.6743 + 36.5023i \\ & -13.6743 - 36.5023i \\ & -5.1253 + 0.0000i \\ & -0.3198 + 0.0000i \\ & 0.2578 + 0.0000i \end{aligned}$$

Then, the number of zeroes of $1 + G_{rotor}G_{pend}K_{pend}(s)$ in the right half plane, Z = 1. Also, the number of poles, of $G_{rotor}G_{pend}K_{pend}(s)$ in the right half plane, P = 1. Then, the number of clockwise encirclements of the point, s = -1, is zero.

Figure 68 displays the Nyquist plot for K = 2000. This behavior is consistent with stability since no encirclement of the s = -1 point occurs.

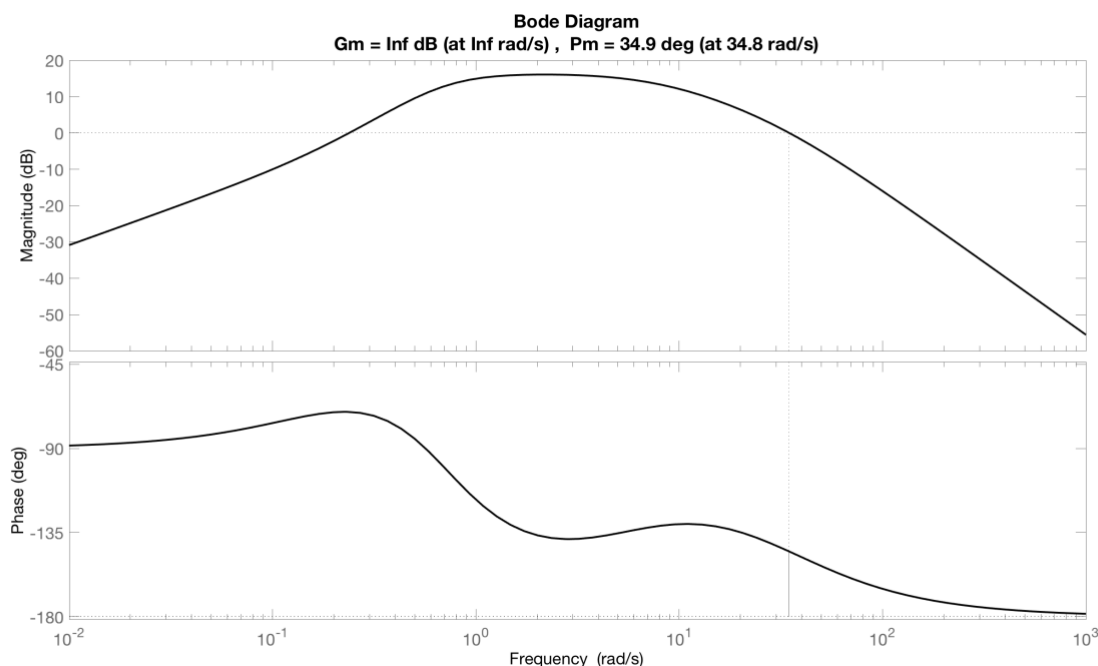


Figure 67. The Bode plot of the Pendulum and Rotor plant with gain and phase margin is shown for gain, K, of 2000.

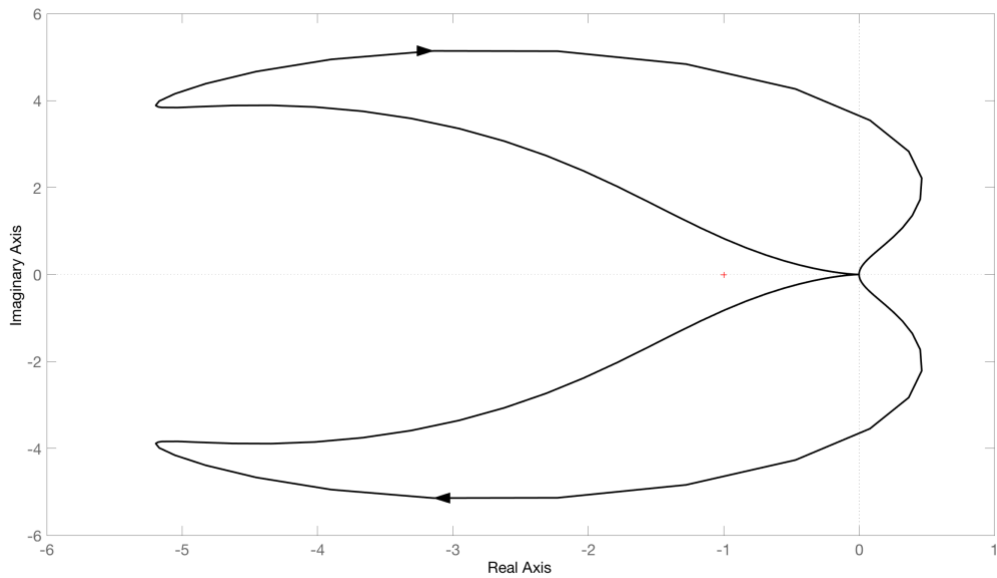


Figure 68. The Nyquist plot of the Pendulum and Rotor plant for gain, K , of 2000.

The dependence of M_s , M_T , and M_{NS} on selection of Gain K will can be evaluated for a range of gain values. The values of each is listed below in Table 8 along with the values of Phase Margin, and Phase Cross Over Frequency for K values of 1000, 2000, and 4000.

Gain	M_s	M_T	M_{NS}	Phase Margin (degrees)	Phase Cross Over Frequency (rad/sec)
1000	1.56	1.34	20013.6	44.6	20.8
2000	1.91	1.67	39999.6	34.9	34.8
4000	2.44	2.24	999969.6	25.8	53.3

Table 8. Values of M_s , M_T , and M_{NS} Phase Margin, and Phase Cross Over Frequency for selections of Gain, K .

The gain value of 2000 is selected as meeting objectives for Phase Margin with relative low values of M_s and M_T , and also yielding an intermediate value of Noise Sensitivity, M_{NS} .

Using this gain, the PID controller becomes

$$K_{rotor}(s) = K_{p-rotor} + \frac{K_{i-rotor}}{s} + K_{d-rotor}s$$

with

$$K_{p-pend} = 2000, \quad K_{i-pend} = K/T_i = 400, \quad K_{d-pend} = KT_d = 300$$

Also, the impulse response of Pendulum angle is shown in *Figure 51*. Note that impulse response characteristic indicates stability. However, this SISO system does not control Rotor Angle. The impulse here induces a drift in Rotor Angle and ultimately unstable behavior. This requires a second controller as described further below and in the next section.

The Integrated Rotary Inverted Pendulum system may be configured with these PID controller values. Suppression of noise resulting from finite resolution and decimation of rotor and encoder angle is provided by a first order filter at corner frequency 5 Hz applied to the derivative computation.

Figure 69 shows experimental system response. It is noted that Pendulum Angle is maintained near zero as required by the system design. Note that the discrete steps associated with the finite resolution of the Pendulum Angle sensor is revealed in this data.

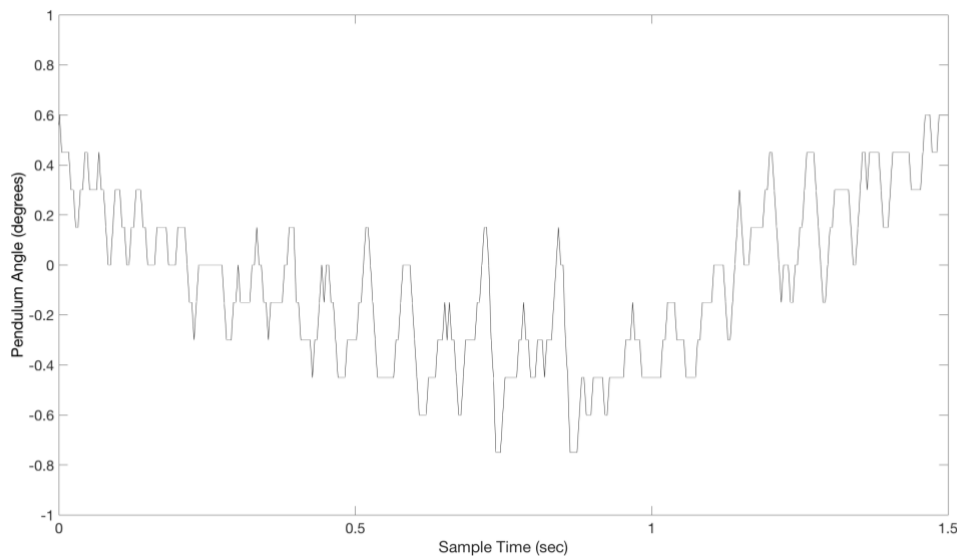


Figure 69. Experimental closed loop operation of the Single Input Single Output PID control system showing Pendulum angle variation. Stable operation is demonstrated. The individual steps observed in this time series data corresponds to the discrete steps in angle measurement by the digital optical encoder.

As noted previously, an important limitation of this Single Input Single Output (SISO) controller appears. Specifically, while the controller stabilizes Pendulum Angle, Rotor Angle does not appear as an input and is not stabilized. Thus, a disturbance in Rotor position is not compensated for by this controller.

The limitations of SISO control may be characterized directly. The response of Rotor Angle, ϕ_{rotor} , to a signal applied to $\theta_{reference}$ may be computed. Examining *Figure 60*, the transfer function from $\theta_{reference}(s)$ to $\phi_{rotor}(s)$ is

$$T_{Rotor-Response} = \frac{\phi_{rotor}(s)}{\theta_{reference}(s)} = \frac{G_{rotor}K_{pend}}{1 + G_{pend}G_{rotor}K_{pend}}$$

The computed response of Rotor Angle, ϕ_{rotor} , to an impulse applied to Pendulum references angle, $\theta_{reference}$, is shown in *Figure 70*. This demonstrates that this SISO system may stabilize Pendulum Angle, but not Rotor Angle. The experimentally measured response of Rotor Angle shown in *Figure 71* confirms that the Rotor Angle is not controlled by this SISO system.

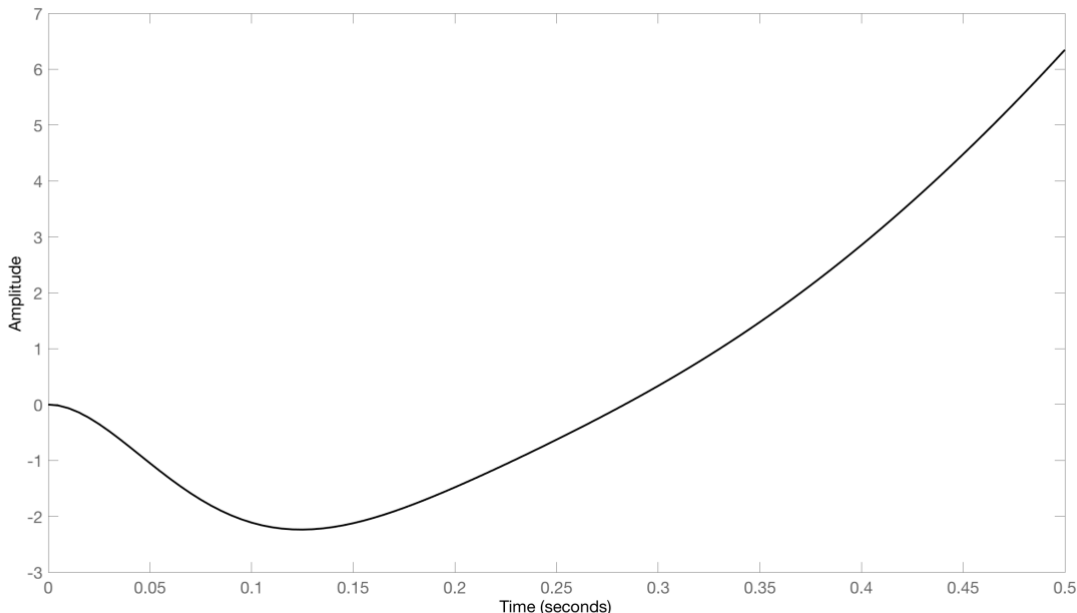


Figure 70. Simulated response of Rotor Angle, ϕ_{rotor} , to an impulse signal applied to Pendulum angle reference, $\theta_{reference}$, at $t = 0$ computed by simulation of the Integrated Rotary Inverted Pendulum. Note the drift in Rotor Angle. During this period, Pendulum Angle remains constant and near zero.

As an experimental example, the Pendulum position for the Integrated Rotary Inverted Pendulum was disturbed, leading to a drift in Rotor position shown in *Figure 71*.

The next section describes the addition of a second PID controller that provides Rotor Angle stabilization relative to a tracking command.

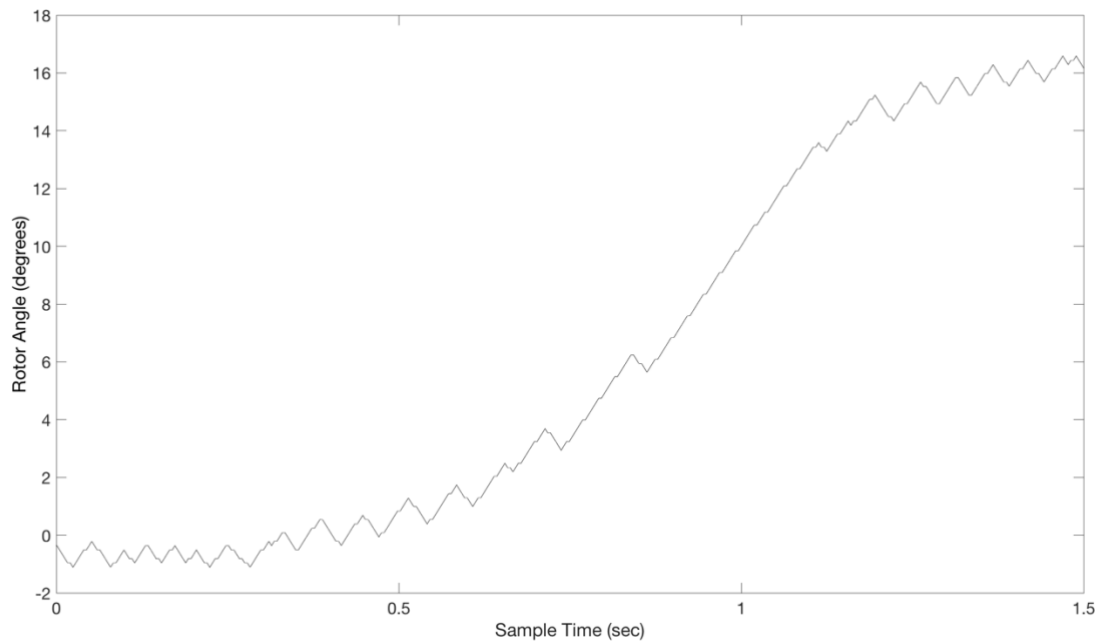


Figure 71. Response of Rotor Angle of the Integrated Rotary Inverted Pendulum as a result of a disturbance applied at $t = 0$. The drift observed is the result of the limitation of this Single Input Single Output controller that stabilizes Pendulum Angle but not Rotor Angle.

Now, as noted, this SISO system controls only Pendulum Angle by providing control input to the Rotor Angle motor actuator. Rotor Angle relative to a tracking reference is not controlled by this SISO system. Thus, Rotor Angle drifts as shown in Figure 71.

Instead a second PID control system is introduced in the next Section that applies rotor angle control input to stabilize rotor angle and enable tracking of a rotor angle command input.

13. Inverted Pendulum Dual PID Controller: Frequency Response Design

The introduction of a second PID controller may enable stabilization of Rotor Angle. This will be accomplished by introducing an Inner Loop and Outer Loop.

The design process will include the steps of:

- 1) Design of Single PID Controller, $K_{pend}(s)$
- 2) Definition of Inner Control Loop including $K_{pend}(s)$
- 3) Definition of Outer Control Loop integrating the Inner Control Loop and a new controller, $K_{rotor}(s)$
- 4) Design of the Rotor Control system, $K_{rotor}(s)$.

The Inner Loop controller will depend on the design of $K_{pend}(s)$ in section 0. This will be held constant while a new Outer Loop controller of Rotor Angle, $K_{rotor}(s)$, is added.

The Inner Loop Controller defines a transfer function from a Rotor Angle Control signal, $\phi_{rotor-control}$ to the Rotor Angle, ϕ_{rotor} . The Outer Loop Controller provides control of Rotor Angle, Rotor Angle, ϕ_{rotor} to a Rotor Angle Tracking Command, $\phi_{rotor-tracking}$.

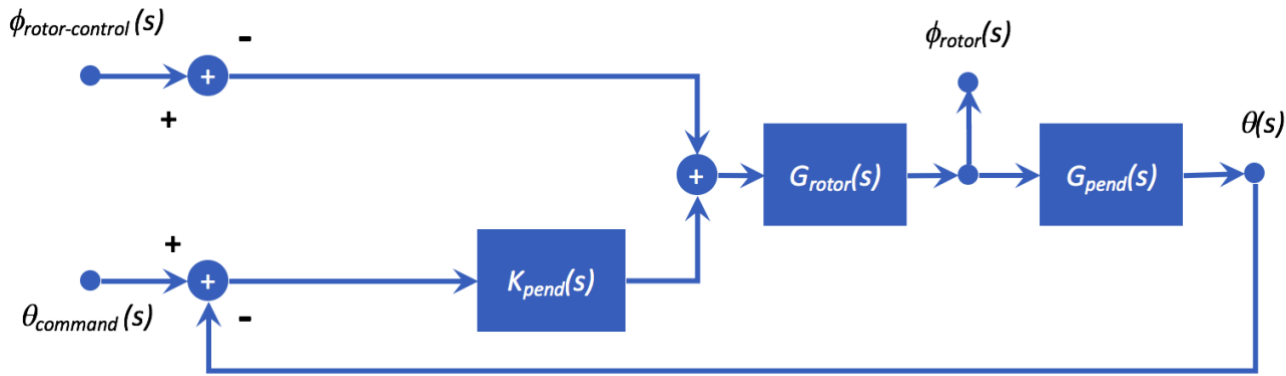


Figure 72. Dual PID Control System Inner Control Loop

Now, the Rotor Angle Control transfer function, $T_{rotor-angle}(s)$ between $\phi_{rotor-control}$ and ϕ_{rotor} will be determined. The input signal, $\theta_{command}(s)$, will be held zero. A summing junction appears at the input to the Pendulum transfer function, $G_{pendulum}$.

$$\phi_{rotor}(s) = (\phi_{rotor}(s)G_{pendulum}(s)K_{pendulum} - \phi_{rotor-control}(s)) G_{rotor}(s)$$

$$T_{rotor-angle}(s) = \frac{\phi_{rotor}(s)}{\phi_{rotor-command}(s)}$$

and

$$T_{rotor-angle}(s) = \frac{-G_{rotor}(s)}{1 + G_{pend}(s)K_{pend}(s) G_{rotor}(s)}$$

This Rotor Angle Control system now introduces the Outer Loop controller to enable control of Rotor Angle. Here, the difference between a Rotor Angle tracking command, $\phi_{rotor-tracking}(s)$ and Rotor Angle, $\phi_{rotor}(s)$, is supplied as an error signal to a new controller, K_{rotor} , and summed with the output of the Pendulum Angle Controller, $K_{pendulum}$ as shown in *Figure 73*.

During subsequent design steps, the configuration of $K_{pend}(s)$ will remain fixed.

The Outer Loop controls ϕ_{rotor} with the goal of tracking the input, $\phi_{rotor-tracking}$.

By definition

$$\phi_{rotor} = \phi_{rotor-command}(s)T_{rotor-angle}(s)$$

Thus, the transfer function from $\phi_{rotor-tracking}$ to ϕ_{rotor} is

$$T_{rotor-tracking}(s) = \frac{\phi_{rotor}(s)}{\phi_{rotor-command}(s)} = \frac{T_{rotor-angle}(s)K_{rotor}(s)}{1 + T_{rotor-angle}(s)K_{rotor}(s)}$$

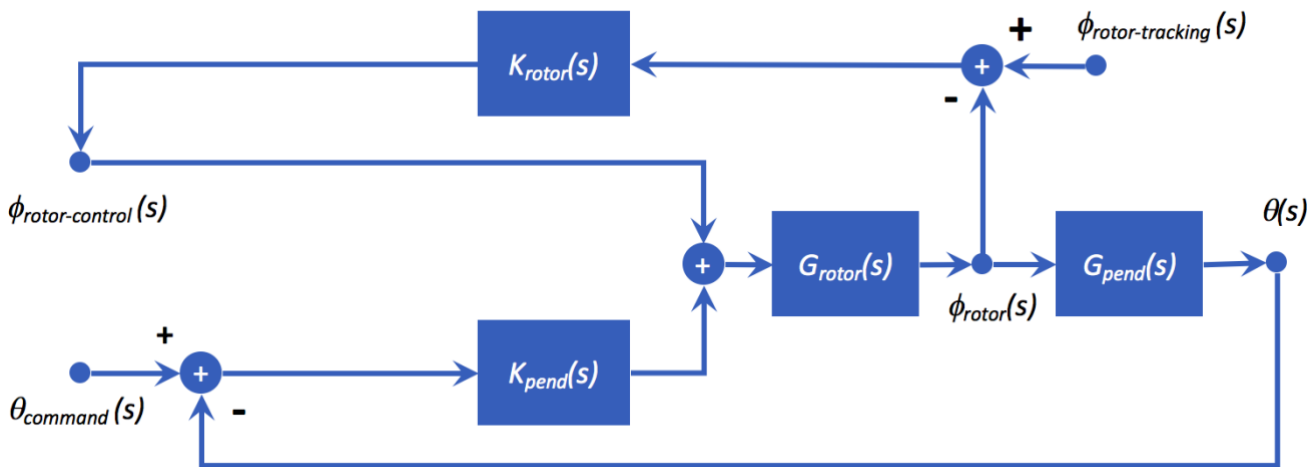


Figure 73. Dual PID Control System Inner and Outer Control Loop

Design of K_{rotor} begins with selection of integral time constant, T_{i-r} , and derivative time constant, T_{d-r} . This is followed by selection of controller gain, K . The form of this controller is:

$$K_{rotor}(s) = K \left(1 + \frac{1}{T_{i-r}s} + T_{d-r}s \right)$$

The selection of optimal values for T_{i-r} , T_{d-r} and K , can also include selection of values for T_i , T_d and K for the Pendulum Angle control PID loop.

To review the characteristics of the Single PID Inverted Mode Pendulum controller of section 0, the closed loop poles, zeroes of $1 + G_{rotor}G_{pend}K_{pend}(s)$ were determined to be:

$$\begin{aligned} & 0.0000 + 0.0000i \\ & -13.6743 + 36.5023i \\ & -13.6743 - 36.5023i \\ & -5.1253 + 0.0000i \\ & -0.3198 + 0.0000i \\ & 0.2578 + 0.0000i \end{aligned}$$

Thus, the integral time constant, T_{i-r} , is then set at the conservative value of 20 seconds. The derivative time constant, T_{d-r} , is set at 4 seconds corresponding to the dominant pole at 0.26 rad/sec. The selected values are.

$$\begin{aligned} T_{i-r} &= 20s \\ T_{d-r} &= 4s \end{aligned}$$

The values may be adjusted after the next cycle of design. These adjustments will be made to meet the design goals described next.

The next step in design is the selection of the gain K . This will be subject to the following objectives:

- 1) The Nyquist Criterion will be met for the plant.
- 2) The Bode characteristic of the plant displays a Phase Margin greater than 30 degrees.
- 3) The maximum values of both the Sensitivity Function and Complimentary Sensitivity Function will be minimized.
- 4) The maximum value of the Noise Sensitivity Function will also be minimized.

As a third example, the value of $K = 2$ is selected. The Bode plot, Nyquist characteristic, and Sensitivity Function plot are shown in *Figure 77*.

As a first example, the value of $K = 8$ is selected. The Bode plot, Nyquist characteristic, and Sensitivity Function plot are shown in *Figure 74..*

As a second example, the value of $K = 4$ is selected. The Bode plot, Nyquist characteristic, and Sensitivity Function plot are shown in *Figure 75.*

For each gain value, N , the number of unstable poles of the plant, $T_{rotor-angle}(s)K_{rotor}(s)$ is one. For each gain value, the number, P , of right half plane zeroes of $1 + T_{rotor-angle}(s)K_{rotor}(s)$ is zero. Therefore, with $N = P - N = -1$, stability requires one encirclement of $s = -1$ in the counterclockwise direction appear in the Nyquist characteristic. Thus, stability is indicated for the gain values of $K = 4$ and $K = 8$.

However, the Gain value of $K = 2$ produces an unstable system with no counterclockwise of of $s = -1$ as shown in *Figure 74.*

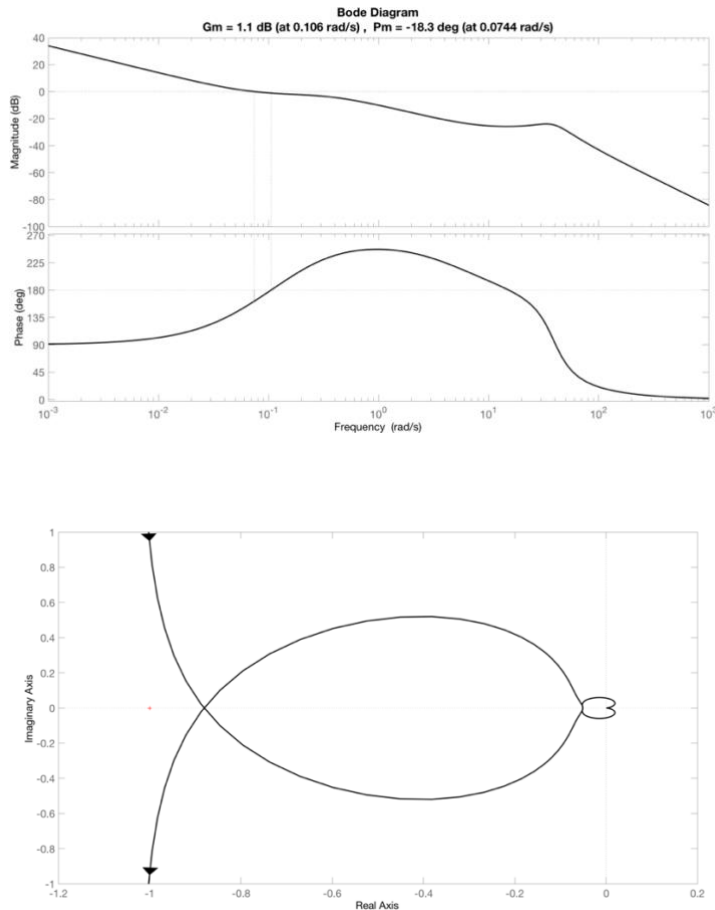


Figure 74. The Bode plot (upper panel) and Nyquist characteristic (lower panel) for $K = 2$. The unstable characteristics for this gain selection are observed in both the negative phase margin as well as the lack of an encirclement of the point $s = -1$.

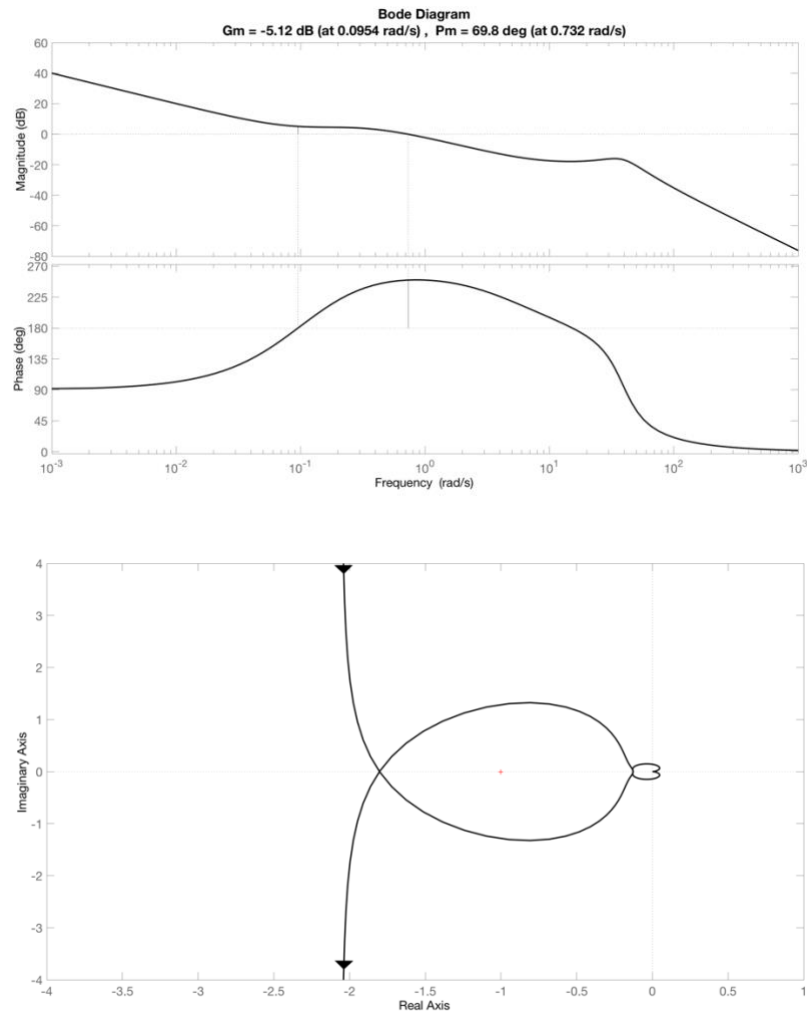


Figure 75. The Bode plot (upper panel) and Nyquist characteristic (lower panel) for $K = 4$. The stable characteristics for this gain selection are observed in both the positive phase margin as well as the counterclockwise encirclement of the point $s = -1$.

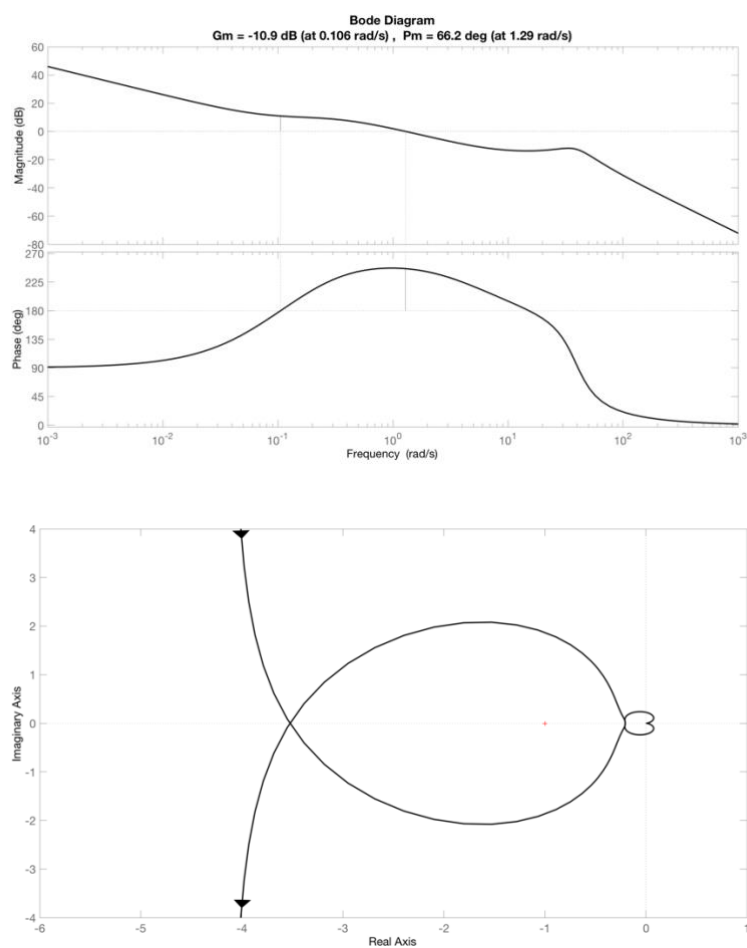


Figure 76. The Bode plot (upper panel), Nyquist characteristic (lower panel) for $K = 8$. The stable characteristics for this gain selection are observed in both the positive phase margin as well as the counterclockwise encirclement of the point $s = -1$.

Each of the examples shown indicate stable operation based on evaluation of the Bode plot Phase Margin.

The dependence of M_S , M_T , and M_{NS} on selection of Gain K will can be evaluated for a range of gain values. The values of each is listed below in Table 9 along with the values of Phase Margin, and Phase Cross Over Frequency for K values of 2, 4, and 8.

Gain	M_s	M_T	M_{NS}	Phase Margin (degrees)	Phase Cross Over Frequency (rad/sec)
2				-18.3	0.07
4	1.29	2.27	631.9	69.8	0.73
8	1.28	2.41	1012.6	66.2	1.29

Table 9. Values of M_s , M_T , and M_{NS} Phase Margin, and Phase Cross Over Frequency for selections of Gain, K. Note that the Gain of K = 2 produces an unstable solution.

The value of gain, K = 4, is selected due to its Phase Margin meeting the design objective and intermediate value of Noise Sensitivity, M_{NS} , and low values of M_s and M_T .

Using this gain value, the PID controller becomes

$$K_{rotor}(s) = K_{p-rotor} + \frac{K_{i-rotor}}{s} + K_{d-rotor}s$$

with

$$K_{p-rotor} = 4.0, \quad K_{i-rotor} = K/T_{i-r} = 0.2, \quad K_{d-rotor} = KT_{d-r} = 16.0$$

Simulated system response to a step input to $\phi_{rotor-command}$, shown in Figure 77 displays stable operation.

Experimentally measured system response to a step input to $\phi_{rotor-command}$, shown in Figure 78, also displays stable operation with a Maximum Overshoot and Time to First Peak value similar to that of the simulated response.

Further development of Dual PID design may continue. However, the challenge for optimizing this MIMO system are clear. The next section introduces Modern Control methods that enable direct optimization of controller design for this system. This produces a dramatic performance advance in overshoot and response time characteristics.

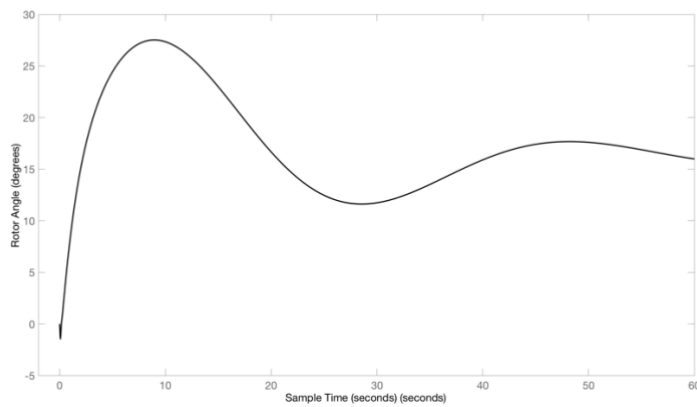


Figure 77. Simulated Rotor Angle response of the Dual PID Control System response for a step input of amplitude 20 degrees to the Rotor Angle command input applied at $t = 0$.

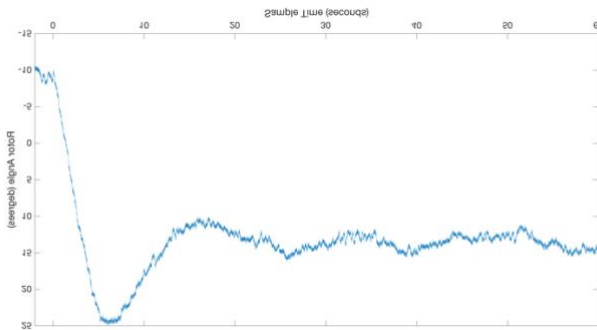


Figure 78. Experimental measurement of Rotor Angle response of the Dual PID Control System response for a step input of amplitude 20 degrees to the Rotor Angle command input applied at $t = 0$.

14. Inverted Pendulum Dual PID Controller: Control of and Unstable Plant

The previous sections have described methods for introduction of Dual PID controller systems for control of the MIMO Integrated Rotary Inverted Pendulum requiring stabilization of both Pendulum Angle and Rotor Angle.

An additional design method for the Integrated Rotary Inverted Pendulum is based on the development of a Rotor Angle Controller with specified and static Controller configuration. Then, design of Pendulum Angle stabilizing controllers is directed to PID controller design including a specified Rotor Angle Transfer Function.

First, the conditions for stabilizing the unstable Inverted Pendulum plant are introduced.

A control system for stabilizing the Pendulum Angle, $\theta_{Pendulum}(s)$ in an inverted position relies on actuation of Rotor Angle, $\phi_{Rotor}(s)$. A controller of Pendulum Angle, $K_{Pend}(s)$, is introduced as shown in Figure 79.

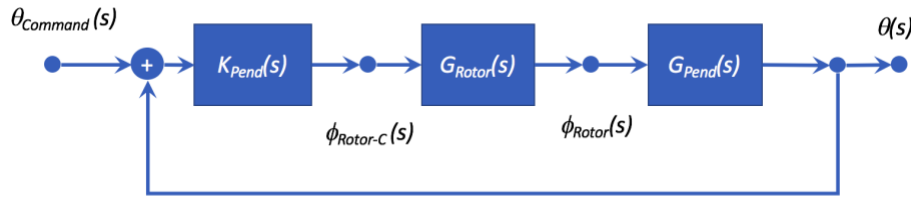


Figure 79.. The Rotary Inverted Pendulum feedback controller of Pendulum Angle.

Evaluating conditions for stability relies on the theory of Strongly Stabilizable systems by Youla. [Youla_1974]. This states that:

A plant is strongly stabilizable if and only if it has an even number of real poles between every pair of real zeros for $Re(s) \geq 0$ including zeroes at $s = \infty$.

Recalling the $G_{Rotor}(s)G_{Pendulum}(s)$ plant of Section 12, the poles of this plant are:

$$\begin{aligned} & 6.4577 + 0.0000i \\ & -6.4577 + 0.0000i \\ & -0.5600 + 0.4200i \\ & -0.5600 - 0.4200i \end{aligned}$$

Also, two zeroes exist for this plant at $s = 0$.

The $G_{Rotor}(s)G_{Pendulum}(s)$ plant does not satisfy the condition since first, there is one RHP pole. However, between the pair of zeroes at $s = \infty$. for $Re(s) \geq 0$ and the zero at $s = \infty$. (Please see the Bode plot of $G_{Rotor}(s)G_{Pendulum}(s)$ in *Figure 90*.)

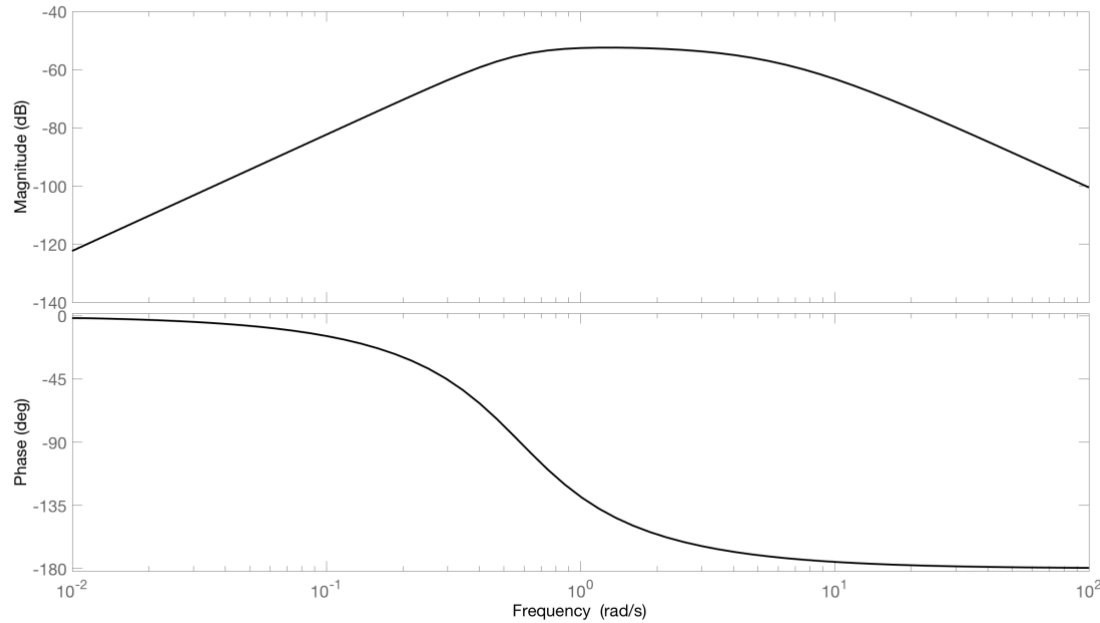


Figure 80. The Bode plot of Pendulum-Rotor plant, $G_{Rotor}(s)G_{Pendulum}(s)$, is shown.

One solution for achieving stability is to modify the system to include dual controllers forming Inner Loop and Outer Loop Controllers as shown in *Figure 90*. Here, $K_{pend}(s)$ of Figure 79 forms the Outer Loop Controller. The addition of a second Inner Loop controller to the system architecture permits addition of a new RHP pole.

It is important to note that since the new Inner Loop controller introduces a RHP pole, it is *unstable*. However, its introduction, along with a stable Outer Loop controller will produce a stable, close loop system.

The Inner Loop operates on Rotor Angle and the Outer Loop on Pendulum Angle as shown in Figure 81.

The Inner Loop transfer function from Rotor Angle Control input to Rotor Angle, is

$$T_{Rotor}(s) = \frac{\phi_{Rotor}(s)}{\phi_{Rotor-C}(s)} = \left(\frac{G_{Rotor}(s)}{1 + K_{Rotor}(s)G_{Rotor}(s)} \right)$$

The transfer function, $T_{Rotor}(s)$, now replaces the actuator transfer function, $G_{Rotor}(s)$, to produce the new architecture of Figure 82.

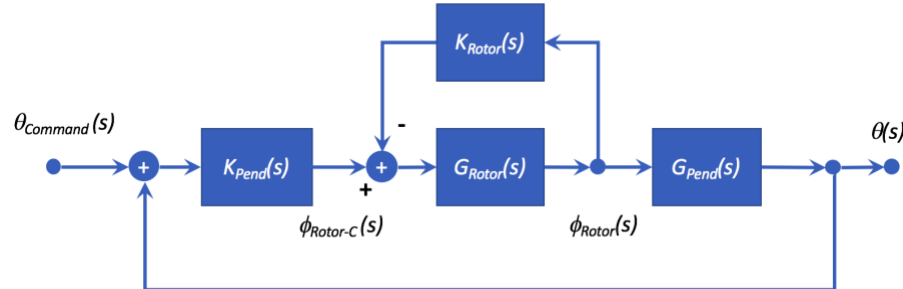


Figure 81. The Inner and Outer Loop control system introduced to create a Strongly Stabilizable system.

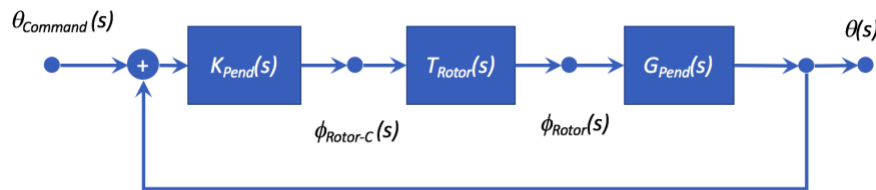


Figure 82. The Inner and Outer Loop Control system with the Inner Loop transfer function represented by $T_{Rotor}(s)$.

The transfer function, $T_{Rotor}(s)$ is based on LQR design and is specified as:

$$T_{Rotor}(s) = \frac{\phi_{Rotor}(s)}{\phi_{Rotor-C}(s)} = \left(\frac{a_{Rotor}}{s^2 - b_{Rotor}s - c_{Rotor}} \right)$$

with $a_{Rotor} = 0.245$, $b_{Rotor} = 1.367$, $c_{Rotor} = 0.549$.

Poles of T_{Rotor} are:

$$\begin{array}{l} 1.6915 \\ -0.3245 \end{array}$$

Inspection of T_{Rotor} shows that this introduces an unstable RHP pole at $s = 1.6915$. Thus, in combination with $G_{Pendulum}(s)$, the plant of $G_{Pendulum}(s)T_{Rotor}(s)$ now includes these poles:

$$\begin{array}{l} -6.4577 \\ 6.4577 \\ 1.6915 \\ -0.3245 \end{array}$$

This system now satisfies the criteria for strongly stabilizable systems since there are now an even number even number of real poles between every pair of real zeros for $\text{Re}(s) \geq 0$ including zeroes at $s = \infty$. The Root Locus plot of $G_{\text{Pendulum}} T_{\text{Rotor}}$ is shown in Figure 83.

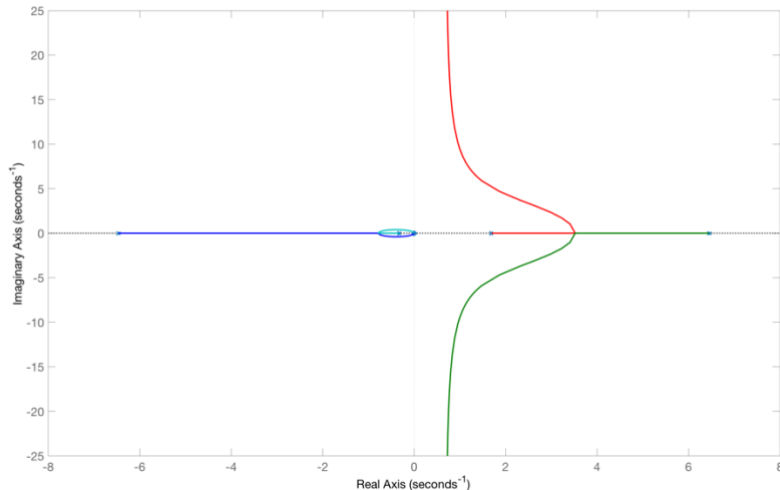


Figure 83. The Root Locus plot of $G_{\text{Pendulum}} T_{\text{Rotor}}$.

Design of a SISO PID controller proceeds using root locus methods. The design objectives for this example will include:

- 5) A damping defined by a Maximum Overshoot, $M_p = 0.1$
- 6) A natural frequency defined by a Time to First Peak, T_p , of 8 seconds

Subsequent to design, stability for this example will be determined by ensuring that

- 2) Phase margin is greater than 30 degrees [Seborg_1989]
- 3) Gain margin is greater than 2 dB [Seborg_1989]

First, a PID controller is selected. Second, for this controller integral and derivative time constants are selected. The Bode plot of the Pendulum-Rotor plant is shown in Figure 47. The influence of poles near 6.46 rad/sec and 0.56 rad/sec is observed.

As a first design choice, the integral time constant is set to the conservative value of 5.0 seconds corresponding to one third of the frequency of the pole at 0.56 rad/sec. The derivative time constant is set at 0.15 seconds, corresponding to the frequency of the pole at 6.46 rad/sec. These values are:

$$T_i = 20.0 \text{ sec} \text{ and } T_d = 0.1 \text{ sec}$$

The form of this PID controller is then,

$$K_{pend}(s) = K \left(1 + \frac{1}{T_i s} + T_d s \right)$$

where K will be found via Root Locus design methods.

The Bode plot for this controller, K_{pend} , the Pendulum and Rotor Plant, $G_{pendulum}G_{rotor}$, and for the open loop combined plant and controller, $K_{pend}G_{pendulum}G_{rotor}$, is shown in

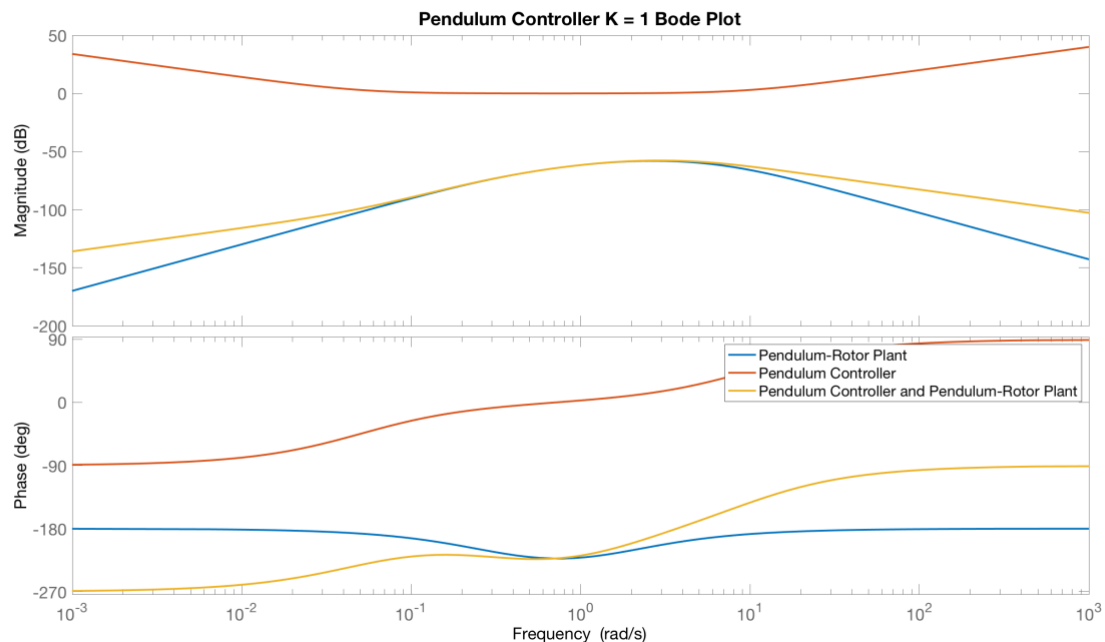


Figure 84. The Bode plot of the Pendulum and T_{rotor} plant, Pendulum controller, and the open loop controller – plant product transfer function is shown for gain, K, of unity.

The controller closed loop response will approximate a second order response and therefore the properties of second order systems can be applied to determine its Natural Frequency, ω_N , and Damping Ratio, ζ , by specifying a Maximum Overshoot, $M_p = 0.1$. [Astrom_2008]

A Damping Ratio is selected based on the criteria for a maximum overshoot. [Nise_2015]

$$\text{Damping Ratio} = \sqrt{\frac{\ln^2(M_p)}{\pi^2 + \ln^2(M_p)}}$$

This produces a Damping Ratio, ζ , of 0.69.

Then, we will select a target Time to First Peak, T_p , of 8 seconds and estimate a corresponding natural frequency. This can be estimated with [Nise_2015]

$$\omega_N = \frac{\pi}{T_p \sqrt{1 - \zeta^2}}$$

This produces a Natural Frequency, ω_N , of 0.46 rad/sec or 2.89 Hz.

The open loop system is

$$G_{open-loop} = G_{rotor} G_{pend} K_{pend}(s)$$

The Root Locus plot for this system is shown in *Figure 85*.

The Root Locus plot shows an arc of constant natural frequency of $\omega_N = 0.46 \text{ rad/sec}$. Also, the lines emanating at the origin are lines of constant Damping Ratio such that points between these lines correspond to solutions with Damping Ratio, ζ , greater than 0.59.

Thus, using Matlab rlocfind, we select a point on the real axis at the intersection of the real axis and the arc of constant natural frequency. This point is indicated by the crosshair symbol on the negative real axis near the arc of $\omega_N = 0.46 \text{ rad/sec}$.

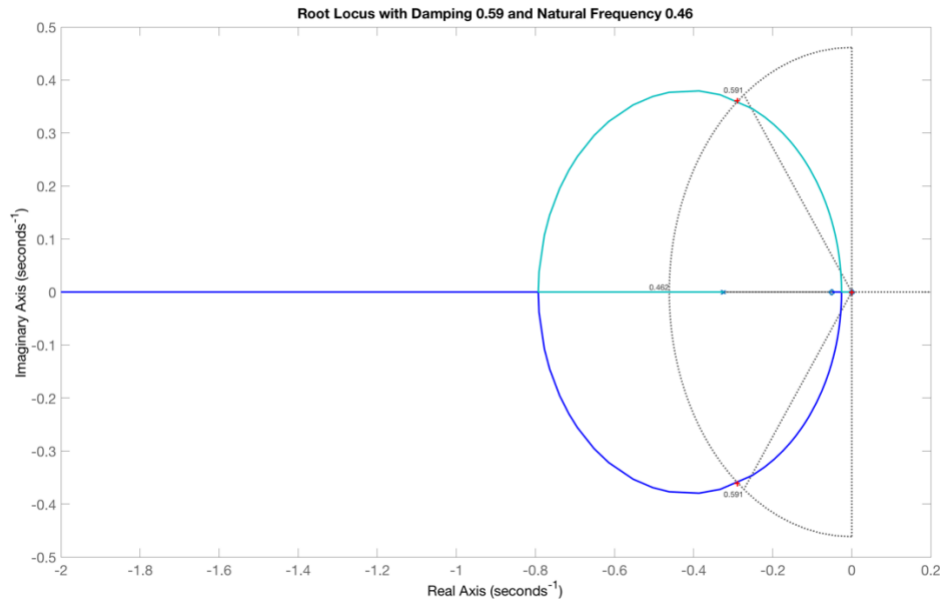


Figure 85. The Root Locus plot of the open loop control system including controller and plant product transfer function is shown. The Matlab rlocfind method has been used to select a point where the arc of constant natural frequency intersects the negative real axis.

This yields a value of gain of $K = 2154.3$. Using this gain scale factor value, the PID controller becomes

$$K_{pend}(s) = K_{p-pend} + \frac{K_{i-pend}}{s} + K_{d-pend}s$$

with

$$K_{p-pend} = 2154.3, \quad K_{i-pend} = K/T_i = 107.7, \quad K_{d-pend} = KT_d = 215.4$$

The poles appearing for the open loop transfer function, $T_{rotor}G_{pend}K_{pend}(s)$ are:

$$\begin{array}{l} 0.0 \\ -31.4159 \\ -6.4577 \\ 6.4577 \\ 1.6915 \\ -0.3245 \end{array}$$

The closed loop poles, zeroes of $1 + T_{rotor}G_{pend}K_{pend}(s)$ are

$$\begin{array}{l} 0.0000 + 0.0000i \\ -10.0953 + 16.1051i \\ -10.0953 - 16.1051i \\ -9.2786 + 0.0000i \\ -0.2898 + 0.3612i \\ -0.2898 - 0.3612i \end{array}$$

An evaluation of stability is provided by the Bode plot of $K_{Pendulum}(s)G_{Pendulum}(s)T_{Rotor}(s)$ with the above gains as shown in *Figure 92*. The Phase Margin of 32.9 degrees meets the stability objective.

For the selected gain value, the number of unstable poles of the plant, $T_{rotor}G_{pend}K_{pend}(s)$ is two. The number, P, of right half plane zeroes of $1 + T_{rotor}G_{pend}K_{pend}(s)$ is zero. Therefore, with N = P - N = -1, stability requires two encirclement of $s = -1$ in the counterclockwise direction appear in the Nyquist characteristic. Thus, stability is indicated as shown in the Nyquist characteristic of *Figure 87*.

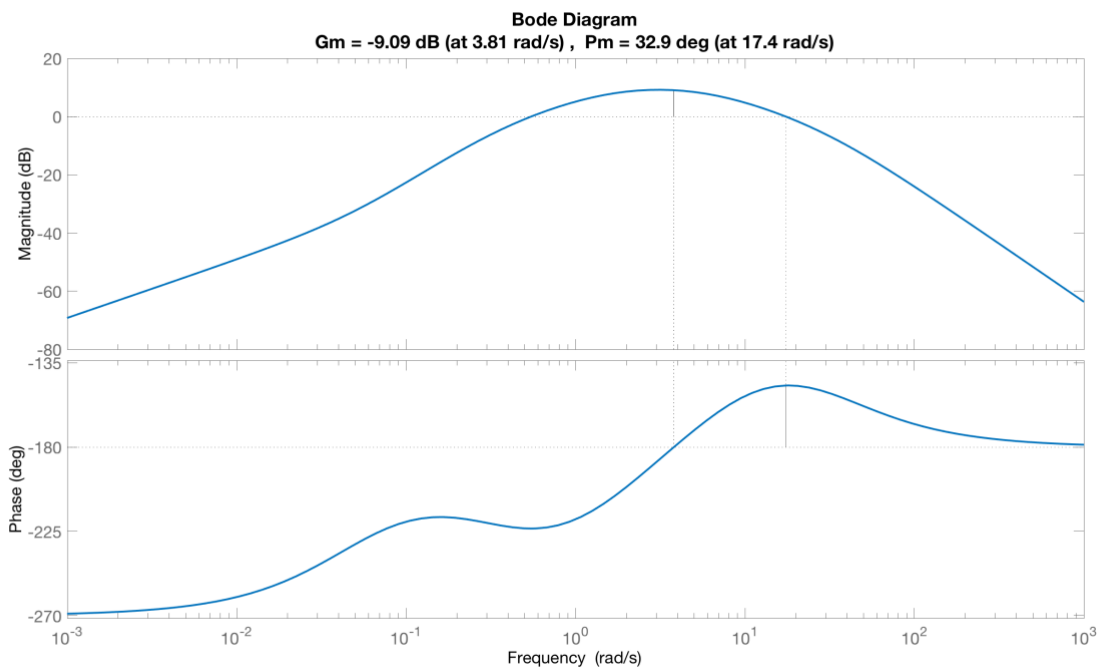


Figure 86. The Bode plot of the open loop control system including controller and plant product transfer function. The phase margin indicates stability with Phase Margin equaling design objectives.

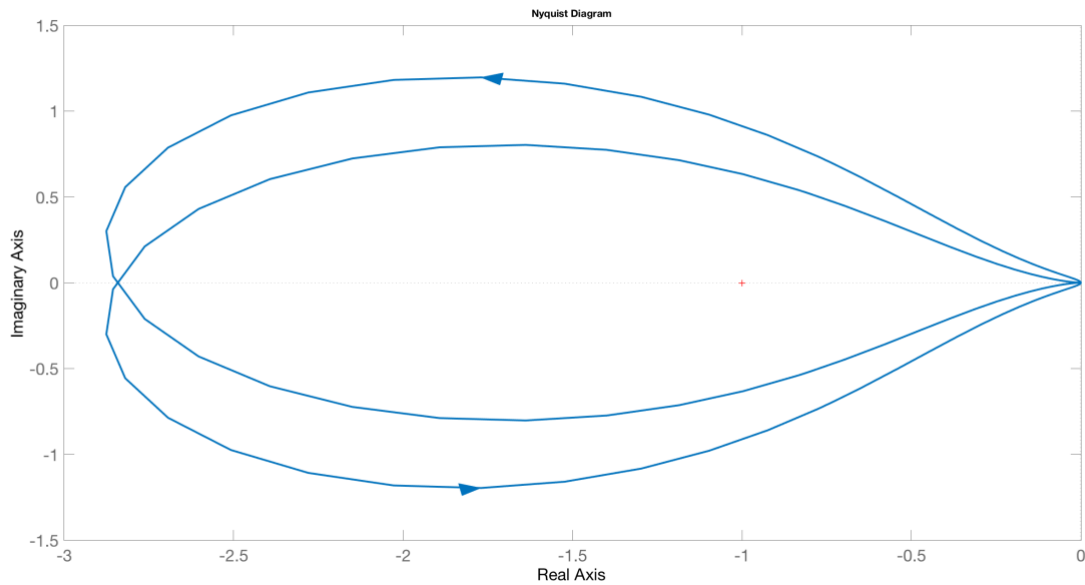


Figure 87. Nyquist characteristic for $K = 2154.3$. The stable characteristics for this gain selection are observed in the presence of two counterclockwise encirclements of the point $s = -1$.

The closed loop transfer function is

$$T_{Pend_cl}(s) = \frac{\theta(s)}{\theta_{Command}(s)} = \left(\frac{K_{Pend}(s)T_{Rotor}(s)G_{Pend}(s)}{1 + K_{Pend}(s)T_{Rotor}(s)G_{Pend}(s)} \right)$$

This may now be applied to determine the closed loop response of the Pendulum Angle control system. The simulated impulse response is shown in *Figure 88*. This is a further confirmation of stability.

The experimentally measured closed loop response of the Pendulum Angle control system is shown in *Figure 89*.

Together, these results demonstrate the accurate agreement between simulated and experimental systems.

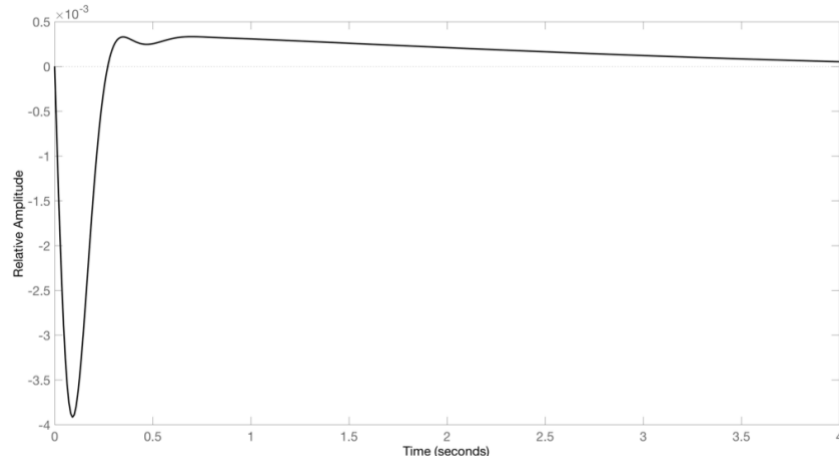


Figure 88. Simulated response of Pendulum Angle, $\theta(s)$, to an impulse signal applied to Pendulum angle tracking command, $\theta_{Command}(s)$, at $t = 0$.

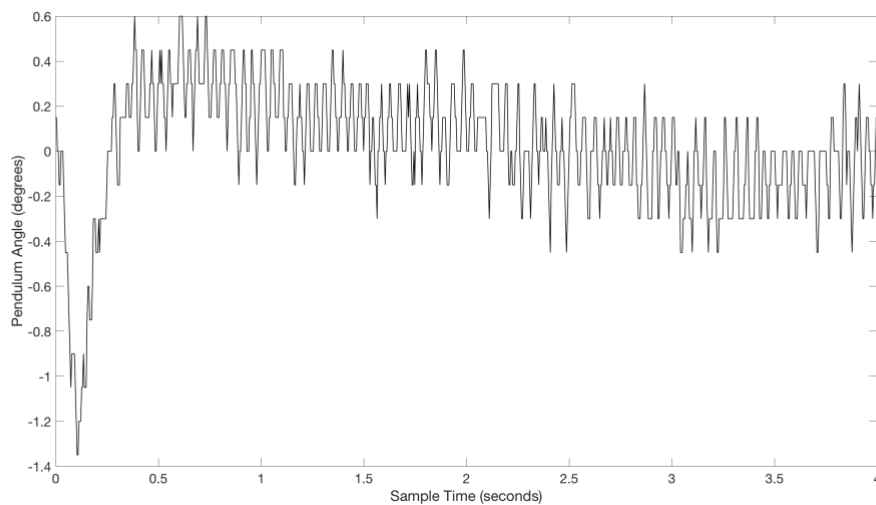


Figure 89. Experimental response of Pendulum Angle, $\theta(s)$, to an impulse signal applied to Pendulum angle tracking command, $\theta_{Command}(s)$, at $t = 0$. Note that the quantization of Pendulum Angle of 0.15 degrees per step is visible.

15. State Space Modern Control: The Linear Quadratic Regulator

The PID controller has been designed by frequency domain methods as well as by root locus techniques. However, these methods are not suited for design of the multi-input multi-output (MIMO) methods required for the rotary inverted pendulum where both pendulum angle and rotor angle require control. The design of a compensator and the placement of its closed loop poles for MIMO systems is challenging. Also, for MIMO systems, the controller systems that produce a set of closed loop poles are not unique. [Speyer_2010]

The Integrated Rotary Inverted Pendulum provides a method for directly comparing classical control, as in the previous section, and methods based on Modern Control described in this section. Modern Control introduces state space methods that enable description of MIMO systems. This also enables development of algorithms providing systematic methods for optimal design. This optimal design also permits optimization methods that permit weighting of response characteristics as well as control effort. This capability, in turn, allows for separate optimization of control system components including the Motor Controller.

A Linear Quadratic Regulator (LQR) system has been developed for the Integrated Rotary Inverted Pendulum. The LQR system has been developed with one input control signal for Rotor Angle Control and two outputs for Rotor Angle and Pendulum Angle. This is developed enabling Rotor Angle tracking of a command signal while maintaining Pendulum Angle at its nominal vertical, zero value.

As described in Section 4, development of the LQR system first requires development of a model for the Stepper Motor system providing Rotor control of Rotor Angle, ϕ , in response to Rotor Angle Control input, ϕ_{RC} .

Development of a Linear Quadratic Regulator (LQR) system may proceed with this model available.

First, the Rotor angle response transfer function differential equation is:

$$\ddot{\phi} = -b\dot{\phi} - c\phi + au$$

where the input control signal, u , is, ϕ_{RC} .

Then, the transfer function between Rotor angle and Pendulum angle is defined by a differential equation:

$$\ddot{\theta} = e\ddot{\phi} + d\theta$$

where

$$e = \frac{r}{l}$$

$$d = \frac{g}{l}$$

Experimental measurements were performed on a system with

$$\begin{aligned} r &= 0.140 \text{ m} \\ l &= 0.235 \text{ m} \end{aligned}$$

Now, substituting for $\ddot{\phi}$ above, pendulum angle is related to input control signal, \mathbf{u} .

$$\ddot{\theta} = e(-b\dot{\phi} - c\phi + a\mathbf{u}) + d\theta$$

or

$$\ddot{\theta} = -be\dot{\phi} - ce\phi + ae\mathbf{u} + d\theta$$

Thus, the state-space form of this system of differential equations relates the Rotor and Pendulum angle state vector, \mathbf{x} , to control vector, \mathbf{u} .

First, the state vector \mathbf{x} is defined

$$\mathbf{x} = \begin{bmatrix} \phi \\ \dot{\phi} \\ \theta \\ \dot{\theta} \end{bmatrix}$$

and

$$\dot{\mathbf{x}} = \mathbf{Ax} + \mathbf{Bu}$$

with

$$\dot{\mathbf{x}} = \begin{bmatrix} \dot{\phi} \\ \ddot{\phi} \\ \dot{\theta} \\ \ddot{\theta} \end{bmatrix}$$

and the state matrix, \mathbf{A}

$$\mathbf{A} = \begin{bmatrix} 0 & 1 & 0 & 0 \\ -c & -b & 0 & 0 \\ 0 & 0 & 0 & 1 \\ -ce & -be & d & 0 \end{bmatrix}$$

with the input matrix, \mathbf{B}

then,

$$\begin{bmatrix} \dot{\phi} \\ \ddot{\phi} \\ \dot{\theta} \\ \ddot{\theta} \end{bmatrix} = \begin{bmatrix} 0 & 1 & 0 & 0 \\ -c & -b & 0 & 0 \\ 0 & 0 & 0 & 1 \\ -ce & -be & d & 0 \end{bmatrix} \begin{bmatrix} \phi \\ \dot{\phi} \\ \theta \\ \dot{\theta} \end{bmatrix} + \begin{bmatrix} 0 \\ a \\ 0 \\ ae \end{bmatrix} u$$

The system output vector, y , including the Rotor Angle, ϕ , and Pendulum Angle, θ , is defined,

$$y = Cx + Du$$

with the output matrix, C

$$C = \begin{bmatrix} 1 & 0 & 0 & 0 \\ 0 & 1 & 0 & 0 \\ 0 & 0 & 1 & 0 \\ 0 & 0 & 0 & 1 \end{bmatrix}$$

and the feedforward matrix, D

$$D = \begin{bmatrix} 0 \\ 0 \end{bmatrix}$$

then

$$y = \begin{bmatrix} 1 & 0 & 0 & 0 \\ 0 & 1 & 0 & 0 \\ 0 & 0 & 1 & 0 \\ 0 & 0 & 0 & 1 \end{bmatrix} \begin{bmatrix} \phi \\ \dot{\phi} \\ \theta \\ \dot{\theta} \end{bmatrix} + \begin{bmatrix} 0 \\ 0 \end{bmatrix} u$$

The state feedback system is defined as

$$u = Kx$$

The Linear Quadratic Regulator (LQR) design method finds the optimal gain matrix, K , that minimizes the cost function of output u ,

$$J(u) = \int_0^{\infty} (x^T Q x + u^T R u) dt$$

The matrix, determines the relative weights of state value contributions to the cost function. For the purpose of this design, the weights of Pendulum Angle, θ , and Rotor Angle, ϕ , are equal thus resulting in a control law that minimizes both with equal weight. The value of R , determines the ratio of weight

of control effort to control error. Increasing value of \mathbf{R} increases the weight of control error at the expense of control effort.

The weight matrix, \mathbf{Q} , is selected with unit diagonal values, and \mathbf{R} is set to 1. Thus,

$$\mathbf{Q} = \mathbf{C} * \mathbf{C}^T$$

and

$$\mathbf{Q} = \begin{bmatrix} 1 & 0 & 0 & 0 \\ 0 & 1 & 0 & 0 \\ 0 & 0 & 1 & 0 \\ 0 & 0 & 0 & 1 \end{bmatrix}$$

Before proceeding, the controllability of the Integrated Rotary Inverted Pendulum system plant may be evaluated.

\mathbf{A} is a 4×4 matrix while \mathbf{B} is a 1×4 matrix. Then the controllability matrix, \mathbf{M}_C , is

$$\mathbf{M}_C = [\mathbf{B} \ \mathbf{AB} \ \mathbf{A}^2\mathbf{B} \ \mathbf{A}^3\mathbf{B}]$$

Applying the numerical values of a , b , e , and d , the controllability matrix, \mathbf{M}_C , is

$$\mathbf{M}_C = [\mathbf{B} \ \mathbf{AB} \ \mathbf{A}^2\mathbf{B} \ \mathbf{A}^3\mathbf{B}] = \begin{bmatrix} 0 & 0.2450 & -0.2744 & -0.0753 \\ 0.2450 & -0.2744 & 0.1873 & -0.0074 \\ 0 & -0.1095 & 0.1226 & 4.6536 \\ -0.1095 & 0.1226 & -4.6536 & -194.2581 \end{bmatrix}$$

Computation of \mathbf{M}_C above shows that the full row rank of \mathbf{M}_C is 4 and that the system is controllable.

The computation of system dynamics for LQR design requires that gains for rotor control and measurement gain of rotor position and measurement gain of pendulum position included the values for the Integrated Rotary Inverted Pendulum experimental system. These include, the Rotor Angle Control Gain, Rotor Angle Measurement Gain and the Pendulum Angle Measurement Gain listed in Table 1. The relationship between Pendulum Angle Measurement Gain and Rotor Angle Measurement Gain requires that the parameter, e , is scaled by the ratio of Pendulum Angle Measurement Gain to Rotor Angle Measurement Gain. Further, the parameter a is scaled by the ratio of Rotor Angle Measurement Gain to Rotor Angle Control Gain.

For the example of $Min_{Speed} = 300$ and $Max_{Speed} = 1000$ steps per second, the Integrated Rotary Inverted Pendulum LQR computed gain values for this Motor Controller configuration are:

$$K_\theta = 4.24; \quad K_{\dot{\theta}} = 9.24; \quad K_\phi = 988.3; \quad K_{\dot{\phi}} = 153.0$$

For the example of $Min_{Speed} = 200$ and $Max_{Speed} = 1000$ steps per second, the Integrated Rotary Inverted Pendulum LQR computed gain values for this Motor Controller configuration are:

$$K_\theta = 4.24; \quad K_{\dot{\theta}} = 10.15; \quad K_\phi = 913.9; \quad K_{\dot{\phi}} = 141.5$$

For the example of $Min_{Speed} = 200$ and $Max_{Speed} = 200$ steps per second, the Integrated Rotary Inverted Pendulum LQR computed gain values for this Motor Controller configuration are:

$$K_\theta = 4.24; \quad K_{\dot{\theta}} = 14.63; \quad K_\phi = 893.9; \quad K_{\dot{\phi}} = 138.4$$

These same gain values were applied to the Integrated Rotary Inverted Pendulum.

First, for the example of $Min_{Speed} = 300$ and $Max_{Speed} = 1000$ steps per second, the step response of this physical system was characterized by application of a step command of amplitude 16 degrees to the Rotor Angle control input. The simulated response of Rotor Angle and Pendulum Angle to this step command is shown in *Figure 90*. The IRIP experimental system response of Rotor Angle is shown in *Figure 91* and response of Pendulum Angle to this step command is shown in *Figure 92*.

Second, for the example of $Min_{Speed} = 200$ and $Max_{Speed} = 1000$ steps per second, the step response of this physical system was characterized by application of a step command of amplitude 16 degrees to the Rotor Angle control input. The simulated response of Rotor Angle and Pendulum Angle to this step command is shown in *Figure 93*. The IRIP experimental system response of Rotor Angle is shown in *Figure 94* and response of Pendulum Angle to this step command is shown in *Figure 95*.

Third, for the example of $Min_{Speed} = 200$ and $Max_{Speed} = 200$ steps per second, the step response of this physical system was also characterized by application of a step command of amplitude 16 degrees to the Rotor Angle control input. The simulated response of Rotor Angle and Pendulum Angle to this step command is shown in *Figure 96*. The IRIP experimental system response of Rotor Angle is shown in *Figure 97* and response of Pendulum Angle to this step command is shown in *Figure 98*.

Comparison of *Figure 91*, *Figure 94*, *Figure 97* and immediately show the change in system performance produced by the change in step rate. This performance improvement, includes a cost of motor system energy demand. Many design opportunities are now possible with a family of motor control configurations, motor response models, and control system architectures.

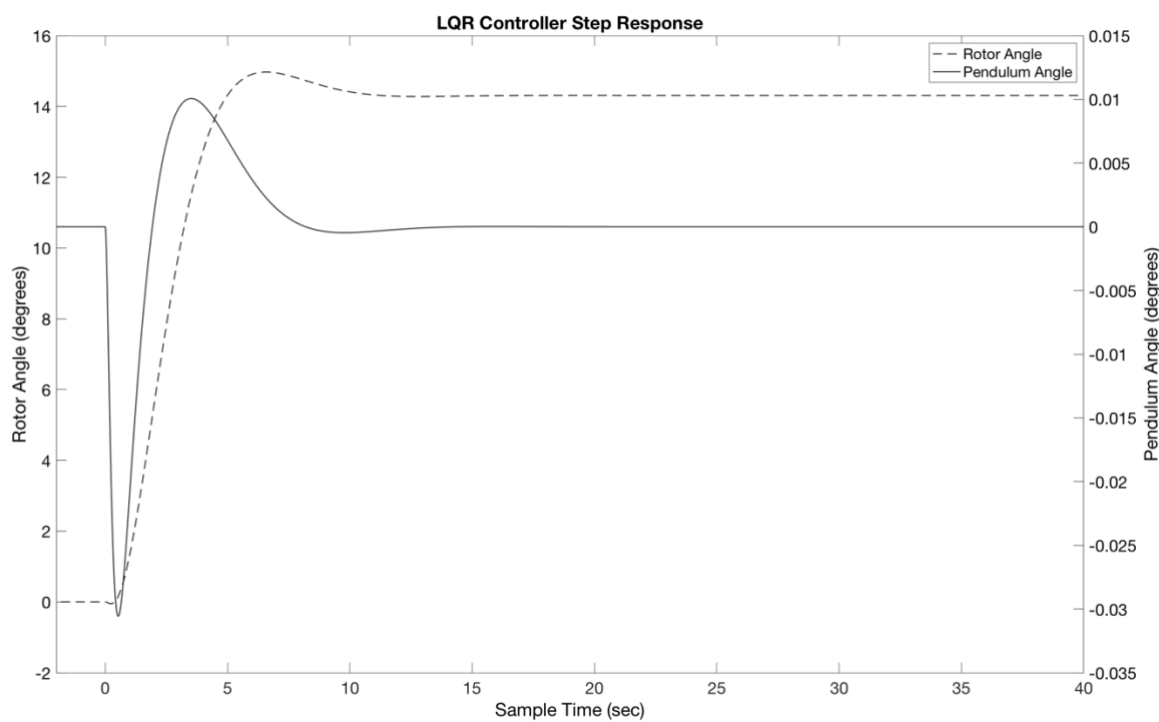


Figure 90. Simulated response of Rotor Angle and Pendulum Angle for the Integrated Rotary Inverted Pendulum with LQR Controller for a step in Rotor Angle Control Input of 16 degrees applied at $t = 0$ s for Motor Controller configuration of $\text{Min}_{\text{Speed}} = 300$ and $\text{Max}_{\text{Speed}} = 1000$ steps per second.

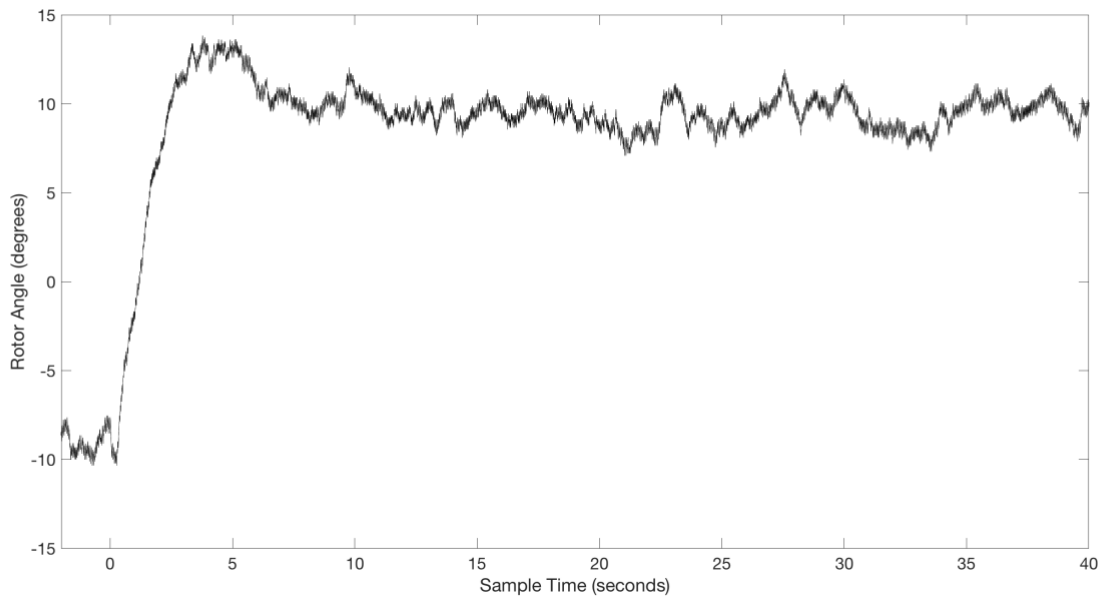


Figure 91. Experimentally Measured step response of Rotor Angle for the Integrated Rotary Inverted Pendulum with LQR Controller for a step of Rotor Angle Control Input of 16 degrees applied at $t = 0$ s for Motor Controller configuration of $\text{Min}_{\text{Speed}} = 300$ and $\text{Max}_{\text{Speed}} = 1000$ steps per second.

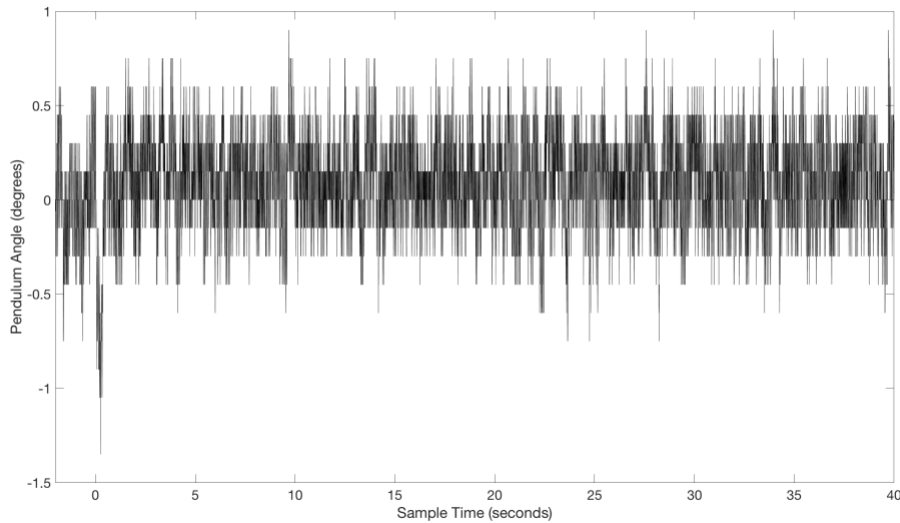


Figure 92 Experimentally Measured step response of Pendulum Angle for the Integrated Rotary Inverted Pendulum with LQR Controller for a step change in Rotor Angle Control Input of 16 degrees applied at $t = 0$ s for Motor Controller configuration of $\text{Min}_{\text{Speed}} = 300$ and $\text{Max}_{\text{Speed}} = 1000$ steps per second.

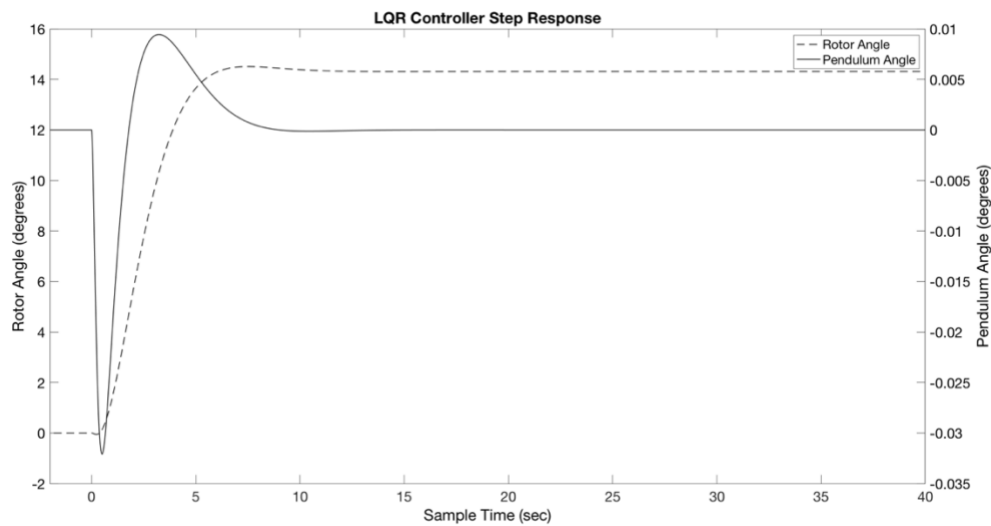


Figure 93. Simulated response of Rotor Angle and Pendulum Angle for the Integrated Rotary Inverted Pendulum with LQR Controller for a step in Rotor Angle Control Input of 16 degrees applied at $t = 0$ s for Motor Controller configuration of $\text{Min}_{\text{Speed}} = 200$ and $\text{Max}_{\text{Speed}} = 1000$ steps per second.

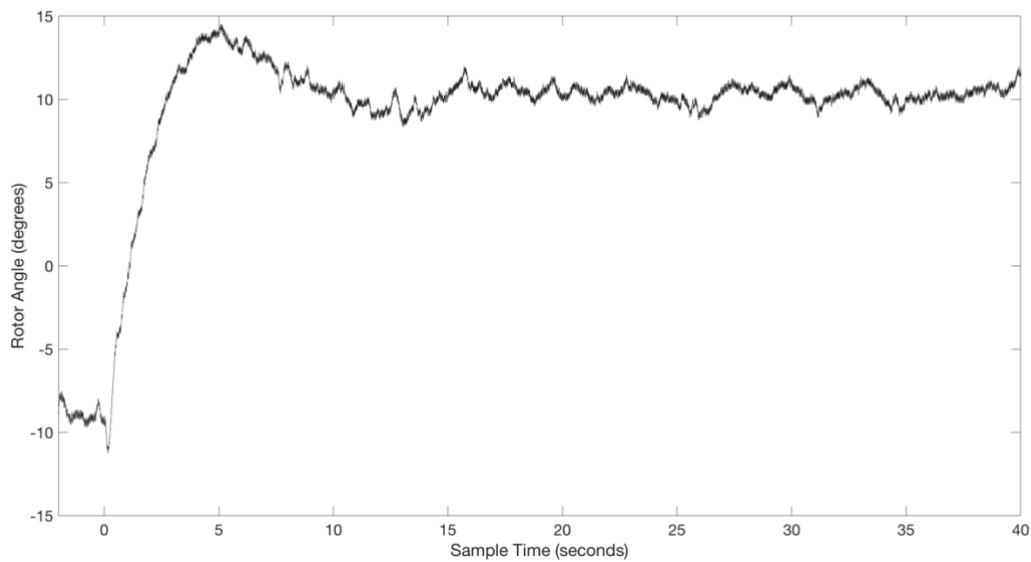


Figure 94. Experimentally Measured step response of Rotor Angle for the Integrated Rotary Inverted Pendulum with LQR Controller for a step of Rotor Angle Control Input of 16 degrees applied at $t = 0$ s for Motor Controller configuration of $\text{Min}_{\text{Speed}} = 200$ and $\text{Max}_{\text{Speed}} = 1000$ steps per second.

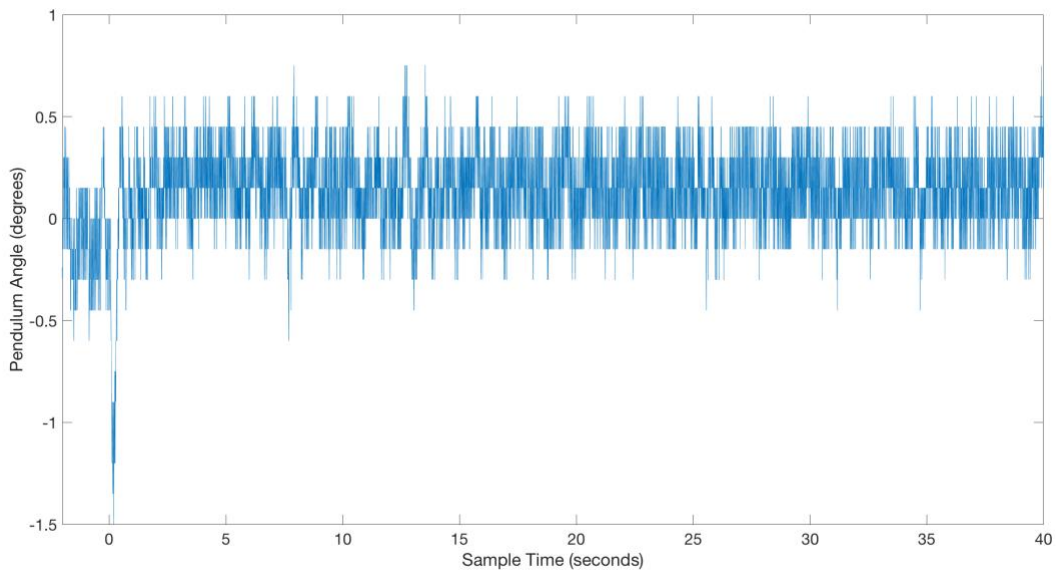


Figure 95 Experimentally Measured step response of Pendulum Angle for the Integrated Rotary Inverted Pendulum with LQR Controller for a step change in Rotor Angle Control Input of 16 degrees applied at $t = 0$ s for Motor Controller configuration of $\text{Min}_{\text{Speed}} = 200$ and $\text{Max}_{\text{Speed}} = 1000$ steps per second.

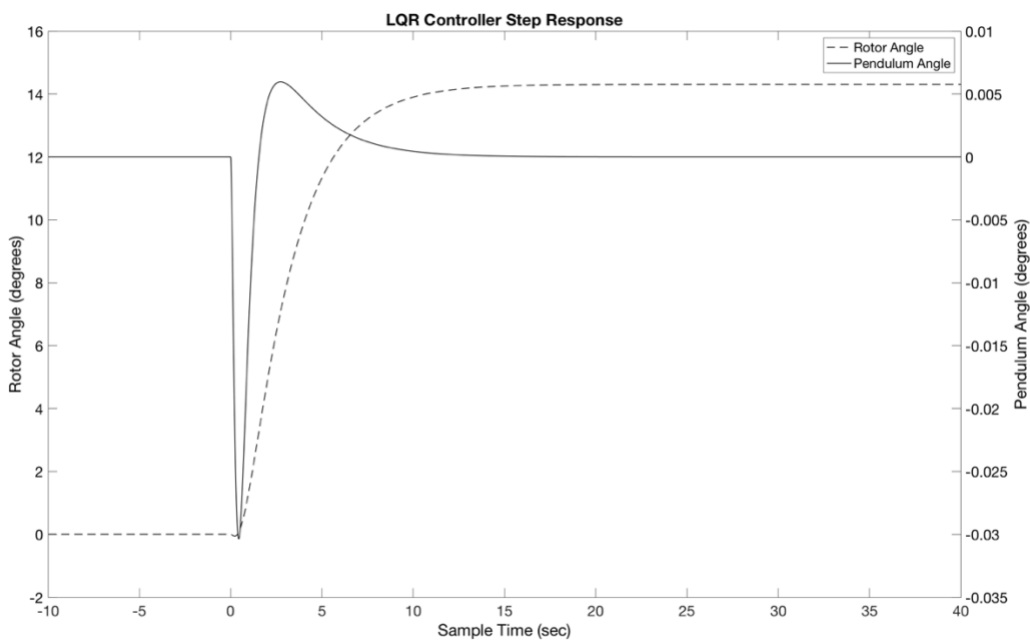


Figure 96. Simulated response of Rotor Angle and Pendulum Angle for the Integrated Rotary Inverted Pendulum with LQR Controller for a step in Rotor Angle Control Input of 16 degrees applied at $t = 0$ s for Motor Controller configuration of $\text{Min}_{\text{Speed}} = 200$ and $\text{Max}_{\text{Speed}} = 200$ steps per second.

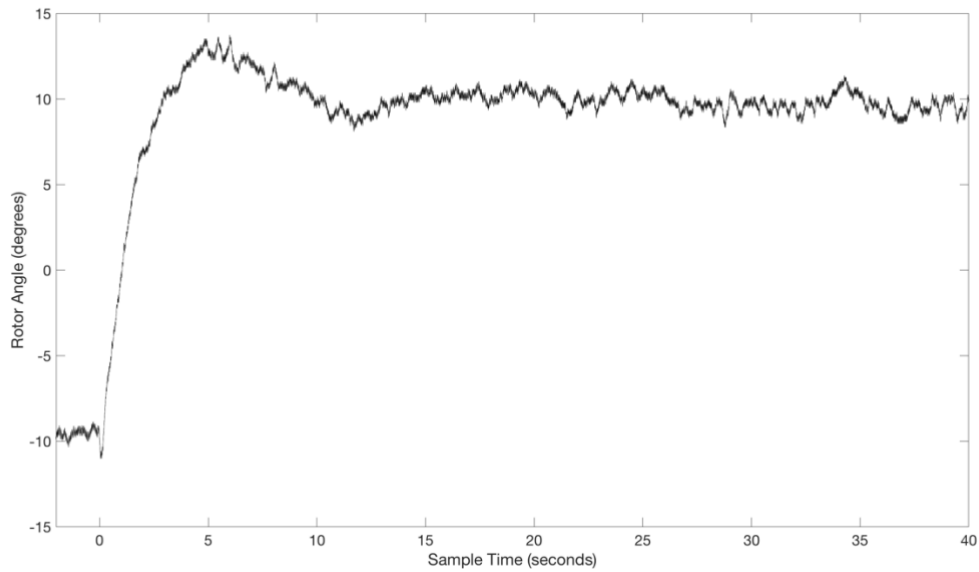


Figure 97. Experimentally Measured step response of Rotor Angle for the Integrated Rotary Inverted Pendulum with LQR Controller for a step of Rotor Angle Control Input of 16 degrees applied at $t = 0$ s for Motor Controller configuration of $\text{Min}_{\text{Speed}} = 200$ and $\text{Max}_{\text{Speed}} = 200$ steps per second.

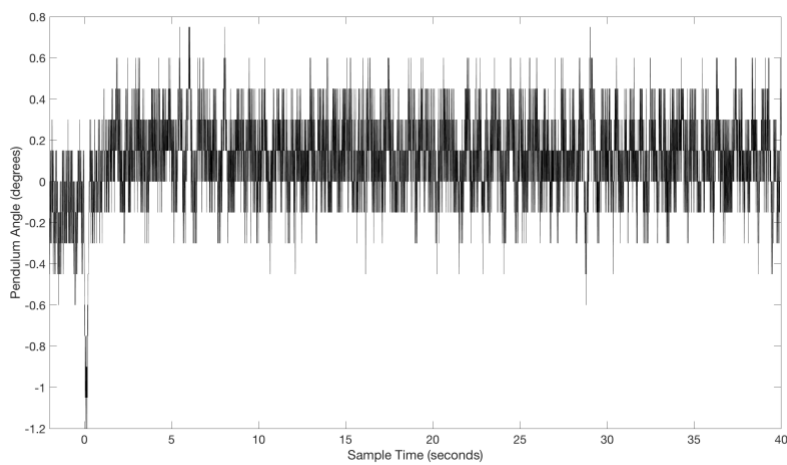


Figure 98 Experimentally Measured step response of Pendulum Angle for the Integrated Rotary Inverted Pendulum with LQR Controller for a step change in Rotor Angle Control Input of 16 degrees applied at $t = 0$ s for Motor Controller configuration of $\text{Min}_{\text{Speed}} = 200$ and $\text{Max}_{\text{Speed}} = 200$ steps per second.

An additional test of the Integrated Rotary Inverted Pendulum with LQR Controller was developed by applying an amplitude modulated sine wave input applied to the Rotor Angle Control Input. The sinusoidal wave frequency is 0.01 Hz and is modulated in amplitude at 0.001 Hz. The input control signal and system response are shown in *Figure 99*. Also, the simulated response of Rotor Angle and Pendulum Angle for the LQR model for this same Rotor Angle Command is shown in *Figure 100*.

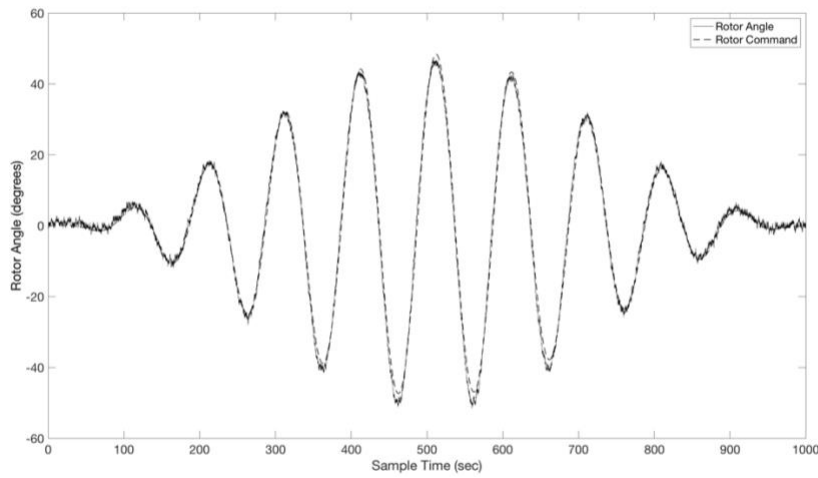


Figure 99. Experimentally measured results for the response of the Integrated Rotary Inverted Pendulum to an amplitude modulated sinusoidal signal applied to the Rotor Angle Control input of amplitude 52 degrees.

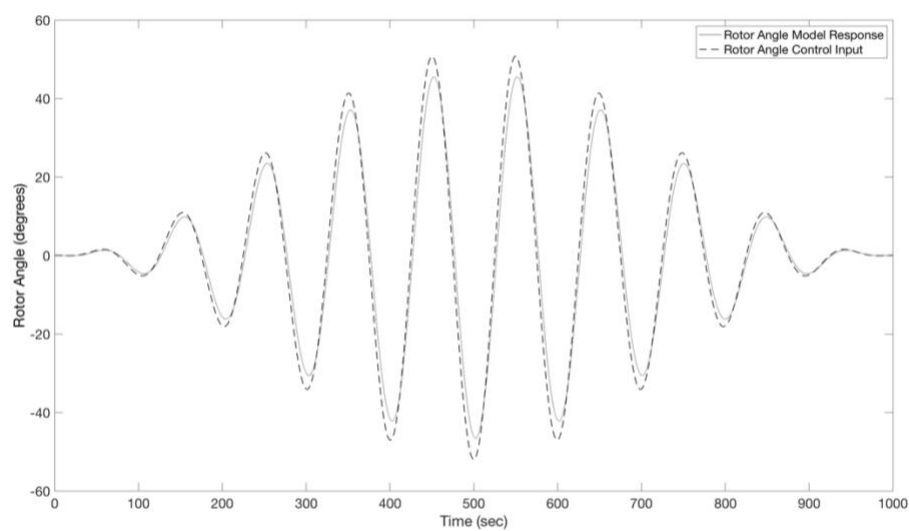


Figure 100. Simulation results for the response of the Integrated Rotary Inverted Pendulum to an amplitude modulated sinusoidal signal applied to the Rotor Angle Control input of amplitude 52 degrees.

16. State Space Modern Control: The Linear Quadratic Regulator for Stable Suspended Pendulum Operating Mode

As described in Section 15, the development of an optimal controller for a MIMO system requires modern control methods. Thus, a Linear Quadratic Regulator (LQR) system has been developed for the Integrated Rotary Inverted Pendulum *operating in the Suspended Pendulum mode described in Section 5*. The LQR system has been developed with one input control signal for Rotor Angle Control and two outputs for Rotor Angle and Pendulum Angle. This is developed enabling Rotor Angle tracking of a command signal while maintaining Pendulum Angle at its nominal vertical, zero value.

As described in Section 4, development of the LQR system first requires development of a model for the Stepper Motor system providing Rotor control of Rotor Angle, ϕ , in response to Rotor Angle Control input, ϕ_{RC} .

Development of a Linear Quadratic Regulator (LQR) system may proceed with this model available.

First, the Rotor angle response transfer function differential equation is:

$$\ddot{\phi} = -b\dot{\phi} - c\phi + au$$

where the input control signal, u , is, ϕ_{RC} .

Then, the transfer function between Rotor angle and Pendulum angle is defined by a differential equation of the same form as that of the *Inverted Pendulum Operating Mode*. For this design, we will proceed first with the approximation of zero damping. Then, as noted in Section 5, the Pendulum Angle to Rotor Angle Transfer Function is:

$$G_{pendulum}(s) = \frac{\theta(s)}{\phi(s)} = \frac{(r/l)s^2}{s^2 + (g/l)}$$

where $\omega_o = g/l$ and $Q = \omega_o(m/l)$.

The differential equation relating Pendulum Angle to Rotor Angle is, therefore,

$$\ddot{\theta} = e\ddot{\phi} - d\theta - \sqrt{d}/Q$$

where

$$e = \frac{r}{l}$$

$$d = \frac{g}{l}$$

Note that this differential equation is of the same form as that of *Inverted Pendulum Operation Mode* with the exception that the polarity of d is now negative. For this model, Q is estimated from Pendulum measurement to be $Q = 10$ as in Section 5.

Experimental measurements were performed on a system with

$$r = 0.140 \text{ m}$$

$$l = 0.235 \text{ m}$$

Now, substituting for $\ddot{\phi}$ above, pendulum angle is related to input control signal, u .

$$\ddot{\theta} = e(-b\dot{\phi} - c\phi + au) - d\theta - \sqrt{d}/Q \dot{\theta}$$

or

$$\ddot{\theta} = -be\dot{\phi} - ce\phi + ae u - d\theta - \sqrt{d}/Q \dot{\theta}$$

Thus, the state-space form of this system of differential equations relates the Rotor and Pendulum angle state vector, x , to control vector, u .

First, the state vector x is defined

$$x = \begin{bmatrix} \phi \\ \dot{\phi} \\ \theta \\ \dot{\theta} \end{bmatrix}$$

and

$$\dot{x} = Ax + Bu$$

with

$$\dot{x} = \begin{bmatrix} \dot{\phi} \\ \ddot{\phi} \\ \dot{\theta} \\ \ddot{\theta} \end{bmatrix}$$

and the state matrix, A

$$\mathbf{A} = \begin{bmatrix} 0 & 1 & 0 & 0 \\ -c & -b & 0 & 0 \\ 0 & 0 & 0 & 1 \\ -ce & -be & -d & \sqrt{d}/Q \dot{\theta} \end{bmatrix}$$

with the input matrix, \mathbf{B}

$$\mathbf{B} = \begin{bmatrix} 0 \\ a \\ 0 \\ ae \end{bmatrix}$$

then,

$$\begin{bmatrix} \dot{\phi} \\ \ddot{\phi} \\ \dot{\theta} \\ \ddot{\theta} \end{bmatrix} = \begin{bmatrix} 0 & 1 & 0 & 0 \\ -c & -b & 0 & 0 \\ 0 & 0 & 0 & 1 \\ -ce & -be & -d & 0 \end{bmatrix} \begin{bmatrix} \phi \\ \dot{\phi} \\ \theta \\ \dot{\theta} \end{bmatrix} + \begin{bmatrix} 0 \\ a \\ 0 \\ ae \end{bmatrix} \mathbf{u}$$

The system output vector, \mathbf{y} , including the Rotor Angle, ϕ , and Pendulum Angle, θ , is defined,

$$\mathbf{y} = \mathbf{Cx} + \mathbf{Du}$$

with the output matrix, \mathbf{C}

$$\mathbf{C} = \begin{bmatrix} 1 & 0 & 0 & 0 \\ 0 & 1 & 0 & 0 \\ 0 & 0 & 1 & 0 \\ 0 & 0 & 0 & 1 \end{bmatrix}$$

and the feedforward matrix, \mathbf{D}

$$\mathbf{D} = \begin{bmatrix} 0 \\ 0 \end{bmatrix}$$

then

$$\mathbf{y} = \begin{bmatrix} 1 & 0 & 0 & 0 \\ 0 & 1 & 0 & 0 \\ 0 & 0 & 1 & 0 \\ 0 & 0 & 0 & 1 \end{bmatrix} \begin{bmatrix} \phi \\ \dot{\phi} \\ \theta \\ \dot{\theta} \end{bmatrix} + \begin{bmatrix} 0 \\ 0 \end{bmatrix} \mathbf{u}$$

The state feedback system is defined as

$$\mathbf{u} = \mathbf{Kx}$$

The Linear Quadratic Regulator (LQR) design method finds the optimal gain matrix, \mathbf{K} , that minimizes the cost function of output \mathbf{u} ,

$$J(\mathbf{u}) = \int_0^{\infty} (\mathbf{x}^T \mathbf{Q} \mathbf{x} + \mathbf{u}^T \mathbf{R} \mathbf{u}) dt$$

The matrix, determines the relative weights of state value contributions to the cost function. For the purpose of this design, the weights of Pendulum Angle, θ , and Rotor Angle, ϕ , are equal thus resulting in a control law that minimizes both with equal weight. The value of \mathbf{R} , determines the ratio of weight of control effort to control error. Increasing value of \mathbf{R} increases the weight of control error at the expense of control effort.

The weight matrix, \mathbf{Q} , is selected with unit diagonal values, and \mathbf{R} is set to 1. Thus,

$$\mathbf{Q} = \mathbf{C} * \mathbf{C}^T$$

now,

$$\mathbf{C} * \mathbf{C}^T = \begin{bmatrix} 1 & 0 & 0 & 0 \\ 0 & 0 & 0 & 0 \\ 0 & 0 & 1 & 0 \\ 0 & 0 & 0 & 0 \end{bmatrix}$$

Also, weight is assigned to the stabilization of Rotor Angle and Rotor Angle Derivative

$$\mathbf{Q} = \mathbf{Q} * \begin{bmatrix} 1 & 0 & 0 & 0 \\ 0 & 0 & 0 & 0 \\ 0 & 0 & 10 & 0 \\ 0 & 0 & 0 & 10 \end{bmatrix}$$

Before proceeding, the controllability of the Integrated Rotary Inverted Pendulum system plant may be evaluated.

\mathbf{A} is a 4×4 matrix while \mathbf{B} is a 1×4 matrix. Then the controllability matrix, \mathbf{M}_C , is

$$\mathbf{M}_C = [\mathbf{B} \ \mathbf{AB} \ \mathbf{A}^2\mathbf{B} \ \mathbf{A}^3\mathbf{B}]$$

Applying the numerical values of a , b , e , and d , the controllability matrix, \mathbf{M}_C , is

$$\mathbf{M}_C = [\mathbf{B} \ \mathbf{AB} \ \mathbf{A}^2\mathbf{B} \ \mathbf{A}^3\mathbf{B}] = \begin{bmatrix} 0 & 0.2450 & -0.2744 & -0.0753 \\ 0.2450 & -0.2744 & 0.1873 & -0.0074 \\ 0 & -0.1095 & 0.1933 & -10.8551 \\ -0.1095 & 0.1933 & 4.3613 & -175.0436 \end{bmatrix}$$

Computation of \mathbf{M}_C above shows that the full row rank of \mathbf{M}_C is 4 and that the system is controllable.

The computation of system dynamics for LQR design requires that gains for rotor control and measurement gain of rotor position and measurement gain of pendulum position included the values for the Integrated Rotary Inverted Pendulum experimental system. These include, the Rotor Angle Control Gain, Rotor Angle Measurement Gain and the Pendulum Angle Measurement Gain listed in Table 1. The relationship between Pendulum Angle Measurement Gain and Rotor Angle Measurement Gain requires that the parameter, e , is scaled by the ratio of Pendulum Angle Measurement Gain to Rotor Angle Measurement Gain. Further, the parameter a is scaled by the ratio of Rotor Angle Measurement Gain to Rotor Angle Control Gain.

For the example of $Min_{Speed} = 200$ and $Max_{Speed} = 1000$ steps per second, the Integrated Rotary Inverted Pendulum LQR computed gain values for this Motor Controller configuration are:

$$K_\theta = 0.236; \quad K_{\dot{\theta}} = 0.314; \quad K_\phi = -0.965; \quad K_{\dot{\phi}} = -0.797$$

It is important to note that modern control methods have yielded gain values dramatically different from the classic design of Sections 6 and 7. As will be shown below, this design based on Modern Control also shows dramatically improved performance.

These same gain values were applied to the Integrated Rotary Inverted Pendulum system.

For the example of $Min_{Speed} = 200$ and $Max_{Speed} = 1000$ steps per second, the step response of this physical system was characterized by application of a step command of amplitude 16 degrees to the Rotor Angle control input. The simulated response of Rotor Angle and Pendulum Angle to this step command is shown in *Figure 101*. The experimental system response of Rotor Angle is shown in *Figure 102* and response of Pendulum Angle to this step command is shown in *Figure 103*.

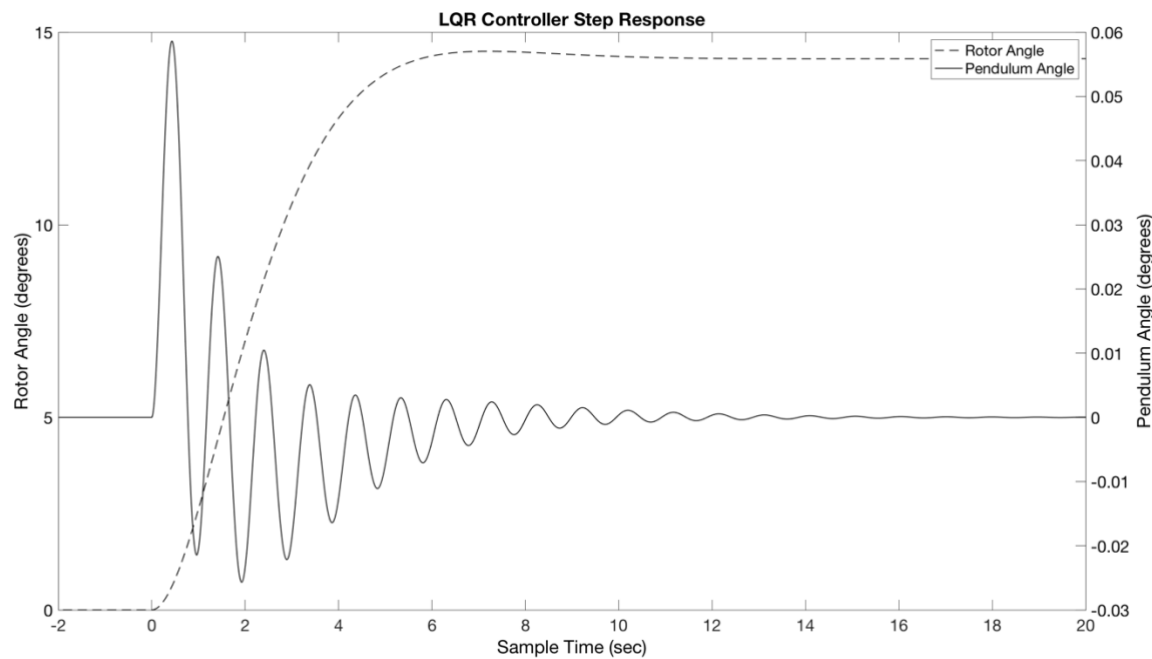


Figure 101. Simulated response of Rotor Angle and Pendulum Angle for the Integrated Rotary Inverted Pendulum with LQR Controller for a step in Rotor Angle Control Input of 16 degrees applied at $t = 0$ s for Motor Controller configuration of $\text{Min}_{\text{Speed}} = 200$ and $\text{Max}_{\text{Speed}} = 1000$ steps per second.

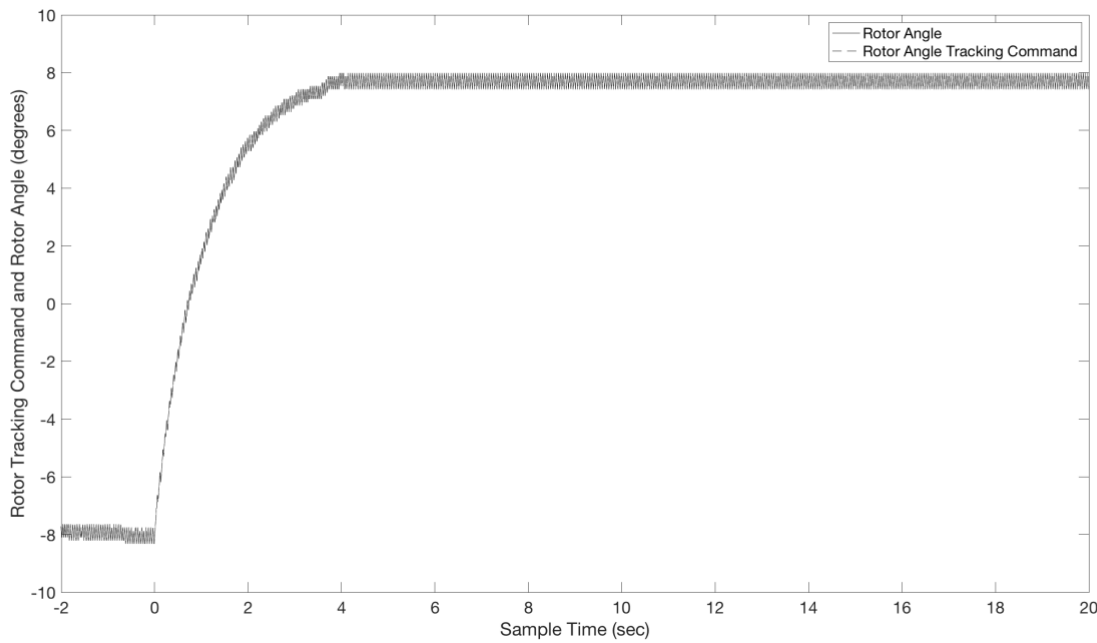


Figure 102. Experimentally Measured step response of Rotor Angle for the Integrated Rotary Inverted Pendulum with LQR Controller for a step of Rotor Angle Control Input of 16 degrees applied at $t = 0$ s for Motor Controller configuration of $\text{Min}_{\text{Speed}} = 200$ and $\text{Max}_{\text{Speed}} = 1000$ steps per second.

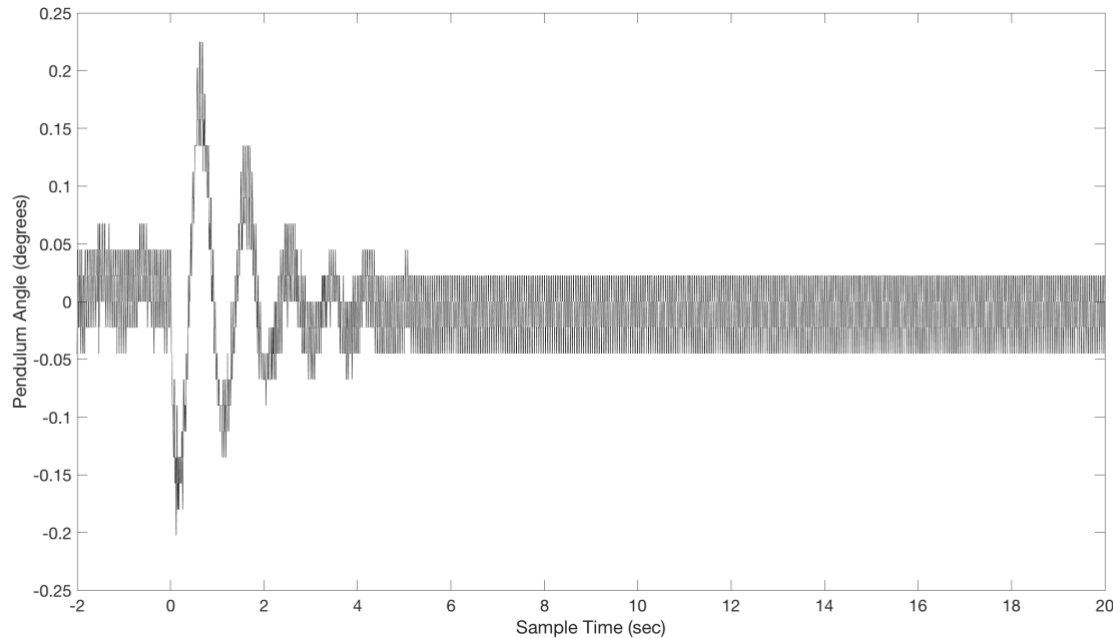


Figure 103 Experimentally Measured step response of Pendulum Angle for the Integrated Rotary Inverted Pendulum with LQR Controller for a step change in Rotor Angle Control Input of 16 degrees applied at $t = 0$ s for Motor Controller configuration of $\text{Min}_{\text{Speed}} = 200$ and $\text{Max}_{\text{Speed}} = 1000$ steps per second. Note that the finite resolution of the Pendulum Angle Optical Encoder of 0.16 degrees accounts for the amplitude quantization visible in this data.

An additional test of the Integrated Rotary Inverted Pendulum with LQR Controller was developed by applying an amplitude modulated sine wave input applied to the Rotor Angle Control Input. The sinusoidal wave frequency is 0.01 Hz and is modulated in amplitude at 0.001 Hz. The input control signal and system response are shown in *Figure 104*. Also, the simulated response of Rotor Angle and Pendulum Angle for the LQR model for this same Rotor Angle Command is shown in *Figure 105*.

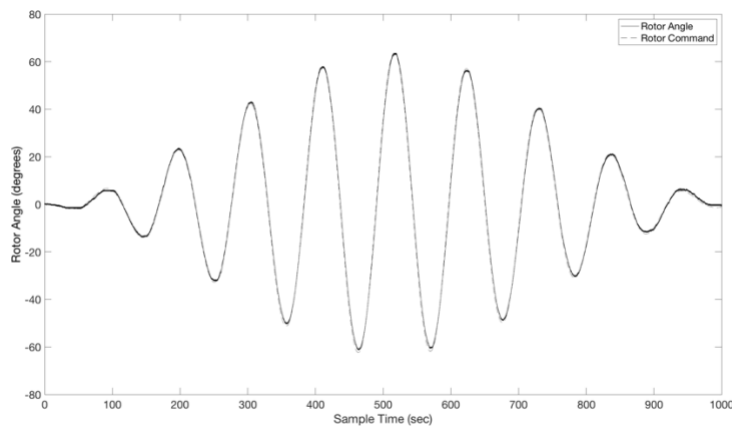


Figure 104. Experimentally measured results for the response of the Integrated Rotary Inverted Pendulum to an amplitude modulated sinusoidal signal applied to the Rotor Angle Control input of amplitude 52 degrees.

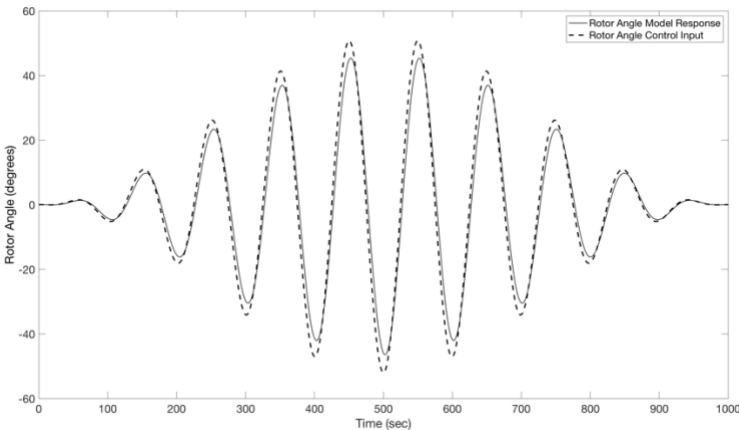


Figure 105. Simulation results for the response of the Integrated Rotary Inverted Pendulum to an amplitude modulated sinusoidal signal applied to the Rotor Angle Control input of amplitude 52 degrees.

17. References

[Astrom_2008] Karl Johan Astrom and Richard M. Murray. 2008. Feedback Systems: An Introduction for Scientists and Engineers. Princeton University Press, Princeton, NJ, USA.

[Furuta_1992] K. Furuta, M. Yamakita, and S. Kobayashi, "Swing-up control of inverted pendulum using pseudo-state feedback," Journal of Systems and Control Engineering, vol. 206, no. 6, pp. 263-269, 1992.

[Nise_2015] Norman S. Nise, 2015, Control Systems Engineering (7th ed.). John Wiley & Sons, Inc., New York, NY, USA.

[Seborg_1989] Seborg, D.E., T.F. Edgar and D.A. Mellichamp (1989). Process Dynamics and Control. John Wiley & Sons.

[Speyer_2010] J. L. Speyer and D. H. Jacobson. Primer on Optimal Control Theory. SIAM, 2010.

[ST_IHM01A1_2019] <https://www.st.com/en/ecosystems/x-nucleo-ihm01a1.html>

[ST_L6474_2019] <https://www.st.com/b/en/motor-drivers/l6474.html>

[ST_Nucleo_2019] <https://www.st.com/b/en/evaluation-tools/nucleo-f401re.html>

18. Appendix A: Pendulum Angle Error Autocompensation System

The Integrated Rotary Inverted Pendulum and other similar systems may be subject to long term drift errors resulting from at least two sources. First, the Pendulum controller requires accurate measurement of Pendulum Angle relative to the gravity vector. An initial offset of this value will lead to drift in the controller system output with a rate dependent on magnitude of the offset error. Pendulum Angle calibration is performed by a process where Pendulum Angle is measured for the Pendulum operating prior to control system operation such that the Pendulum Angle corresponds to the Pendulum operating in a suspended, vertical mode. Prior to initiation of control operation, the Pendulum is manually rotated into a near vertical orientation. At this time, the control system measures Pendulum Angle and subtracts the angle of 180 degrees from all subsequent measurement, yielding an angle measured relative to the gravity vector.

One error source results from the finite resolution of the optical encoder. This finite resolution implies that at initiation of the Pendulum Angle control operation, the recording of vertical down position and subsequent vertical upwards position will include a small offset error of the order of one optical encoder step or, 0.16 degrees. During control operation, this small bias error will induce a drift Rotor Position as the control system seeks to eliminate this error.

A second error source results from tilt in the Rotary Inverted Pendulum structure relative to the gravity vector. A departure of the structure from vertical orientation (due to a slope in the base support structure relative to earth level) will introduce an error in operation. This results from the small, but finite difference between the normal to the plane of rotation of the Rotary Inverted Pendulum and the gravity vector. This will also lead to an error as the Rotor Control system seeks to ensure the Pendulum Angle is zero.

The error in operation appears as a drift and long term error between ϕ_{rotor} and $\phi_{rotor-control}$. A control system, referred to as Autocompensation compensates for the platform slope and encoder offset errors. Autocompensation introduces an additional PID control operating on the input of the low pass filtered difference between ϕ_{rotor} and $\phi_{rotor-control}$ and providing an output summed with the measured pendulum angle, $\theta(s)$. A first order low pass filter, $H_{as}(s)$, at corner frequency of f_{as} is applied to the difference between ϕ_{rotor} and $\phi_{rotor-control}$.

The Autocompensation introduces, therefore, a filter and PID control block into the Dual PID controller. The block diagram for the Autocompensation control is shown in *Figure 106*.

It is important to note that the implementation of the Integrated Rotary Inverted Pendulum offers three operating modes for Autocompensation:

- 1) Autocompensation Operation Disabled
- 2) Autocompensation Operation Enabled for all operating time
- 3) Autocompensation Operation Enabled for an initial period, T_{as} , and with Autocompensation control suspended for later time. This option enables errors to be removed during a short initial operating period and then suspension of Autocompensation control for all later time.

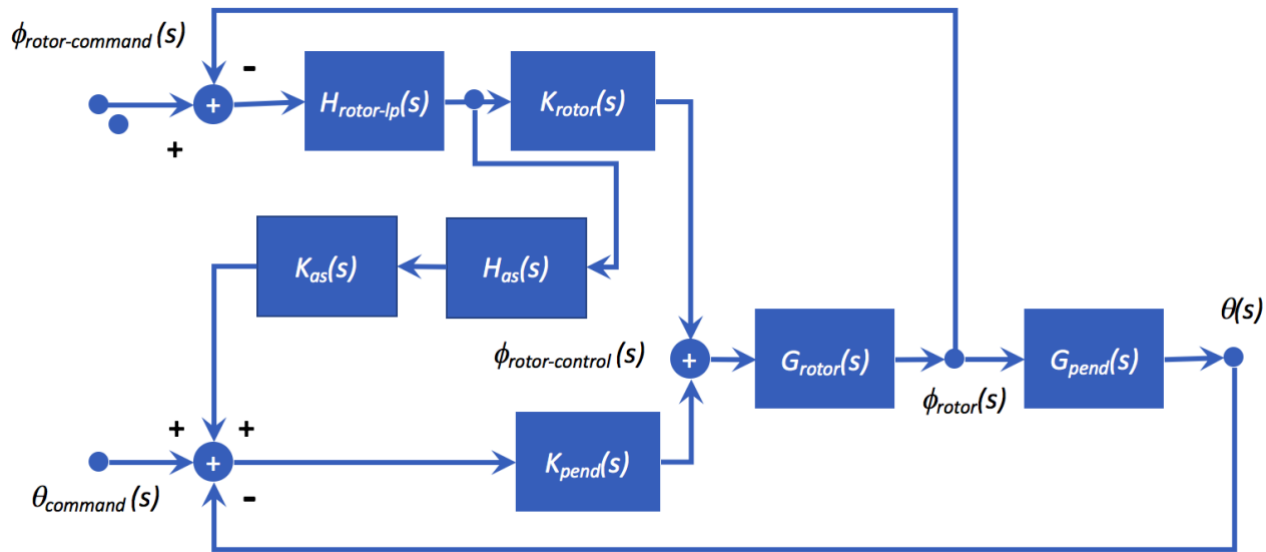


Figure 106. The Autocompensation PID Control System

The relationship between ϕ_{rotor} and $\phi_{rotor-control}$ is below.

$$\begin{aligned}\phi_{rotor}(s) = & \phi_{rotor}(s)G_{pendulum}(s)K_{pend}(s)G_{rotor}(s) \\ & + (\phi_{rotor-command}(s) - \phi_{rotor}(s))H_{rotor-lp}(s)K_{rotor}(s)G_{rotor}(s) \\ & + (\phi_{rotor-command}(s) - \phi_{rotor}(s))H_{as}(s)K_{as}(s)K_{pend}(s)G_{rotor}(s)\end{aligned}$$

Finally, noting the negative feedback contribution of K_{pend} , the transfer function from rotor command angle to rotor angle is.

$$\frac{\phi_{rotor}(s)}{\phi_{rotor-command}(s)} = \frac{(H_{rotor-lp}(s)K_{rotor}(s)G_{rotor}(s) - H_{as}(s)K_{as}(s)K_{pend}(s)G_{rotor}(s))}{(1 + H_{rotor-lp}(s)K_{rotor}(s)G_{rotor}(s) - H_{as}(s)K_{as}(s)K_{pend}(s)G_{rotor}(s) + G_{pendulum}(s)K_{pend}(s)G_{rotor}(s))}$$

The contribution of K_{as} to the input of K_{pend} includes the gain relating measured rotor angle position (Rotor Angle Measurement Gain) with encoder angle position of (Encoder Angle Measurement Gain). Further, the output of the controller, is scaled by the gain factor between measured angle and motor control angle gain (Rotor Angle Control Gain). This control system, operating at low relative frequency, is stable and requires only proportional control.

The Integrated Rotary Inverted Pendulum control system for rotor angle applies these typical values:

$$\begin{aligned}K_p &= 0.005; K_i = 0; K_d = 0 \\ f_{as} &= 0.01 \text{ Hz} \\ T_{as} &= 80 \text{ seconds}\end{aligned}$$

19. Appendix B: Integrated Rotary Inverted Pendulum: Real Time Viewer and Matlab Interface

The Integrated Rotary Inverted Pendulum may operate independently of a computing platform. Its control system implementation is supported in a high speed, real time C code implementation operating on the STM32 processor.

However, all control system real time parameters may be viewed and system configuration may be modified via standard USB serial interfaces.

Real time viewing of control system operation is also available. *Figure 107* shows the Real Time Viewer output where the traces for Rotor Angle, Pendulum Angle, and Rotor Angle Tracking Command are all displayed. This provides both opportunity to visualize signals while viewing the physical system response and also to evaluate performance. The Real Time Viewer also provides a method for selecting Motor Control Configurations. The image of *Figure 107* is a snapshot of operation of the LQR controller showing system response to a 16 degree step in the Rotor Angle Tracking Command.

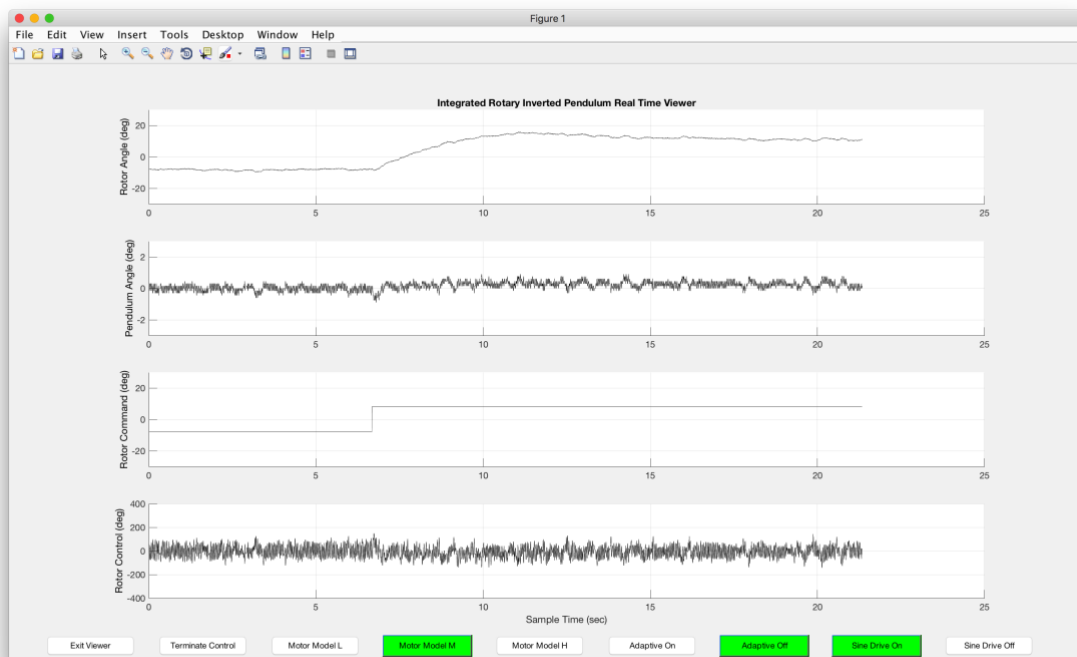


Figure 107. The Integrated Rotary Inverted Pendulum real time viewer in Matlab. This shows part of a trace of real time data corresponding to operation of the Dual PID controller showing system response to a 16 degree step in the Rotor Angle Tracking Command.

1. Appendix C: Integrated Rotary Inverted Pendulum: Serial Control Interface

The IRIP system may be configured and experimental testing may be performed using an interactive session provided by the IRIP system. Serial communication may be established at the rate of 115,200 baud via a USB serial link from Mac OSX or Windows environments.

Upon reset action of the Nucleo processor system, the interactive session starts.

The user is requested to enter a starting mode. These modes include:

Input Mode Command Entry	Mode Description
1	Inverted Pendulum Control with Motor Speed Profile - Medium
2	Inverted Pendulum Control with Motor Speed Profile - High
3	Inverted Pendulum Control with Motor Speed Profile - Low
4	Suspended Pendulum Control with Motor Speed Profile - Medium
s	Single PID mode requiring entry only of Pendulum PID Control gains with model Rotor Transfer Function as described in Section 14
g	General mode enabling entry of PID gains for both Pendulum PID and Rotor PID
t	Test mode for testing of Rotor Actuator and Pendulum Angle Encoder

Response Messages from IRIP System

After system boot or after the user depresses the reset switch, the following messages will appear at the serial interface:

```

System Starting Prepare to Enter Mode Selection...
*****
 System Start Mode Selections *****
Enter 1 at prompt for Inverted Pendulum Control with Motor Speed Profile - Medium
Enter 2 at prompt for Inverted Pendulum Control with Motor Speed Profile - High
Enter 3 at prompt for Inverted Pendulum Control with Motor Speed Profile - Low
Enter 4 at prompt for Suspended Pendulum Control with Motor Speed Profile - Medium
Enter 's' at prompt for Single PID: With Prompts for Pendulum Controller Gains
Enter 'g' at prompt for General Mode: With Prompts for Both Pendulum and Rotor Controller Gains
Enter 't' at prompt for Test Mode: Test of Rotor Actuator and Pendulum Angle Encoder
  
```

Enter Mode Selection Now or System Will Start in Default Mode in 2 Seconds: 1

```

Mode 1 Configured
Enter 1 to Enable Rotor Chirp Drive; 0 to Disable: 0
Enter 1 to Enable Step Drive; 0 to Disable: 1
Enter 1 to Enable Sine Drive; 0 to Disable: 0
Rotor Step Drive enabled
  
```

Motor Profile Speeds Min 200 Max 1000
 Prepare for Control Start - Initial Rotor Position: 0
 Test for Pendulum at Rest - Stabilize Pendulum Now
 Pendulum Now at Rest and Measuring Pendulum Down Angle
 Adjust Pendulum Upright By Turning CCW Control Will Start in 3 Seconds

Initial Rotor Position: 0

0.000	0	4	0	-1881	71.11	1	-51585	-49704
0.005	5	4	0	-3039	71.11	2	-75095	-72055
0.010	5	4	-1	-2749	71.11	3	-35557	-32807
0.015	5	3	-2	-2023	71.11	4	-17192	-15168
0.020	5	2	-3	-1038	71.11	5	-8373	-7334
0.025	5	2	-4	-624	71.11	6	-4543	-3919
0.029	4	1	-5	-116	71.11	7	-2604	-2488
0.033	4	1	-6	206	71.11	8	-1735	-1941
0.037	4	0	-7	632	71.11	9	-1151	-1783
0.041	4	0	-8	883	71.11	10	-908	-1791
0.045	4	-1	-8	1246	71.11	11	-577	-1823
0.050	5	-2	-10	1911	71.11	12	47	-1863
0.054	4	-2	-10	2044	71.11	13	98	-1945
0.058	4	-2	-11	1833	71.11	14	-165	-1998
0.063	5	-2	-10	1646	71.11	15	-306	-1953
0.068	5	-2	-11	1482	71.11	16	-348	-1831
0.073	5	-2	-12	1337	71.11	17	-431	-1769
0.078	5	-4	-13	2150	71.11	18	333	-1817
0.083	5	-5	-13	3086	71.11	19	1221	-1865
0.088	5	-5	-12	3130	71.11	20	1344	-1786
0.093	5	-4	-11	2370	71.11	21	832	-1538
0.098	5	-2	-10	885	71.11	22	-312	-1198

The reported IRIP data is best viewed using the IRIP Real Time Viewer.

Data can also be recorded using the IRIP Data Acquisition System.

The data values, observed in tab-separated columns includes these values:

IRIP Data Description		
	Variable	Definition
1	test_time	Time computed from Nucleo processor 1 ms clock tick
2	cycle_time	Time for current control system cycle in milliseconds
3	encoder_position	Pendulum angle in 6.667 steps per degree
4	rotor_position	Rotor angle in 8.887 steps per degree
5	pendulum_angle_controller	Output of Pendulum Angle PID controller in 17.778 steps per degree)
6	rotor_command	Rotor tracking command in 8.889 steps per degree
7	chirp_cycle	Cycle count for chirp cycle operation
8	rotor_position_target	Target angle for motor position supplied to motor controller (in 17.778 steps per degree) includes difference of rotor_position to compensate for addition of reference rotor angle required in motor drive interface.
9	rotor_angle_controller	Output of Pendulum Angle PID controller in 17.778 steps per degree)

2. Appendix D: Integrated Rotary Inverted Pendulum: Individualization for Instruction

The benefits of hands-on instruction apply when every student acquires individual experience in design, implementation, testing, and verification. This Appendix describes instructional approaches that enable this individual support.

First, the mission to support a large student population requires a precise, reproducible system kit that may be assembled directly and tested.

Second, while precise, the Integrated Rotary Inverted Pendulum is also sensitive to conditions including platform tilt and small variations in the characteristics of Motor systems, Encoder systems, clock frequency, and the Pendulum structure. For this reason, experimental measurements on any two platforms will be distinguishable. This enables a system where student assignment submissions will be distinguishable.

Third, at the same time, it is important to enable additional platform configuration that distinguishes the response of each platform from any other. This enables the same assignment to be presented to all students in a course while ensuring that each student's contribution may be independently verified.

Fourth, the Integrated Rotary Inverted Pendulum includes configurable Motor Control configuration. Small changes in these configuration values produce system responses that are unique. A class may be assigned a single design task. At the same time, subsets of the students, or individual students may receive unique Motor Control configurations.